UNIVERSIDADE FEDERAL DE SANTA CATARINA

CENTRO TECNOLÓGICO

PROGRAMA DE PÓS-GRADUAÇÃO EM ENGENHARIA ELÉTRICA

Guilherme Brasil Pintarelli

Sensing electroporation during pulsed electric fields

Florianópolis, 2022

2022

Guilherme Brasil Pintarelli

Sensing electroporation during pulsed electric fields

> Thesis submitted to the Graduate Program in Electrical Engineering at the *Universidade Federal de Santa Catarina* for the Doctorate Degree in Electrical Engineering.
> Supervisor: Daniela Ota Hisayasu Suzuki, Dr. Eng.

Florianópolis

2022

Ficha de identificação da obra elaborada pelo autor,

através do Programa de Geração Automática da Biblioteca Universitária da UFSC.

Guilherme Brasil Pintarelli

Sensing electroporation during pulsed electric fields

Sensoriamento da eletroporação durante campos elétricos pulsados

O presente trabalho em nível doutorado foi avaliado e aprovado por banca examinadora composta pelos seguintes membros:

Prof. Pedro Xavier de Oliveira, Dr.
Universidade Estadual de Campinas

Prof. Joaquim Miguel Maia, Dr.
Universidade Tecnológica Federal do Paraná

Prof. Wuqiang Yang, Ph.D.
The University of Manchester (UK)

Certificamos que esta é a **versão original e final** do trabalho de conclusão que foi julgado adequado para obtenção do título de Doutor em Engenharia Elétrica no Programa de Pós-Graduação em Engenharia Elétrica (PPGEEL–UFSC).

Prof. Telles Brunelli Lazzarin, Dr. Eng.
Coordenação do Programa de Pós-Graduação em Engenharia Elétrica

Profa. Daniela Ota Hisayasu Suzuki, Dra. Eng.
Orientadora

Florianópolis, 2022.

'If we are ever to discover the laws of nature, we must do so by obtaining the most accurate acquaintance with the facts of nature, and not by dressing up in philosophical language the loose opinions of men who had no knowledge of the facts which throw most light on these laws.'

'… the medium [vast interplanetary and interstellar regions] has other functions and operations besides bearing light from man to man, and from world to world, and giving evidence of the absolute unity of the metric system of the universe. Its minute parts may have rotatory as well as vibratory motions, and the axes of rotation form those lines of magnetic force which extend in unbroken continuity into regions which no eye has seen, and which, by their action on our magnets, are telling us in language not yet interpreted, what is going on in the hidden underworld from minute to minute and from century to century.'

'On Action at a Distance' by James Clerk Maxwell. Original text from the Proceedings of the Royal Institution of Great Britain, 1876. Reprinted by Cambridge University Press in 1980 (MAXWELL, 1980).

ABSTRACT

Pulsed electric fields (PEF) can improve and be an alternative to traditional methods in the areas of medicine and biotechnology. PEF can open pores in the cell membrane; this phenomenon is called electroporation. Electroporation can be used to transfer substances to cells, treat cancers or non-thermal pasteurisation. Electroporation is a dynamic phenomenon characterized by altering the cell membrane permeability. This thesis aims to develop a sensing method for electroporation during the PEF protocol. We propose using the PEF current reading to get treatment feedback. This approach is non-invasive and can be implemented using the existing PEF electrodes. Ultimately the proposed methods can be used to better understand (*e.g.,* modelling) and control electroporation. We executed four experiments to support the objective: (i) We investigated the effects of irreversible electroporation pulse amplitude on *S. cerevisiae* using cell viability tests, macroscopic impedance measurements, scanning electron microscopy and numerical simulations. Irreversible electroporation proved to reach active yeast limits established by wine standards within 500 kV/m. We detected a 15% increase in the pulse current measurements for a 100-fold yeast viability decrease to 10^5 cells/ml. Scanning electron microscopic show details of PEF-triggered yeast surface damage. The direct current is affected by other effects rather than electroporation as PEF contain a broad spectrum of frequencies, mainly sub-10 kHz (typically pulsed high voltage signals). (ii) We investigate the use of alternating current superposing the PEF protocol to mitigate other effects interferences. We used COMSOL simulations with yeast electroporation model to demonstrate that the cell membrane and wall are susceptible to the passage of the displacement current starting between 10 kHz to 10 MHz. The biological media have specific characterization in the broad frequency spectrum. Those contribute with most of macroscopic dispersion β, which is used to development of biological sensors. We show that certain frequencies could be used to detect the occurrence of electroporation, *i.e.,* dielectric dispersion modulated sensing. (iii) We developed a custom signal generator capable of creating the PEF protocol with overlapping arbitrary signals. The system generates waveforms up to ± 85 V, 12 A and 100 kHz (THD < 2.5% at ± 30 V_{pp}). We used gel phantoms (with conductivity similar to the biological tissues, 0.1 S/m in tens of kHz) and likely to accumulate ions in the electrodes interface to study polarization effects. The results showed no significant changes at 100 kHz due to electrode polarization. It can be concluded that the reading at 100 kHz mitigates errors due to the electrodes polarization, and the system is satisfactory for evaluating responses at 100 kHz with DC bias. (iv) We executed *in vitro* study on *S. Tuberosum* using PEF and 100 kHz superposed sine. The analysis of the complex impedance as a function of the PEF has not yet been discussed in the literature. Our results show that certain levels of PEF induce a reduction in the sample's capacitive effect at 100 kHz (β dispersion shift), and the capacitance is no longer the main characteristic of the sample at tissue's irreversible electroporation experiments.

Keywords: Pulsed Electric Fields. Electroporation. Dielectrics. Sensors. Impedance. High Voltage. β-Dispersion.

RESUMO

Os campos elétricos pulsados (PEF) podem melhorar ou ser uma alternativa a métodos tradicionais nas áreas de medicina e biotecnologia. Os PEF provocam abertura de poros na membrana celular (eletroporação). A eletroporação pode ser utilizada na transferência de substâncias para células, tratamento de cânceres ou pasteurização não térmica. A eletroporação é um fenômeno dinâmico caracterizado por alterar a permeabilidade da membrana. Esta tese tem como objetivo desenvolver um método de sensoriamento para eletroporação durante o protocolo PEF. Propomos usar a corrente do PEF para feedback. Essa abordagem não é invasiva e pode ser implementada usando os eletrodos existentes. Os métodos de detecção propostos podem ser usados para modelagem e controle da eletroporação. Foram executados quatro experimentos: (i) Investigação dos efeitos da amplitude de PEF para eletroporação irreversível em *S. cerevisiae* com medição da viabilidade celular, medidas de impedância macroscópica, microscopia eletrônica de varredura e simulações numéricas. A eletroporação irreversível com 500 kV/m reduz os números de levedura aos níveis industriais para vinho. Foi detectado um aumento de 15% nas medições de corrente do PEF para uma diminuição de 100 vezes na viabilidade para 10^5 células/ml. A microscopia eletrônica mostra detalhes de danos na levedura. A corrente contínua é afetada por outros efeitos além da eletroporação, pois o PEF contém um amplo espectro de frequências, principalmente sub-10 kHz (tipicamente sinais pulsados de alta tensão). (ii) Investigamos o uso de corrente alternada sobreposta ao protocolo PEF para mitigar outros efeitos de interferências. Com COMSOL foram realizadas simulações de eletroporação de leveduras e demonstrado que a membrana e parede celular são suscetíveis à passagem da corrente de deslocamento iniciando entre 10 kHz a 10 MHz. Meios biológicos possuem uma caracterização particular no espectro de frequências. Esses contribuem com a maior parte da dispersão macroscópica tipo β, característica de interesse no desenvolvimento de sensores. A medição de impedância em certas frequências pode ser usada para detectar eletroporação. (iii) Foi desenvolvido um gerador de sinais capaz gerar PEF com sobreposição de sinais arbitrários. O sistema desenvolvido gera formas de onda de até ± 85 V, 12 A e 100 kHz (THD < 2,5% a ± 30 Vpp). *Phantoms* de gel (com condutividade semelhante aos tecidos biológicos, 0,1 S/m em dezenas de kHz) e propensos a acumular íons nos eletrodos foram usados para estudar os efeitos da polarização. Os resultados não mostraram mudanças significativas de impedância em 100 kHz devido à polarização do eletrodo. A leitura em 100 kHz reduz erros devido à polarização dos eletrodos, e o sistema é satisfatório para avaliar respostas em 100 kHz com polarização DC. (iv) Foi realizado o estudo *in vitro* com *S. Tuberosum* utilizando protocolos PEF com seno sobreposto de 100 kHz. A análise da impedância complexa em função do PEF ainda não foi discutida na literatura. Os resultados mostram que certos níveis de PEF induzem uma redução no efeito capacitivo da amostra em 100 kHz (deslocamento de dispersão β), e a capacitância não é mais a principal característica da amostra em experimentos de eletroporação irreversível do tecido.

Palavras-chave: Campos Elétricos Pulsados. Eletroporação. Dielétricos. Sensores. Impedância. Alta Tensão Elétrica. Dispersão β.

[blank page]

RESUMO EXPANDIDO

Introdução

Os campos elétricos pulsados (PEF) podem ser utilizados como um processo não térmico baseado em eletricidade para controle celular (*i.e.*, eletroporação). As aplicações de PEF necessitam condições específicas de controle de eletroporação. Essa tese é concentrada no sensoriamento de eletroporação usando medidas elétricas. As medições macroscópicas de propriedades elétricas podem ser usadas para detectar indiretamente a eletroporação. A membrana celular intacta é um material dielétrico e a abertura de poros por eletroporação, vazamento de íons e destruição da membrana aumentam a condutividade do sistema. A espectroscopia de impedância elétrica e a aquisição de tensão de corrente (ou densidade de corrente de eletrodos) são técnicas usadas para detectar a condutividade do meio. As medições elétricas macroscópicas podem utilizar os eletrodos já utilizados no aplicador de PEF, o que facilita a implementação em ambientes sanitários controlados. No entanto, existem desafios para medir a corrente elétrica de eletroporação "real", pois outros efeitos (como a polarização dos eletrodos) podem afetar a medição, e, a análise de impedância requer a interrupção do PEF, o que pode ser uma limitação desses procedimentos. Além da complexidade de caracterizar amostras biológicas usando medições abaixo de 10 kHz, a eletroporação em si não é totalmente compreendida. Assim, os sistemas PEF geralmente não têm feedback de eletroporação porque não existe um método adequado de sensoriamento. Técnicas de detecção de eletroporação em tempo real podem beneficiar as aplicações de eletroporação e o entendimento de sua dinâmica. Os benefícios esperados são melhorar a segurança e a otimização do PEF, aumentar a eficiência energética, reduzir o efeito térmico e eletroquímico e aumentar a qualidade do produto ou do tratamento final. Nesta tese, avaliaremos uma nova abordagem para detectar a eletroporação durante sua ocorrência. Propomos um método e sistema de detecção, que pode ser estendido para controle celular, no qual a própria amostra colabora com a transdução do efeito (ou seja, sensoriamento tipo bioeletrônico). Nosso método de detecção é não invasivo e foi implementado em paralelo ao PEF, utilizando os mesmos eletrodos de aplicação e sobrepondo-se ao protocolo primário do PEF.

Objetivos

O objetivo desse projeto é desenvolver um método de detecção para eletroporação baseado em medições e análises de impedância durante o protocolo PEF. Em particular, usar a leitura atual do próprio protocolo para obter feedback sobre o tratamento. Os métodos de detecção propostos podem ser usados para entender melhor (por exemplo, modelar) e controlar a eletroporação. Existem duas linhas de estudo dentro da tese proposta: (i) O modelo computacional, que é importante para fazer cálculos desde propriedades absolutas de materiais até propriedades equivalentes. (ii) O estudo in vitro com tecido vegetal e levedura, onde foram extraídos os dados biológicos e os dados de corrente e tensão.

Metodologia

Foram utilizadas leveduras *in vitro Saccharomyces cerevisiae* ATCC®36900™, em baixa concentração ($2,5 \times 10^7$ células/mL), para investigar os efeitos do PEF na viabilidade celular (usando o método do azul de metileno, 0,2% C16H18N3SCl), morfologia celular (usando microscópio eletrônico de varredura), condutividade (usando medições de tensão de corrente e espectroscopia de impedância) e energia absorvida. O protocolo PEF foram 8 pulsos retangulares de 100 μs e uma taxa de repetição de 1 Hz. Além disso, foi realizado um estudo

in silico para avaliar o número de poros na membrana celular, tensão elétrica transmembrana e tensão elétrica diferencial na parede celular. Investigamos os efeitos das mudanças de amplitude, pois a eletroporação depende principalmente dela. Foi avaliado o efeito de protocolos PEF de amplitude de 200 a 600 kV/m. Com o modelo *in sílico* da levedura foi realizado um experimento de resposta em frequência no tempo do sistema em três situações experimentais (buffers). Usamos a suposição de que o sistema é invariante no tempo em pequena escala para espectro dielétrico da suspensão. Foi utilizado tecido *in vitro* de *Solanum Tuberosum* e protocolos PEF com seno sobreposto de 100 kHz, com variações monopolar (100 μs) e bipolar (50 + 50 μs), com repetição de 0,1 Hz taxa e amplitude entre 1 e 50 kV/m, e pulsos dente de serra de diferentes $\Delta V/\Delta t$, para estudar o comportamento da dinâmica complexa da eletroporação (antes, durante e depois do tratamento), estudo histológico para verificar a destruição das células e a coloração do tecido para detectar a eletroporação do tecido. Foi executado um modelo do tecido usando uma geometria infinitesimal 2D com células hexagonais. O software COMSOL Multiphysics® versão 4.4 foi usado para modelagem por elementos finitos, aplicação de correntes nos meios biológicos e estudos das dispersões elétricas.

Resultados e Discussão

(i) A eletroporação irreversível com 500 kV/m reduz os limites de levedura viável à níveis estabelecidos por padrões da indústria de vinhos. Os resultados mostram um aumento de 15% nas medições de corrente do PEF para uma diminuição de 100 vezes na viabilidade da levedura para 10^5 células/ml. As imagens de microscopia eletrônica de varredura mostram detalhes de danos na superfície da levedura que podem ser desencadeados pelo PEF. No entanto, não é possível detectar eletroporação reversível usando as medições em corrente contínua. Além disso, a corrente contínua é afetada por outros efeitos além da eletroporação. O PEF é tipicamente alta tensão pulsada, e, esses sinais contêm um amplo espectro de frequências, principalmente abaixo de 10 kHz, que estão sujeitos a fenômenos dispersivos intrínsecos de baixa frequência (*e.g.*, os efeitos dispersivos do tipo α e a polarização da interface amostra-eletrodo). Para evitar e mitigar a medição de outros efeitos que não são eletroporação, foi investigado o uso de corrente alternada sobrepondo o protocolo PEF. Os meios biológicos não são homogêneos, o que lhes confere uma caracterização particular no amplo espectro de frequências. Por exemplo, a barreira celular, ou seja, a membrana celular, causa a chamada dispersão β na faixa de frequência de dezenas a milhares de kHz. (ii) Foram conduzidos, no COMSOL, simulações com células isoladas e tecidos em frequências entre 1 kHz e 100 MHz que demonstram que a membrana e parede celular são suscetíveis à passagem da corrente de deslocamento iniciando entre 10 kHz a 10 MHz. Esses contribuem com a maior parte da dispersão macroscópica tipo β, característica de interesse no desenvolvimento de sensores biológicos. Foi demonstrado mudanças no espectro de frequência devido à eletroporação e buffers externos. Foi demonstrado que é possível detectar o sucesso (ou não) da eletroporação baseado em alteração do espectro. (iii) Para desenvolver o quarto estudo, foi desenvolvido um gerador de alta tensão personalizado capaz de criar o protocolo PEF com sobreposição de sinais arbitrários. O sistema PEF desenvolvido para esta tese gera formas de onda de até ± 85 V, 12 A e 100 kHz (THD < 2,5% a ± 30 Vpp). O sistema foi testado no âmbito desta tese, que é a utilização do protocolo ESOPE e pulsos dente de serra, ambos com sinal senoidal superposto de 1,75 VRMS 100 kHz. A medição de impedância do sistema apresenta erros de até 5% para o módulo e 12% para a fase (testado em cargas que simulam dispersão). *Phantoms* de gel com condutividade semelhante aos tecidos biológicos (0,1 S/m em dezenas de kHz) e propensos a acumular íons nos eletrodos foram usados para estudar os efeitos da polarização, que é uma das principais causas de dispersão abaixo de 10 kHz. Os resultados não mostraram mudanças significativas de impedância em

100 kHz devido à polarização do eletrodo. Pode-se concluir que a leitura da impedância em 100 kHz mitiga erros devido ao acúmulo de íons nos eletrodos, e o sistema PEF é satisfatório para avaliar respostas em 100 kHz com bias DC. (iv) Foram conduzidos estudos *in vitro* (*Solanum Tuberosum*) utilizando protocolos PEF com seno sobreposto de 100 kHz – o protocolo de PEF foi o ESOPE adaptado, com variações monopolar (100 µs) e bipolar (50 + 50 µs), com repetição de 0,1 Hz taxa e amplitude entre 1 e 50 kV/m; e pulsos dente de serra de diferentes $\Delta V/\Delta t$ –. O objetivo deste estudo é apresentar um método de detecção baseado na medição de impedância centrada na frequência de 100 kHz como alternativa para evitar os efeitos dispersivos dos eletrodos. A análise da impedância complexa na dispersão β em função do PEF ainda não foi discutida na literatura. O método pode ser usado para detectar a ocorrência de eletroporação e desenvolver modelos que descrevem mudanças em parâmetros elétricos de membranas complexas (*e.g.*, condutividade e permissividade). Os resultados mostram que determinados níveis de PEF induzem uma redução no efeito capacitivo da amostra em 100 kHz, e a capacitância não é mais a principal característica da amostra em experimentos de eletroporação irreversível (> 25 kV/m). Se estiver operando em eletroporação irreversível, a leitura de impedância DC pode ser satisfatória para detectar eletroporação. Esta tese contribui para a detecção de eletroporação irreversível usando baixa fração celular usando medição de corrente contínua, propõe um modelo numérico do comportamento da dispersão β durante PEF para detectar a eletroporação usando suspensão de levedura e relata o comportamento da dispersão β durante a eletroporação de tecidos.

Considerações Finais
Esta tese mostra métodos de detecção para o tratamento baseado em PEF. Propomos utilizar a leitura atual do próprio protocolo para obter feedback sobre o tratamento. O método de detecção é não invasivo e foi implementado em paralelo à assinatura do PEF, utilizando os mesmos eletrodos de aplicação e sobrepondo-se ao protocolo primário do PEF. Esta tese contribui para a detecção de eletroporação irreversível usando baixa fração celular e medição de corrente contínua; propõe um modelo numérico do comportamento da dispersão-β durante o PEF para detectar a eletroporação usando suspensão de levedura; e relata o comportamento da dispersão-β durante a eletroporação dos tecidos.

Palavras-chave: Campos Elétricos Pulsados. Eletroporação. Dielétricos. Sensores. Impedância. Alta Tensão Elétrica. Dispersão β.

[blank page]

PUBLISHED CONTENT

The following content was published during the doctoral period (Oct. 2018 to June 2022). Some parts of this thesis text are based on the underlined publications. The updated list of authors' publications is on the author webpage (gpintarelli.com) and CNPq Lattes (http://lattes.cnpq.br/6921758272697669).

Journal papers:

1. Dielectric Dispersion Modulated Sensing of Yeast Suspension Electroporation. MDPI Sensors, 2022. **G. B. Pintarelli**, J. R. da Silva, W. Yang & D. O. H. Suzuki.

2. Electrochemotherapy treatment safety under parallel needle deflection. Nature Scientific Reports, 2022. D. L. L. S. Andrade, R. Guedert, **G. B. Pintarelli**, M. M. M. Rangel, K. D. Oliveira, P. G. Quadros & D. O. H. Suzuki.

3. Computer Optimization of Conductive Gels for Electrochemotherapy. Medical Engineering & Physics, 2021. L. B. Lopes, **G. B. Pintarelli**, C. S. F. Santos & D. O. H. Suzuki

4. Sensing of Yeast Inactivation by Electroporation. IEEE Sensors Journal, 2021. **G. B. Pintarelli**, C. T. S. Ramos, J. R. Da Silva; M. J. Rossi & D. O. H. Suzuki.

5. Computer simulation of commercial conductive gels and their application to increase the safety of electrochemotherapy treatment. Medical Engineering & Physics, 2019. **G. B.Pintarelli**, J. A. Berkenbrock, A. Rassele, M. M. M. Rangel & D. O. H. Suzuki.

Book chapters:

1. Electrochemotherapy Effectiveness Loss due to Electrode Bending: An *In silico and In vitro* Study. Springer IFMBE Proceedings, XXVII Brazilian Congress on Biomedical Engineering, 2022. D. L. L. S. de Andrade, J. R. da Silva, R. Guedert, **G. B. Pintarelli**, J. A. Berkenbrock, S. Achenbach & D. O. H. Suzuki.

2. Conductive Gels as a Tool for Electric Field Homogenization and Electroporation in Discontinuous Regions: *In Vitro* and *In Silico* Study. Springer IFMBE Proceedings, XXVII Brazilian Congress on Biomedical Engineering, 2022. L. Lopes, **G. B. Pintarelli** & D. O. H. Suzuki.

3. *Eletroquimioterapia. Manual Prático de Quimioterapia Antineoplásica em Cães e Gatos*, chapter 7, 2021. M. M. M. Rangel, D. O. H. Suzuki & **G. B. Pintarelli**.

4. Computational Study of Parameters of Needle Electrodes for Electrochemotherapy. Springer IFMBE Proceedings, 17th International Conference on Electrical Bioimpedance, 2020. J. R. Silva, R. Guedert, **G. B. Pintarelli** & D. O. H. Suzuki.

5. A Short Review of Membrane Models for Cells Electroporation. Springer IFMBE Proceedings, 17th International Conference on Electrical Bioimpedance, 2020. J. R. Silva, R. Guedert, **G. B. Pintarelli** & D. O. H. Suzuki.

6. Evaluation and Quantification of Electrode Arrangement Performance for Electrochemotherapy. Springer IFMBE Proceedings, XXVI Brazilian Congress on Biomedical Engineering, 2019. R. Guedert, **G. B. Pintarelli**, A. C. Antonio Jr. & D. O. H. Suzuki.

7. Electric Field Distribution and Electroporation in Discontinuous Regions Using Vegetal Model: *In Vitro* and *In Silico* Study. Springer IFMBE Proceedings, XXVI Brazilian Congress on Biomedical Engineering, 2019. A. B. Heyse, **G. B. Pintarelli** & D. O. H. Suzuki.

8. *Simulações de Distribuição de Campo e Corrente Elétrica em Tecidos Biológicos. As Engenharias frente a Sociedade, a Economia e o Meio Ambiente*, chapter 26, 2019. **G. B. Pintarelli**, A. C. Antonio Jr., R. Guedert, S. Cossul & D. O. H. Suzuki.

9. *Tratamento de Cânceres com Eletroquimioterapia. Novas Tecnologias Aplicada à Saúde: Desenvolvimento de Sistemas Dinâmicos - Conceitos, Aplicações e Utilização de Técnicas Inteligentes*, chapter 13, 2019 D. O. H. Suzuki, **G. B. Pintarelli**, L. C. Ramos, J. A. Berkenbrock & M. M. M. Rangel.

Intellectual property:

1. *Dispositivo de Aplicação de Campos Elétricos em Cavidades* (BR 10 2021 019917 2), 2021. **G. B. Pintarelli**, D. O. H. Suzuki., A. C. Antonio Jr., R. Guedert, D. L. L. S. Andrade, J. R. da Silva, L. B. Lopes, C. T. S. Ramos, J. V. Rosa & P. J. T. Pagano.

2. Electrochemotherapy Effectiveness Calculation V1.0 (BR 51 2019 000032 3), 2019. **G. B. Pintarelli**, R. Guedert, A. C. Antonio Jr. & D. O. H. Suzuki.

3. *Equipamento para aplicação de pulsos de tensão elétrica de amplitude, período e forma de onda variáveis e análise de efetividade para técnicas de eletroporação na transfecção genética e tratamento de neoplasias* (BR 10 2019 018097-8 A2), 2019. **G. B. Pintarelli**, A. C. Antonio Jr. & D. O. H. Suzuki.

LIST OF FIGURES

LIST OF ABBREVIATIONS AND ACRONYMS

Acronym	Description
AC	Alternating Current
BLM	Bilayer Lipid Membrane
DC	Direct Current
DUT	Device Under Testing
ECT	Electrochemotherapy
EP	Electroporation or Electropermeabilization
ESOPE	European Standard Operating Procedures of Electrochemotherapy
HVDC	High Voltage Direct Current (in the context of this thesis it is over 100 V_{DC} or 100 V_{RMS})
IGBT	Insulated-Gate Bipolar Transistor
IoT	Internet of Things
IRE	Irreversible Electroporation
MCU	Microcontroller
MOSFET	Metal Oxide Semiconductor Field Effect Transistor
PEF	Pulsed Electric Fields
STEM	Science, Technology, Engineering, and Mathematics
UFSC	*Universidade Federal de Santa Catarina*

LIST OF SYMBOLS

Symbol	Description	Unit
A ∥ B	Two Electrical Components ('A' and 'B') in Parallel	-
C_X	Capacitor 'X'	Farad (F)
$\vec{D}$	Electrical Induction or Electric Flow Density	C/m²
$\vec{E}$	Electric Field (Vector)	V/m
E	Electric Field Vector Absolute Value	V/m
$\vec{H}$	Magnetic field	A/m
I	Electric current	Ampère (A)
J	Electric Current Density	A/m²
J_c	Conductive Current Density	A/m²
J_d	Displacement Current Density	A/m²
Q	Energy	Joule (J)
R_X	Resistor 'X'	Ohm (Ω)
S	Area	m²
V	Electric potential	Volt (V)
V_m	Transmembrane Differential Voltage	Volt (V)
Y	Admittance ($Y = Z^{-1}$)	Siemens = 1/Ω
$Z_{W,V}$	Complex Impedance at a 'W' Frequency and 'V' Voltage Bias	Ohm (Ω)
$|Z|_{W,V}$	Impedance Absolute Value at a 'W' Frequency and 'V' Voltage Bias	Ohm (Ω)
$\angle Z_{W,V}$	Impedance Phase Angle at a 'W' Frequency and 'V' Voltage Bias	Degree (°)
j	$\sqrt{-1}$	-
q	Electric Charge	Coulomb (C)
r	Spherical Cell Radius	Metre (m)
t	Time	Segundos (s)
t_s	Rise time (from 10% to 90%)	s
t_d	Down time (from 10% to 90%)	s
ε	Electrical Permittivity	Farad/m (F/m) ou C²/N.m²
μ	Magnetic Permeability	Henry/m (H/m)
ρ	Volumetric Charge Density	C/m³
σ	Electric Conductivity	Siemens per metre (S/m)
∂A/∂t	Time derivate of 'A'	'A unit'/s
ℓ	Length	m
ω	Angular Frequency	rad/s

[blank page]

CONTENTS

1 INTRODUCTION

Dependence on energy in the form of electricity is the basis of our human beings and societies. Energy consumption is one of the indicators of a society's economic development, human well-being, and technological growth pace. Current scientifical studies of techniques, processes, and instruments will shape the new technologies of the future. In this thesis, we will discuss the Pulsed Electric Fields (PEF). PEF is a non-thermal electricity-based process to control cells. PEF applications require specific levels of electroporation control. We will concentrate on the sensing of electroporation using electrical measurements which can be used to study the phenomenon or to feedback and control electroporation systems. Briefly, the electroporation technique can improve or be an alternative to traditional medical and biotechnological methods. In some cases, electroporation delivers unique results with high added value or improves the quality of life. Electroporation is commonly used for gene transfer, cancer treatment, non-thermal pasteurization, and extracellular material extraction (MIKLAVCIC, 2016). Due to the SARS-CoV2 pandemic, there is also an active effort to use electroporation to enable mass DNA vaccination (WALTZ, 2021). Because of these reasons, the theme is promising and with a strong social impact. These motivate the development of this work.

The PEF and electroporation research area involve a wide field of professionals from Science, Technology, Engineering, and Mathematics (STEM), medical sciences, and biotechnology. Its research and professional practice have growing numbers (*i.e.*, papers, equipment, and professionals). However, the understanding of the 'electro'-pores physical mechanism of formation and expansion is not yet understood. Yet, the pore formation is the best hypothesis to explain the phenomenon and is currently supported by simulation of molecular dynamics at the atomic level (DELEMOTTE; TAREK, 2012) and molecular transport across membranes (KOTNIK; PUCIHAR; MIKLAVČIČ, 2010). Obtaining direct experimental evidence (*e.g.*, pore images) is still not possible due to pore dynamics being near nanoseconds and nanometres. Thus, there is still no 'absolute response' to the sensing of the electroporation occurrence, and because of that, electroporation is applied in an open loop, without feedback. Therefore, electroporation's requirements are typically specified as PEF signature, which depends on the biological characteristics and application.

Macroscopic electrical properties measurements can be used to indirectly sense electroporation. The intact cell membrane is dielectric, and the opening of pores by

electroporation, ion leakage and membrane destruction increases bulk conductivity. The conductivity increase due to electroporation was observed in high cell fraction suspensions of animal cells (KINOSITA; TSONG, 1979; PAVLIN *et al.*, 2005; SUZUKI *et al.*, 2011), bacteria (EMANUEL; ROMAN; CAHAN, 2019) and yeast (EL ZAKHEM *et al.*, 2006; RAMOS; FARIAS D., 2013), and tissues (CASTELLVÍ; MERCADAL; IVORRA, 2017; LANGUS *et al.*, 2016; NEAL *et al.*, 2012; SUÁREZ *et al.*, 2014). Electrical impedance spectroscopy and current-voltage acquisition (or electrodes current density) are used to sense media conductivity. Macroscopic electrical measurements can use the electrodes already used for PEF application, which facilitates implementation at sanitary controlled environments (BARBA *et al.*, 2015; BATISTA NAPOTNIK; MIKLAVČIČ, 2018; CASTELLVÍ; MERCADAL; IVORRA, 2017). Nevertheless, there are challenges to measure the 'real' electroporation electrical current as other effects as electrodes polarization can affect the measurement, and impedance analysis requires PEF interruption, which may be a limitation of those procedures (BATISTA NAPOTNIK; MIKLAVČIČ, 2018).

Besides the complexity of characterizing biological samples using sub-10 kHz measurements, the electroporation itself is not entirely understood. Thus, PEF systems usually do not have electroporation feedback because there is no adequate PEF probing method. Techniques and sensing electroporation in real-time[1] could benefit electroporation applications and dynamics understanding. The expected benefits are to improve safety and optimization of PEF, increase energy efficiency, reduce the thermal and electrochemical effect, and increase product or final treatment quality. In this thesis, we will evaluate a novel approach to sensing electroporation during its occurrence. We propose a sensing method and system, which can be ultimately extended to a cell's number or cell's uptake controlling method, in which the sample itself collaborates with the effect transduction (*i.e.*, bioelectronic sensing). Our sensing method is non-invasive and was implemented in parallel to the PEF signature, using the same application electrodes and overlapping the primary PEF protocol. A specific electric current signal can be used to investigate changes in the dielectric membrane of the cell in real-time and, thus, can be processed in a computerized electronic system to probe cell electroporation during the PEF and can feed a closed-loop control system. From the engineering point of view, reading electrical currents is practical and can be easily implemented. It is important to highlight that the tools and techniques proposed in this work

---

[1] A real-time system is a system which comply with a time requirement. This thesis will demonstrate that the sensing of a cell membrane may require up to microseconds and milliseconds wavelengths. Thus, suitable to meet time requirements.

can be integrated into the Internet of Things (IoT) systems or any other industrial instrumentation systems for systems integration and interoperability. Our studies use well-known engineering tools, such as computing electromagnetic wave distribution, power supply superposition, and independent component analysis of mixed signals. This thesis uses *in silico* and *in vitro* experimental activities (using a vegetal model and yeast). During the studies, we will execute electrical measurements, seeking to find correlations, mainly in electrical impedance, cell viability, current standards on electroporation levels and PEF protocol.

1.1 THESIS STRUCTURE

This thesis is divided into six chapters. Chapters 3 to 6 describes an independent study that supports the final objective.

Chapter 2: 'Theoretical Foundations' is an outline of PEF proceedings and our knowledge of how to sense electroporation using electrical measurements.

Chapter 3: 'Impedance Sensing and PEF System' describes the system and techniques implementation to measure impedance during PEF protocol. Those methods will be used in further chapters.

Chapter 4: 'Sensing of Yeast Inactivation by Electroporation' describes an *in vitro* study using electrical measurements, electronic microscopy, and cell viability used to access the yeast irreversible electroporation.

Chapter 5: 'Dielectric Dispersion Modulated Sensing of Yeast Suspension Electroporation' describes a theoretical study to show the impact of electroporation and its buffers at the biological system frequency response.

Chapter 6: 'Sensing the Dynamics of Complex Electrical Properties under PEF: *In vitro* vegetal study' describes the use of a sinusoidal signal superposition the primary electropermeabilization protocol to access the membrane state.

1.2 OBJECTIVES

We aim to develop a sensing method for electroporation based on impedance measurements and analysis during the PEF protocol. In particular, use the current reading of the protocol itself to get feedback on the treatment. Ultimately the proposed sensing methods

can be used to better understand (*e.g.* modelling) and control electroporation. We have two lines of study within the proposed thesis: (i) The computational model, which is important for making calculations from absolute properties of materials to equivalent properties. We prefer to use the finite element tool and not analytical methods because the biological systems have complex geometry, which can make analytical calculation unfeasible. (ii) The *in vitro* study with vegetal tissue and yeast, which is where the biological data and current and voltage data will be extracted. Our main objective contemplates some specific goals:

1. Develop computer models of biological cells and tissues;

2. Perform computer simulations to identify frequency response due to passive electrical properties and geometry;

3. Develop electronics for switching electrical voltage compatible with PEF;

4. Develop configuration of electrodes for the production of electric fields of the order of tens to hundreds of kilovolts per meter compatible with PEF;

5. Develop a method and circuit for acquiring voltage and current compatible with the switching circuit developed;

6. Apply methods for analysing electrical properties before, during, and after electroporation treatments;

7. Prepare biological samples. Potato tuber for tissue study and *Saccharomyces Cerevisiae* yeast for cell suspension studies;

8. Conduct experiments related to cell integrity using compatible microscopes and methods;

9. Conduct experiments, applying electric fields pulsed using *in vitro* biological media.

2 THEORETICAL FOUNDATION

In this chapter, we will focus on detailing the specific applied background to this thesis, which is an overview of pulsed electric fields, characterization of biological materials by impedance, cell sensing, and β-dispersion. We must note that the electroporation topic involves areas of electromagnetism, circuits, power electronics, and biology. We recently discussed the history of electroporation, pore formation theories, applied bioelectromagnetism, ionic currents, effects of current passage in a biological system, PEF power electronics, and electroporation applications (PINTARELLI, G. B. *et al.*, 2019; PINTARELLI, 2018; SUZUKI *et al.*, 2019). We also observe that multiple authors carried out extensive reviews of the electroporation (CHEN *et al.*, 2006; JIANG; DAVALOS; BISCHOF, 2015; MIKLAVČIČ; PUC, 2006; MISHRA, 2008; WEAVER; CHIZMADZHEV, 1996) and books that contemplate the theme (CHANG, 1992; ESCOBAR-CHÁVEZ *et al.*, 2012; JARM; KRAMAR, 2016; JORDAN; NEUMANN; SOWERS, 1989; PAKHOMOV; MARKOV; MIKLAVČIČ, 2010; RUBINSKY, 2010; ZIMMERMANN; NEIL, 1996).

2.1 OVERVIEW OF PULSED ELECTRIC FIELDS FOR ELECTROPORATION

Pulsed Electric Fields (PEF) treatment is a non-thermal electricity-based method to control biological cells in different media. PEF results depend on biological conditions and pulse parameters. The PEF approach can be configured mainly based on the combination of pulse amplitudes, pulse durations, and pulse repetitions, which is also called PEF signature. Usually, high amplitude (tens to hundreds of kV/m), short duration (usually 100 μs duration), and rectangular PEF are used for electroporation. If PEF is configured as low amplitude and long duration (tens of kV/m and tens milliseconds), it is possible to primarily cause electrolysis which may induce chemical ablation (KLEIN *et al.*, 2020; WEAVER *et al.*, 2012).

Electroporation can arise as reversible or irreversible which is mostly dependent on the PEF amplitude. If operating at reversible electroporation, it is desired to enable cell membrane recovery after PEF. Reversible electroporation facilitates mass transport through the cell membrane and can improve chemotherapy (known as electrochemotherapy) (GEHL *et al.*, 2018) and *in vivo* (DNA vaccines), and *in vitro* gene electro transfer (ROSAZZA *et al.*, 2016). The current standard for clinical cancer treatment using electrochemotherapy is eight

100 μs duration, 110 to 120 kV/m, and a rectangular pulse train (GEHL *et al.*, 2018); This protocol is part of the European Standard Operating Procedures for Electrochemotherapy and Electrogenetherapy (ESOPE). ESOPE also provide guidelines for equipment and surgical procedures. Similar procedures are also widely used at the veterinary practice (RANGEL *et al.*, 2019). The 110 to 120 kV/m range is designed for reversible electroporation of most animal cells. Yet, it is expected to have some irreversible electroporation (COROVIC *et al.*, 2013; PINTARELLI, G.B. *et al.*, 2019). In gene electro transfer, electroporation systems are optimized depending on the cell, and often manufacturers provide a 'ready to use' protocol, depending on the tissue or cell and molecule to be uptake[2] (POTTER; HELLER, 2018; ZAMPAGLIONE *et al.*, 2005). Irreversible electroporation causes excessive damage which disrupts cell homeostasis and provokes cell death. The irreversible electroporation can directly treat the neoplasm (LV *et al.*, 2019) and preserve food (as can be used for eliminating bacteria and yeast) (GOLBERG; FISCHER; RUBINSKY, 2010; SALE; HAMILTON, 1967; TOEPFL; HEINZ; KNORR, 2007). The irreversible electroporation cancer treatment (IRE) usually uses bursts of 100 pulses, few to hundreds of μs duration, 120 kV/m and higher protocols (CASTELLVÍ *et al.*, 2018; JIANG; DAVALOS; BISCHOF, 2015). In industrial systems it is possible to use irreversible electroporation for pasteurization of wine and beer, and intracellular material extraction; those systems usually continuously switch tens of kV and produce up to hundreds to thousands kV/m in a flow process (GANEVA; GALUTZOV; TEISSIÉ, 2003; KEMPKES, 2017).

PEF equipment contains a high voltage waveform generator and uses applied metallic parts, *i.e.*, electrodes, to transfer the pulsed energy to the biological media. The generator uses high power pulse technology (REDONDO, 2017; SUZUKI *et al.*, 2019); This approach uses a conversion-storage-conversion system: (i) First step is the conversion of energy from a source low voltage and low power density primary (*e.g.*, conventional AC mains or battery) to high voltage; (ii) The second step is temporary internal storage of the converted energy, usually made with capacitors; (iii) Finally, the stored energy is converted and quickly delivered to the load in a pulsed at high voltage and high-power density. Sometimes the PEF generator is referred as 'electroporator'. There are several commercial PEF systems. The cancer treatment clinical equipment are: Cliniporator (IGEA, Carpi, Italy) and NanoKnife (AngioDynamics Inc, New York, USA). The current DNA vaccine equipment

---

[2] Gene eletrotransfer systems usually include an electroporation buffer and programed higher rectangular electroporation pulse followed by other lower voltage to steer molecules into the cell by electrophoresis.

under clinical trial is the Cellectra (Inovio Pharmaceuticals, Pennsylvania, USA). Some of the veterinary equipment are: OnkoDisruptor (Biopulse Biotech, Naples, Italy), ElectroVet EZ and S13 (Leroy Biotech, St-Orens-de-Gameville, France) and VetCP 125 (Implastic, São Paulo, Brazil). Some of the laboratorial equipment are: ECM630 and CytoPulse family (BTX Harvard Apparatus, SanDiego, California, USA), Neon Electroporation System (Invitrogen/ThermoFisher Scientific, Waltham, MA, USA) and MicroPulser electroporator (Bio-Rad, California, USA). Some of industrial equipment are: ELEA (Quakenbrück, Germany), ScandiNova (Uppsala, Sweden) and PulseMaster (Hapert, Netherlands).

PEF temporarily provokes excessive accumulation of transmembrane ionic charges. The transmembrane potentials (V_m) are reported to be 0.2 to 1 V for reversible electroporation (SUZUKI *et al.*, 2011) and above 1 V for irreversible electroporation (GOLBERG; FISCHER; RUBINSKY, 2010). The maximum V_m for a spherical cell of radius r is approximately determined by the steady-state Schwan equation $1.5 \times r \times E$, where E is the PEF amplitude (KOTNIK *et al.*, 2012) [3]. The electroporation theory is based on formation of nano-pores in the cell membrane due to excessive accumulation of transmembrane ionic charges. Pore hypothesis evidence is given by measurements showing the increase in ionic permeability due to PEF. Pore creation and expansion is described to change the membrane electrical properties (*e.g.*, electrical conductivity) (ZHUANG; KOLB, 2015). The pore number can be described by the Smoluchowski equation (MESCIA *et al.*, 2018). The membrane changes affect the macroscopic scale electrical properties, which can be modeled using a macroscopic current. This concept is mostly used to describe PEF tissue response, which enables the pre-treatment of PEF-based cancer therapies (KOTNIK *et al.*, 2019; ZHAO *et al.*, 2018) (this topic will continue in section 2.5).

2.2 FROM ELECTRICAL PROPERTIES TO EQUIVALENT CIRCUIT

If we have a cylinder 'A', with certain values of conductivity σ, permittivity ε, and a time-harmonic voltage ($V = V_0 e^{j\omega t}$, and an electric field equal to $E = V/\ell$), an electrical current I will flow, as shown in Figure 1a. The S is the base area and ℓ the cylinder length. The conductive part creates a conductive current density ($J_c = \sigma E$), and the reactive part creates a

---

[3] Maximum V_m occour at cells poles θ = 0° and θ = 180°. Where θ is the angle measured from the center of the cell with respect to the direction of the field. The full equation is $1.5 \times r \times E \times \cos(\Theta)$.

displacement current density[4] ($J_d = d(\varepsilon E)/dt = j\omega\varepsilon E$) (BASTOS; SADOWSKI, 2017-). We can disregard inductance as the magnetic permeability (μ) is not expressive in dielectrics such as biological materials (GRIMNES; MARTINSEN, 2014). Hence, the total expected current is J (Equation (1)). When moving to the volumetric approach, we integrate the J over the entire surface cylinder base (with the S area); thus, we can calculate the I current (Equation (2)). The I is the sample electrical current (which can be read externally and macroscopically) due to an externally generated V. We observe that the time-harmonic assumption, *i.e.*, all vector fields are periodic in time, is important to further usage of Fourier transform to analyse mixed signals (OPPENHEIN; WILLSKY; NAWAB, 1996).

$$J = J_c + J_d = \sigma E + j\omega\varepsilon E = (\sigma + j\omega\varepsilon)\frac{V}{\ell} \tag{1}$$

$$I = \int_S J = (\sigma + j\omega\varepsilon)\frac{VS}{\ell} \tag{2}$$

Figure 1 – (a) Hypothetical homogeneous nondispersive cylinder 'A' with a voltage difference V being applied. (b) Electrical circuits approach to the homogeneous cylinder (parallel model).
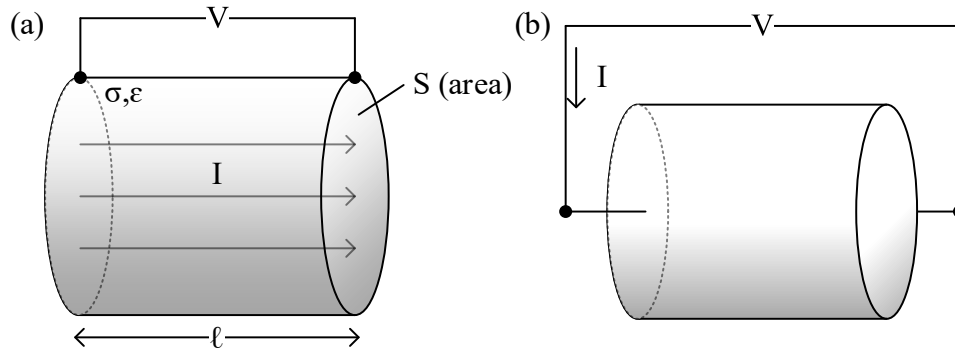
Source: Autor.

The current I through Figure 1a can also be calculated using the electrical circuits approach. Therefore, a resistance ($R = \ell/(\sigma S)$) parallel to a capacitor ($C = \varepsilon S/\ell$) can model the dielectric cylinder as Figure 1b (parallel model). By using Kirchhoff's laws, the total I is the

---

[4] The displacement current ($d\mathrm{D}/dt$ or $d(\varepsilon E)/dt$) is a Maxwell's concept, which is not a 'real current' but the change of electric field in the dielectric material. The displacement current is sometimes not considered depending on the PEF study. $J_d = d\mathrm{D}/dt = d(\varepsilon E)/dt$.

net sum of the resistor (I_R = V/R) and capacitor current (I_C = C ∂V/∂t) as Equation (3), which gives the same result as Equation (2).

$$I = I_R + I_C = \frac{V}{R} + C\frac{dV}{dt} = \frac{V}{R} + j\omega CV_0 e^{j\omega t}$$

$$\text{Thus, } I = \frac{\sigma VS}{\ell} + \frac{j\omega\varepsilon VS}{\ell} = (\sigma + j\omega\varepsilon)\frac{VS}{\ell} = \text{Equation (2)}$$

(3)

If we have the Figure 2a, dispersive cylinder 'B' with heterogeneous electrical characteristics, *i.e.* a conductive σ and a capacitive ε part, a counter displacement electric field E_c will exist. The conductive element will have a conductive current density ($J = J_c = \sigma\Delta E$), and the capacitive part will have a displacement current density ($J = J_d = j\omega\varepsilon E_c$). Hence, the total expected current is J (Equation (4)). Integrating the J over the S area, we calculate the I current (Equation (5)).

$$J = J_c = \sigma(E - E_c) = \sigma\left(\frac{V}{\ell} - \frac{J}{j\omega\varepsilon}\right)$$

$$\text{Thus, } J = \left(\frac{j\omega\varepsilon\sigma}{j\omega\varepsilon+\sigma}\right)\frac{V}{\ell} = \left(\frac{1}{\frac{1}{\sigma}+\frac{1}{j\omega\varepsilon}}\right)\frac{V}{\ell}$$

(4)

$$I = \int_S J = \left(\frac{1}{\frac{1}{\sigma} + \frac{1}{j\omega\varepsilon}}\right)\frac{VS}{\ell}$$

(5)

Figure 2 – (a) Hypothetical non-homogeneous dispersive cylinder with a voltage difference V being applied (b) Electrical circuits approach to cylinder 'B' (series model).
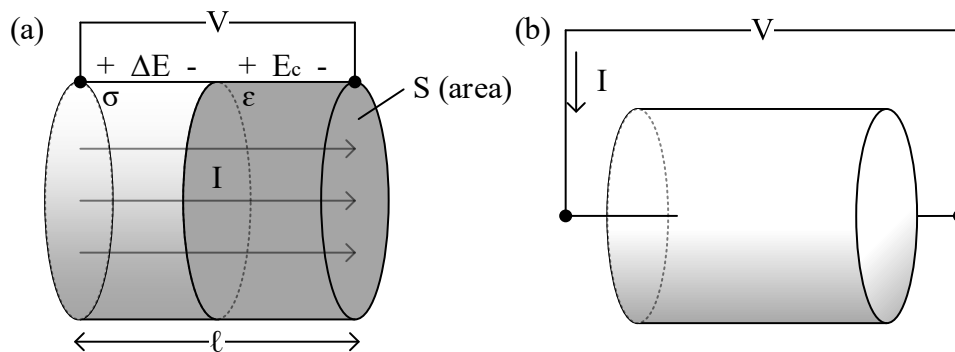
Source: Autor.

Using the electrical circuits approach, we model the dispersive cylinder as Figure 2b (series model) and the total I is as Equation (6), which gives the same result as Equation (5).

$$I = \frac{V}{Z}, \text{ where Z is the total impedance, } i.e., Z = R + X_c, \text{ and } X_c = \frac{-j}{\omega C}$$

$$\text{Thus, } I = \frac{V}{R - \frac{j}{\omega C}} = \frac{V}{\frac{\ell}{\sigma S} - \frac{j\ell}{\omega \varepsilon S}} = \left(\frac{1}{\frac{1}{\sigma} + \frac{1}{j\omega\varepsilon}}\right) \frac{VS}{\ell} = \text{Equation (5)}$$

(6)

The cylinder of Figure 1 frequency response or admittance ($Y1(\omega) = I/V = 1/Z$) is as Equation (7). The capacitor provides means (displacement field) for high-frequency current passage, thus, acting as a short circuit at high frequencies. The cylinder of Figure 1 can be called nondispersive as ε and σ are constants. Figure 2 cylinder frequency response ($Y2(\omega)$) is as Equation (8). This system has a pole at σ/ε; thus, it is a first-order high pass filter with the -3 dB cut frequency at this frequency. The cylinder of Figure 2 can be called dispersive as ε and σ are not constants in its axis which is the. current direction. Figure 3 shows the frequency response of both hypothetical cylinders.

$$Y1(\omega) = (\sigma + j\omega\varepsilon)K, \text{ where } K = \frac{S}{\ell} \tag{7}$$

$$Y2(\omega) = \left(\frac{1}{\frac{1}{\sigma} + \frac{1}{j\omega\varepsilon}}\right) K = \left(\frac{j\omega\sigma\varepsilon}{\sigma + j\omega\varepsilon}\right) K \tag{8}$$

Figure 3 – The frequency response of cylinders of (a) Figure 1 and (b) Figure 2. The lowest value of (b) is '1'. Variables are $\varepsilon = \sigma = K = 1$.
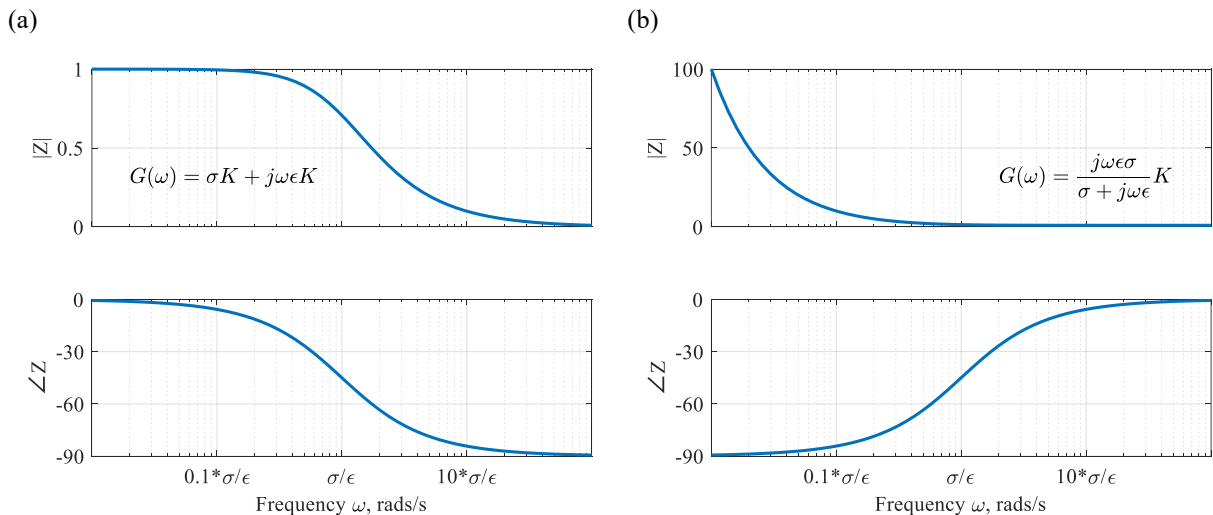
Source: Autor.

The two components' arrangements presented (the resistor and capacitor; both series and parallel) are the basis for understanding the electrical properties and modelling of biological media. The simplest biological model contains a parallel capacitor and resistor as Figure 1b. However, the two components modelling diverge if representing the bottom end (near DC frequency) or the high frequency. Hence, more elements can be included to describe the sample's impedance better and represent the biological states. For instance, we can combine Figure 1 and Figure 2, *i.e.* four-element circuit as Figure 4a (this circuit is also known as a single dispersion Debye circuit model) (GRIMNES; MARTINSEN, 2014). Where, the C_β describes the insulating cells membranes; thus R_β-C_β dispersive branch is the electrical path across the membranes (β-dispersion); The C_∞ can represent the polarization of water molecules at GHz; And the R_s is the sample's static conductivity (CASTELLVÍ, 2014; GRIMNES; MARTINSEN, 2014; RAMOS; SUZUKI, 2017). Figure 4b shows the four-element model circuit response. The low frequency cannot pass through the capacitive membrane (C_β); thus, its passage is through the intercellular media (R_s). The 100 kHz and over frequencies can pass through C_β; therefore, the total equivalent impedance is lower (MA; SOLEIMANI, 2020; ROY *et al.*, 2020). Figure 4b combined circuit model helps the understanding of this thesis as it has a main dispersion (at approximately 20 kHz). A dielectric dispersion is defined as the variation in the equivalent permittivity ε of a material due to the frequency. A dispersion exists due relaxation or resonance at the sample. The conductivity σ also changes at a dispersion, as σ and ε are dependent. A dispersion can be described by an RC series branch. The cell membrane (which this thesis aims to sense) has its dispersion between 100 Hz to 1 MHz. Figure 5 depicts the current paths at low and high frequency at biological media. The low-frequency paths are more perturbed than at high frequencies due to cell membranes. Thus, electrical current flow is lower at lower frequencies.

Figure 4 – (a) A biological tissue model, containing a branch with a 'static' R_s and parasitic capacitance C_∞, and a branch simulating a single β-dispersion (R_β and C_β). This is the combined model. (b) Its impedance spectrum. For this example, we used $C_\infty = 1$ ηF, $R_s = 10$ Ω, $C_\beta = 1$ μF and $R_\beta = 5$ Ω.
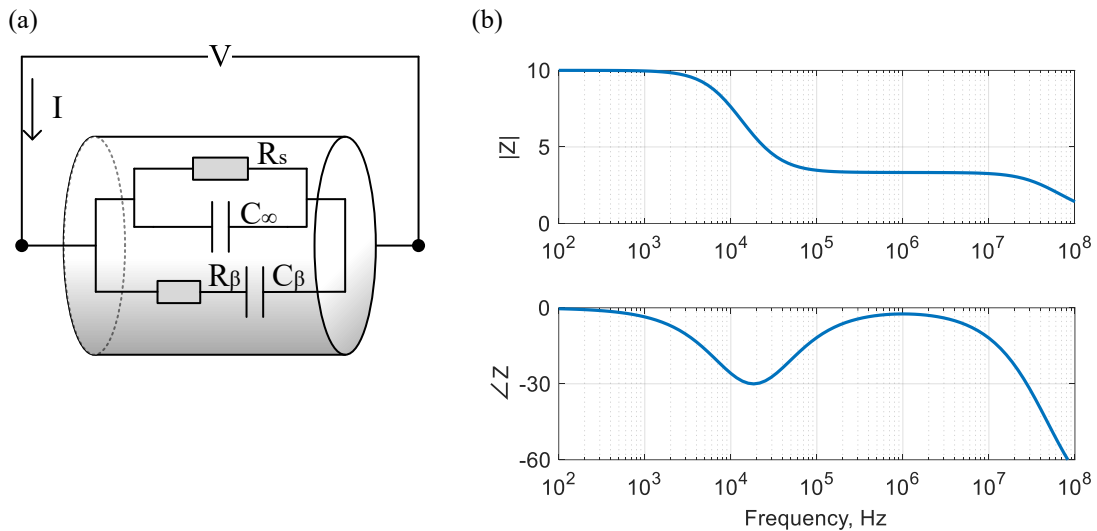
Source: Autor.

Figure 5 – Illustration of the current passage in (a) suspended cells (yeast) and (b) cells in a tissue (potato tissue). The (b) blue stain is methylene blue, showing the potato tissue cell barrier.
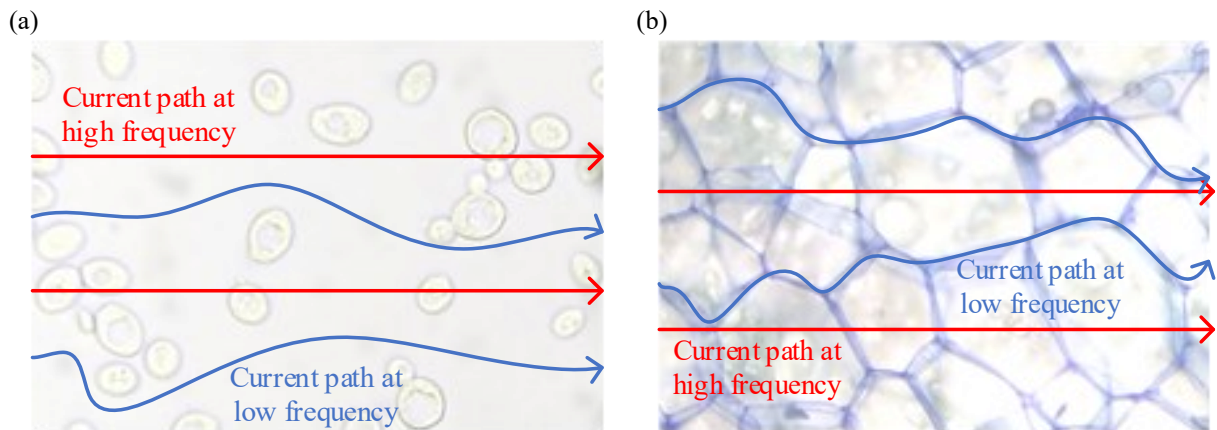
Source: Author.

2.3 SENSING OF BIOLOGICAL MATERIALS BY IMPEDANCE

The biological media are mainly conductive aqueous electrolytes separated by thin dielectric cell membranes with active channels. Therefore, biological systems are extremely

heterogeneous concerning their passive electrical properties[5] and have a non-linear electrical interaction mechanism[6]. The impedance spectroscopy is a common technique for analysing heterogeneous systems, and it indirectly contains information about the biological aspects. Electrical impedance is defined as the ability of a material to restrain and delay the electric current passage and its electromagnetic fields, which are consequences of Maxwell's equations. If the material is a biological material, we can refer to its passive electrical properties as bioimpedance (GRIMNES; MARTINSEN, 2014). We will describe the biological materials using conductivity σ and relative permittivity ε_r ($\varepsilon_r = \varepsilon/\varepsilon_0$) which is the most common procedure in this thesis area. Some authors use σ and ε as part of a single complex variable (called complex dielectric constant or complex permittivity, which is equal to $\varepsilon(\omega) - j \cdot \sigma(\omega)/\omega$) or even use a similarly complex conductivity. The magnetic permeability (μ) is not studied as it is not expressive in dielectrics such as biological materials. We will use the term impedance (and not bioimpedance) because we will study electrical response of the whole biological material, rather than the individual electrical properties. Using impedance to assess cell status is practical, as it is easy to use and flexible for systems design and biosensors fabrication. Impedance systems are non-invasive as they can use external electrodes; compatible with real-time control systems as measurements can accomplish time requirements; scalable as materials can be described per length (*e.g.,* conductivity is S/m and permittivity is F/m); low cost when compared to microscopy and chemical techniques; and, portable as it can be embedded with other electronic systems. During impedance sensing, the electrical response of the system or cell's dielectric properties can be determined by measuring the system response to frequency-dependent excitation signals (MORGAN *et al.*, 2007).

The biological systems have a characteristic impedance 'feature', which is the main interferences or dielectric changes (termed α, β-, and γ-dispersions) due to electromagnetic field frequency ω. Those three dispersions are originated from the electrical polarization delay (also called dielectric relaxation) that occurs in three different regions/levels of the system (*i.e.* atmosphere around the cells, cell membrane interfaces, and molecule level). We observe that the polarization delay is given in the time domain, and it is called relaxation, which can be transposed to the frequency domain, so-called dispersion. Those are major caused by the

---

[5] We refer to the polarization and relaxation mechanisms, *i.e.*, dispersions, and orientation dependent properties (anisotropy).
[6] We refer to active membrane responses, heating conductivity changes, and electroporation.

cell membrane transport, ionic diffusion processes and gap junctions (α-dispersion, centred at approximately 100 Hz), cell membranes interfacial polarization[7] (β-dispersion, centred at approximately 100 kHz), and ions and molecules mobility through water (γ-dispersion, centred at approximately 10 GHz). The approximate centre locations of the dispersions, *i.e.* changes in the equivalent conductivity $\sigma(\omega)$ and permittivity $\varepsilon(\omega)$, are also shown in Figure 6a (HEILEMAN; DAOUD; TABRIZIAN, 2013; SCHWAN, 1957, 1963). A comparable circuit model can describe those as Figure 6b, where each of the RC branches represents a dispersion (RAMOS; SUZUKI, 2017).

Figure 6 – (a) Conductivity and permittivity spectrum of a biological sample. The α, β, and γ are distinctive dispersions which occur approximately at 100 Hz, 100k and 10 GHz. (b) Equivalent circuit model of a biological sample containing all the dispersions.
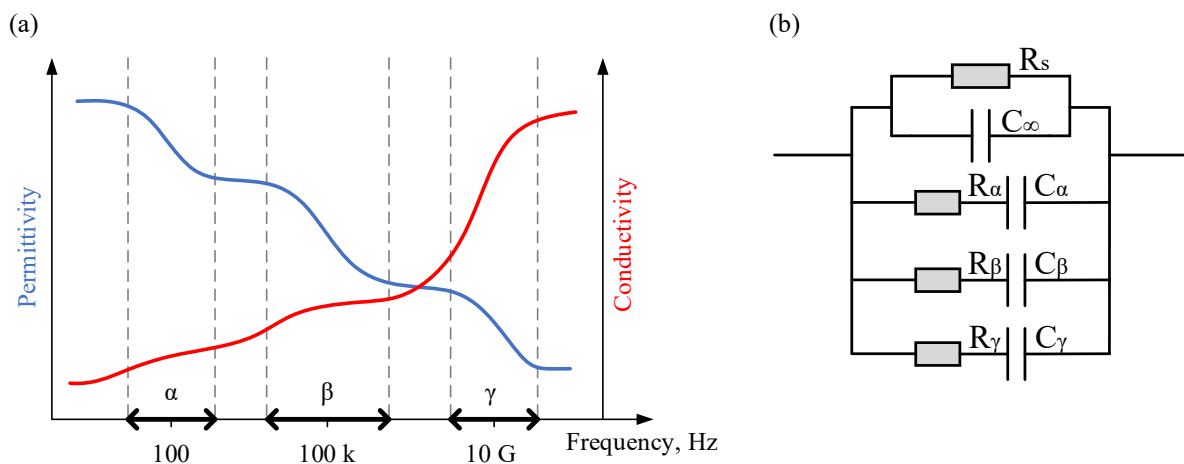
Source: (a) Adapted from (HEILEMAN; DAOUD; TABRIZIAN, 2013; SCHWAN, 1957, 1963); (b) Adapted from (RAMOS; SUZUKI, 2017).

Currently, few Hz to 1 GHz spectrum is used for monitoring cell suspensions and tissues, and the β-dispersions changes are especially interesting for biosensor development, as the alterations foremost explain them in the intrinsic capacitive characteristic of the membrane and electrolyte group (*i.e.* cytoplasm and external environment) (HEILEMAN; DAOUD; TABRIZIAN, 2013; SCHWAN, 1957). At cell suspension level, β-dispersions can be used for evaluating cell concentration, growth phases, cell size, the effect of biotic and abiotic factors, membrane organization and cell behaviour (FLORES-COSÍO *et al.*, 2020). At the tissue level, they can be used for characterizing tissues, anomalies (*e.g.* cancer), the pathological status of patients and structure deterioration (ADLER; BOYLE, 2017; IBBA *et*

---

[7] The heterogeneity of layered or inhomogeneous dielectrics are responsible for creating the interfacial polarization. This effect is also called the Maxwell-Wagner effect.

al., 2020). If we use specific β-dispersion's frequency range signals, we can incorporate α into the static components (R_s and $C_∞$) and β into dispersive branch ($R_β$ and $C_β$) as the circuit of Figure 4a.

There are some challenges related to sensing the biological media, for instance, the formation of double layers (also called diffuse layers) are reported as the leading cause of low frequency dispersion. Electrical double layers may be measured in terms of how far its electrostatic effect persists. This length is called Debye length (HÜCKEL, 1924). There are two locations suitable to accumulate ions and charged molecules. The first is the interface solution-electrodes (*i.e.* electrodes polarization), which is usually modelled as a series impedance[8] (C_{DL} and R_{DL}) as Figure 7. The second is the cells itself; their charges attract ions and charged molecules to their interfaces (α-dispersion). The double-layer effect may impose a parasitic voltage drop which partially shields the electric field at the cells. Also, the low frequency dispersion may affect the β-dispersion as whole spectrum is 'connected' (DI BIASIO; AMBROSONE; CAMETTI, 2010; RIOU *et al.*, 2014; SCHWAN, 1963; ZHANG; ZHAO, 2009). Double layer interference is expected for frequencies lower than approximately 100 kHz (ISHAI *et al.*, 2013), and frequencies less than 10 kHz are generally discarded because of this interference. On the other hand, there is an upper limit to sense cells, as above approximately 10 MHz, the cells membrane are conductors; thus, cells become 'electrically invisible' (see Figure 5). Therefore, if the sense is based on membrane dispersion, the optimized range is 10 kHz to 1 MHz (ARNDT *et al.*, 2004; GOWRISHANKAR; WEAVER, 2003; XU *et al.*, 2016). Despite the sensing level (*i.e.* tissues or cells level), it is possible to describe the biological media as an equivalent circuit model. If studying cell suspensions, it is possible also to consider the effects of the medium, since it can also conduct electrical current (HOLMES *et al.*, 2009; MORGAN *et al.*, 2007; SUN; GREEN; MORGAN, 2008; XU *et al.*, 2016).

We note that some instrumentation techniques are used to mitigate unwanted effects: (i) 4-point probe measurement can mitigate the dispersion due to solution-electrodes interface; (ii) characterization of system's series inductance and parallel capacitance and its further compensation can mitigate parasite effects; (iii) the chamber/cell constant compensation can mitigate chamber fringe effect[9] due to electrode format or high measurement frequency (over

---

[8] When modelling electric double layer at micro devices, C_{DL} and R_{DL} may be used in parallel with the sample as the diffuse layer spreads to a wide range.
[9] Fringe effect is the electric field spreading to a larger space and affecting the neighbouring area.

1 MHz) (LAUFER *et al.*, 2010; MA; SU; NATHAN, 2015; RHOADES; VAN SCHILFGAARDE, 1976; YANG, 2010).

Figure 7 – Parallel electrodes with a sample and a signal source. The single dispersion equivalent circuit (R_s and C_∞ are the static resistance and capacitance of the model and R_β-C_β the dispersive branch). The R_{DL} and C_{DL} are the equivalent circuits composed by resistance and capacitance of the electric double layer effect (or polarization). The R_{DL} and C_{DL} are shown only on the left electrode, which is a sum of both (left and right) polarization $R_{DL}/2$ and $C_{DL}/2$.
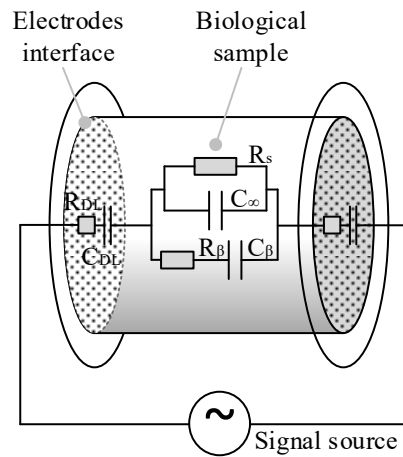
Source: Author.

2.4 ELECTRIC CURRENT IMPACTS ON BIOLOGICAL MEDIA

Biological media are electrolytes, also called 'ionic conductors'. The electrolytes are aqueous media containing ions, which can be created by dissociation or ionization. The diluted ions are susceptible to move according to the electric field. The ionic current is the sum of ionic conduction current (*i.e.* ionic displacement due to electric potential gradient) and ionic diffusion current (*i.e.* ionic displacement due to concentration gradient). The electrolyte conduction mechanism is different from the electric materials, which the electric current is due to the flow of free electrons (*i.e.* electron displacement current) (GRIMNES; MARTINSEN, 2014).

All cells have an idling physiological transmembrane potential V_m (*i.e.* potential difference between cell's inside-outside) which they are naturally being regulated due to transport structures (*i.e.* channels and ionic pumps). The V_m is held by the cell membrane, which generally prevents the passage of charges (*i.e.* ions and molecules). If the cell is

immersed in an exogenous electric field, ions approach the cell membrane (in the extracellular medium and the intracellular medium); thus, the induction of transmembrane potential V_m occurs, *i.e.* stimulus or electroporation (GRIMNES; MARTINSEN, 2014).

The PEF desired outcome is electro-manipulation (*i.e.* electroporation, electrofusion and electrotransformation/electrodeformation). However, there are some PEF intrinsic (and usually undesired) impacts. Those can change the physical state and the sample electrical characteristics. This fact can difficult individual electro-manipulation. There are three types of intrinsic PEF effects: electrokinetics, electrochemical and joule heating.

- The electrokinetics is related to cell suspensions, and it can be electrodeformation or dielectrophoresis (*e.g.* electro-orientation). Electrodeformation is reported using sub-millisecond PEF at giant cells (*e.g.* cell transient ellipsoidal shape deformation) (RISKE; DIMOVA, 2005), and electro-orientation is reported in dipole charged cells exposed to over hundreds of milliseconds PEF (*e.g.* yeast alignment in pearl chains) and strong non-homogeneous electric field (*e.g.* microdevice cell sorting) (VOLDMAN, 2006).

- The electrochemical electrolytic processes are a consequence of the interface of the electrolyte-electrode conduction mechanism. There are two processes: the electrolysis of the medium water[10] and its chlorides[11] and dissolution of the electrodes alloying metals (*e.g.* iron, chrome, nickel, and aluminium). Electrolysis of the medium can cause a electrical double layer, pH gradients and bubbles near the electrodes. PEF over milliseconds range is likely to have strong electrolytic effects which can be harmful to cells and interfere with electroporation (RUBINSKY *et al.*, 2016). Typically, an unstable electric double layer is formed after few microseconds, and a stable double layer is formed after tens of milliseconds (SHIMIZU *et al.*, 2006). Bubbles are usually a concern if gases overcome the solution dissociation factor, which is more common at the micro and nanoscale. The bubbles provoke diffraction of the electric field. Mitigating the electrode-solution double layer effects is a challenge in the PEF application and sense, as a capacitor can represent it in series with the sample (see Figure 7). The usage of alternating current (*e.g.* bipolar rectangular pulses) and low conductivity mediums are known to reduce electrolysis (KOTNIK;

---

[10] Releases oxygen (O_2), hydrogen (H_2), hydrogen ions ($H+$) and hydroxyl ions ($OH-$).
[11] Releases chlorine gas (Cl_2).

MIKLAVČIČ; MIR, 2001; SAULIS *et al.*, 2005). PEF metal electrodes dissociation usually is lessened using stainless-steel electrodes (yet, the iron part may dissolve) (TOMOV; TSONEVA, 2000). We observe that Ag/AgCl electrodes are non-polarizable electrodes and are widely used in the clinical (*e.g.* ECG, EMG and EEG) and electrophysiology measurements (*e.g.* patch clamp equipment). However, stainless steel is mostly used with PEF since it is resistant with most aggressive chemical reagents and high DC current stress.

- The electrical current thermally stresses the media (*i.e.* joule effect). The cell membrane is sensitive to temperature, and temperature changes can change the rigidity of the membrane and its electrical properties. Over 42 ℃ seconds exposure is known to be harmful to cells. Moreover, the ion mobility is affected by the temperature (thus, change its electrical properties). Temperature rise is reported for long burst and low pulse inter pause PEF protocol and electrodes with sharp edges (DAVALOS; RUBINSKY, 2008). The temperature rise (ΔT) can be estimated using $\Delta T = EF^2 t\sigma/c$, where EF is the absolute value of the PEF, t is the PEF duration, σ the media conductivity and c is the specific heat at constant pressure (this equation assumes homogeneous electric field, resistive sample, all energy being converted into heat homogeneously, no heat dissipation and solution density of 1 kg/L).

2.5 ASSESSMENT OF ELECTROPORATION USING ELECTRICAL MEASUREMENTS

Electroporation pores occur in the order of nanoseconds and nanometres. Currently, there is no established method for direct pores imaging (direct electroporation sensing). There is an attempt on photographing electro-pores using rapid-freezing and electron microscopy (CHANG; REESE, 1990). However, the observations have some criticism, as the electron microscopy processing methods interfere within the sample. The molecular models and molecular transport across membranes play a role in explaining pore dynamics (DELEMOTTE; TAREK, 2012; FERNÁNDEZ; RISK, 2017; KOTNIK; PUCIHAR; MIKLAVČIČ, 2010; WEAVER; VERNIER, 2017). Electroporation can be evaluated indirectly with the import of exogenous molecules, leakage of cell components or physical and chemical methods (*e.g.* electrical properties, voltage clamp and cell swelling) (BATISTA NAPOTNIK; MIKLAVČIČ, 2018).

Macroscopic electrical properties measurements can be a quick and minimally invasive way to indirectly monitor the 'poration'. The intact cell membrane is dielectric, and the opening of pores by electroporation causes a decrease in the membrane's electrical resistance. Moreover, leakage of intracellular ions may occur or complete cell membrane destruction. We note that cell death is expected if operating irreversible electroporation. Intracellular ion leakage and membrane destruction can contribute to increasing the macroscopic conductivity. There are two main sensing approaches, measuring before and after the pulse (by using electrical impedance spectroscopy) or during an electroporation pulse (by current-voltage acquisition or electrodes current density). Macroscopic electrical measurements may take advantage of using the PEF-electrodes themselves, which facilitates implementation at sanitary controlled environments (BARBA *et al.*, 2015; BATISTA NAPOTNIK; MIKLAVČIČ, 2018; CASTELLVÍ; MERCADAL; IVORRA, 2017) without the need of extra equipment contacting the sample (SIMONIS; GARJONYTE; STIRKE, 2020). The basic experimental setup for measuring electrical properties is shown in Figure 8.

Figure 8 – Basic setup for measuring electrical properties of electroporation. Instantaneous voltage and current are measured with an oscilloscope or compatible equipment. Impedance analyser measures impedance before and after EP protocol.
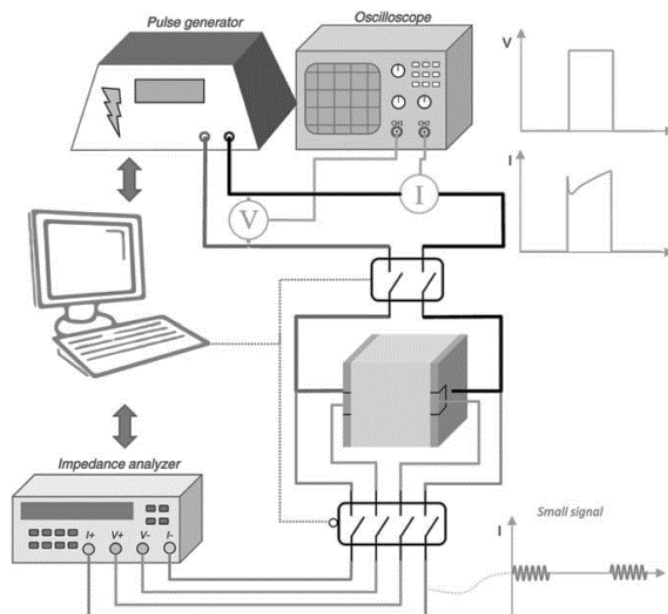
Source: (CASTELLVÍ; MERCADAL; IVORRA, 2017).

Analysis by electrical impedance spectroscopy may provide a wide range of information. The optimal cell sensing frequency range is between 100 Hz to 100 kHz

(ARNDT *et al.*, 2004; KRINKE *et al.*, 2009; XU *et al.*, 2016). Nevertheless, electrodes polarization up to 1 kHz is expected (XU *et al.*, 2016). The impedance analysis method usually requires interruption in the electroporation protocol, and analysis may take seconds to complete, which may be a limitation of this procedure since electroporation occurs in nanoseconds (BATISTA NAPOTNIK; MIKLAVČIČ, 2018). Analysis during individual PEF pulses can be performed by measuring current and voltage. This method is also called 'instantaneous' or 'apparent' conductivity analysis, *i.e.*, the ratio between current and voltage at a given time point. The conductivity increase due to electroporation was observed in high cell fraction suspensions of animal cells (KINOSITA; TSONG, 1979; PAVLIN *et al.*, 2005; SUZUKI *et al.*, 2011), bacteria (EMANUEL; ROMAN; CAHAN, 2019) and yeast (EL ZAKHEM *et al.*, 2006; PINTARELLI *et al.*, 2021; RAMOS; FARIAS D., 2013), and tissues (CASTELLVÍ; MERCADAL; IVORRA, 2017; LANGUS *et al.*, 2016; NEAL *et al.*, 2012; SUÁREZ *et al.*, 2014).

PEF is usually delivered in the signature of 100 µs rectangular pulses burst (monopolar) or 50+50 µs (bipolar). Thus, those PEF contains a broad spectrum of frequencies, and mostly sub-4.4kHz frequencies, as shown in Figure 9, which are subject to α-dispersive effects which interfere in the measurement. Current models use instantaneous current-voltage measurements to describe the PEF electrical current (LOPES *et al.*, 2021; PAVLIN *et al.*, 2005; SEL *et al.*, 2005; ZHAO *et al.*, 2018), which is a sum of conduction current, dispersive effects (due to sample reactance), electrode-biological-media polarization, and electroporation. From the engineering point of view, differentiating the electroporation current from other PEF-current is complex. We call the electroporation current the superimposed non-physiological displacement current in the cell membrane due to pore opening. It is known that the biological systems are electrolytes and charges are subject to changes in polarization, *i.e.*, orientation and displacement of charges, and biological systems are characterized by the three most expressive relaxation factors: ions diffusion outside the cells, cell's membrane interface charging, and molecule orientation, which contribute to Schwan's dispersions, α, β, and γ, respectively (see section 2.3). The α-dispersion and electrode-biological-media-dispersion are located at sub-10 kHz, which is where the PEF burst energy spectrum is. Those phenomenon dynamics have not been completely understood, interfering in the direct current measurement.

Another method to access electroporation is the usage of a sinusoidal signal superposing the PEF. This method resembles the impedance measurement using DC bias

which is used to analyse non-linear capacitor (*e.g.* ceramic capacitors which the capacitance depends on the DC voltage). Early work has been done using 10 kHz sinusoidal signal added to a primary 1 ms PEF protocol to avoid dispersive effects (RAMOS *et al.*, 2012). The authors found differences between the AC (*i.e.* 10 kHz) conductivity and 'DC instantaneous' current and voltage measurements. The 10 kHz was selected as the location which the sample was mainly resistive (on yeast samples).

Figure 9 – (a) A 100 µs rectangular pulse. (b) Analytical Fourier transform of a 100 µs PEF pulse. The half-power is at 4.4 kHz, and most of the PEF energy is between DC to 4.4kHz
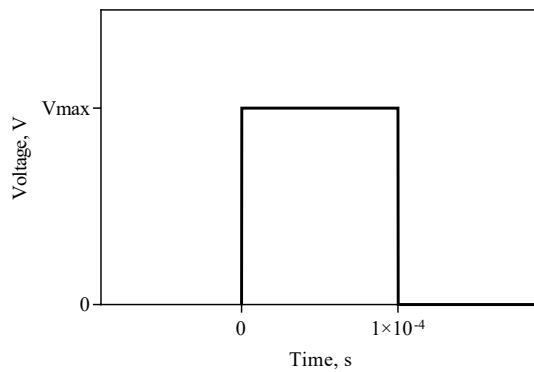
(a)   (b)
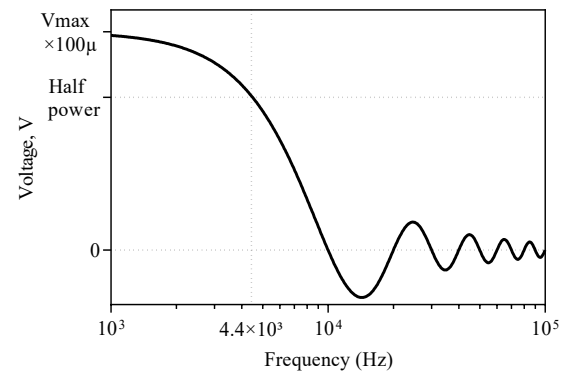
Source: Autor.

[blank page]

3 IMPEDANCE SENSING AND PEF SYSTEM

It is known that electroporation is related to pulse amplitude, pulse train repetition rate, pulse shape, pulse number and repetition rate. The combination of several parametric possibilities, inserted by electroporator operator, makes it possible to reach (reversible or irreversible) electroporation to the cellular systems of animal and plant cells, whether being suspension of cells or tissue, *in vivo* or *in vitro*. The PEF equipment corresponds to a wave generator of electrical voltage, with an amplitude of up to kilovolts and period in the order of microseconds. The electroporator uses electrodes to impose pulsed electric field on the sample biological. The electric field amplitude used for electroporation mainly depends on the cell size, and typically the range is 10 to 1000kV/m (WEAVER *et al.*, 2012).

This chapter aims to develop a system and methods to enable customizable PEF experiments and perform alternate current analysis during the PEF. The change in the complex electrical properties may allow a novel study of electroporation which are essential for developing new electroporation models. Those may indirectly probe the electroporation, thus, may trigger future PEF control systems. We notice that there are few considerations in the literature using mixed signals approach to sense electroporation. One reason is the technical difficulty in developing fast linear amplifiers for high voltages and currents. Linear amplifiers operate with elevated voltage drops in the switches, which generally reflects extensive power efforts. The high voltage rectangular pulses are more easily obtained with IGBT or MOSFET switching.

3.1 MATERIALS AND METHODS

The complex impedance $Z(\omega)$ of a linear system can be calculated as Equation (9). Usually, a small sinusoidal voltage signal $V(\omega)$ (*i.e.* excitation signal) is applied to the tested sample, and the electrical current response $I(\omega)$ is measured. The $j=\sqrt{-1}$ and ω is the frequency. The real Z_{RE} (R) and imaginary Z_{IM} (X) parts of the $Z(\omega)$ are called resistance and reactance, respectively. The magnitude $|Z|$ and phase angle $\angle\theta$ of $Z(\omega)$ are accordingly to Equation set (10). We will use the polar description $|Z|\angle\theta$) because it is more convenient when working with the two AC signals (*i.e.* is simpler to compare V and I time-variant signals using the polar description) and samples' spectrum can be compared with analogue filters. Moreover, the cartesian R-X description is more adequate when the equivalent circuit is the

R-X itself, in the case of biological media the R-X elements are frequency-dependent and can be confused with the four-element equivalent circuit.

$$Z(\omega) = \frac{V(\omega)}{I(\omega)} = Z_{RE} + jZ_{IM} \tag{9}$$

$$|Z| = \sqrt{(Z_{RE})^2 + (Z_{IM})^2} \text{ and } \theta = \arctan\left(\frac{Z_{IM}}{Z_{RE}}\right) \tag{10}$$

3.1.1 Signal Generator

For an economical and portable generation of electrical pulses for clinical and laboratory electroporation, it is applied to the electroporator 'high power pulse technology'. For treatments in the food industry and nano electroporation, other types of technology can be used (KEMPKES, 2017). Similar procedures are used in defibrillators, plasma generation, lasers, and welding machines. The electroporator power system has energy transformation and storage steps. The change of energy is usually done with static converters. The first step is the conversion of energy from a source primary low voltage and low power density (*e.g.* conventional 127/220 V mains or battery) for high voltage. The second step is the temporary storage of the converted energy, which can be done with a capacitor bank. Arrangements of parallel and series capacitor are used with auxiliary diodes and resistors (to stabilize the voltage during storage and discharge). The capacitor bank usually has low equivalent series resistance (ESR). We note that energy can be stored in capacitors (electrical energy) or in inductors (magnetic energy). In electroporators for laboratory and clinical use it is usually stored in capacitors, as it is the least costly procedure, and there is no interruption of currents (in inductors). Finally, the stored energy is converted and quickly delivered to the cargo in a pulsed at high-voltage and high-power density. The basic operation is as shown in Figure 10. Considering that electrical energy is already stored in a charged capacitor, the generation of monopolar pulses can be performed with a single switch controlled capacitive discharge circuit. The generation of bipolar pulses can be done with an inverter circuit (push-pull, half-bridge or full-bridge) (PAI; ZHANG, 1995; REDONDO, 2017).

During the master's period, the author developed three custom electroporators of up to 1 kV and 30 A, using topologies of a single switch and full-bridge and with embedded V-I recording. The electroporators are shown in Figure 11 (PINTARELLI, 2018; PINTARELLI; ANTÔNIO JR; SUZUKI, 2019). Those electroporators power electronics were adapted to this

thesis experiments. This chapter highlights the adaptation to generate and record PEF with superposing sines.

Figure 10 – Example of energy conversion processes in electroporator. Primary energy (from the electricity grid or battery) is converted and stored at high voltage. Rectifiers or CC-DC converters are used in this step. Capacitive storage is generally adopted in electroporators. The energy stored in capacitors is delivered in electrical pulses to the electrodes. In this step, the topologies of CC/AC converters can be used. The most common are controlled capacitive discharge (for monopolar pulses) and inverter (for bipolar pulses).
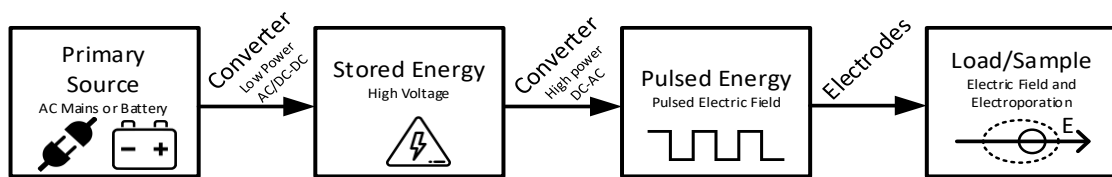
Source: Adapted from (SUZUKI *et al.*, 2019).

For the application of arbitrary forms, a push-pull MOSFET topology for pulsed energy application was developed (pair of IRFP240 and IRFP9240). This system operates as a linear amplifier. We note that in the audio engineering area this topology is called a class A amplifier. The linear amplifier supports up to ±85 V. The generation of arbitrary signals is done digitally with the Espressif Systems ESP32-D0WDQ6, which is an integrated solution with a microcontroller (MCU) and peripherals. This MCU was particularly selected due its two individually controlled 240 MHz cores, large RAM storage for fast interruption routines, the capability of running real-time operating system (*e.g.* FreeRTOS), two 8-bit digital-to-analogue converter channels (DAC) and embed 802.11b/g/n Wi-Fi radio (ESPRESSIF SYSTEMS, 2017). The system schematic is shown in Figure 12. The MCU was programmed using the manufacturer ESP-IDF framework at Visual Studio Code and PlatformIO. The first core (core 0) manages all Wi-Fi related requests and the HTTP web server (Wi-Fi and HTTP server tasks). The second core (core 1) runs a RAM-stored task which is assigned to control both DAC (pulse manager task). DAC signals are conditioned and summed using a pre-amplifier stage (Analog Devices AD826). We configured one of the DACs to connect to the MCU embedded cosine waveform generator; thus, precise sinewaves can be easily superposed with other arbitrary waves. A semaphore routine was used within FreeRTOS to guarantee real-time during PEF.

Figure 11 – PEF equipment prototypes: (a) up to 120 V, 10 A, monopolar, with fine voltage adjustment; (b) up to 800 V, 20 A, monopolar, with embedded current-voltage datalogger; (c) up to 800 V, 30 A, bipolar, with embedded current-voltage datalogger and its electronics (d). (e) European Standard Operating Procedures of Electrochemotherapy (ESOPE) adapted pulse (800V, 20 A, 100 µs monopolar, 5 kHz repetition rate eight pulse train).

a)

b)

c)

d)

e)
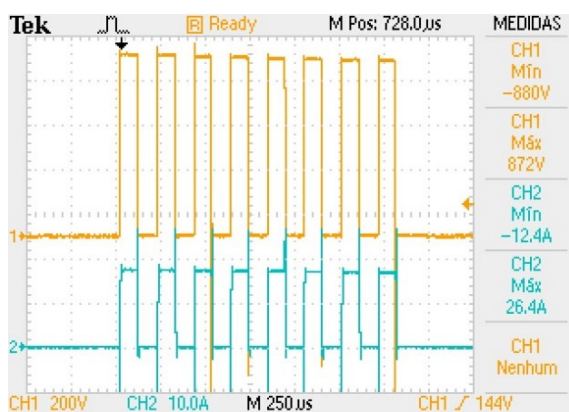
Source: Author and (PINTARELLI, 2018).

The system is controlled by the user using a web applet interface, accessible by any navigator at smartphone or computer Wi-Fi capable. The system has some pre-defined

waveforms. The arbitrary waveform can be generated by uploading RAW waves to the MCU. With the applet, user can set diverse protocol (*e.g.* rectangular, triangular, sawtooth, inverted triangular, sines from 1 kHz to 250 kHz, monopolar and bipolar waveforms, individual wavelength ranging from 50 μs to 1 ms, diverse burst pulse number, sinusoidal superposition and peak amplitude). The web interface is shown in Figure 13. There are several sliders to operate the equipment. The 'mode' slider sets the pre-defined pulses, where '1' is the square pulse train (monopolar) with overlapping sine, '2' is the sawtooth pulse train with overlapping sine, '3'is the triangle pulse train with overlapping sine, '4' is the fixed duration cycle sine, and '5' is the bipolar square pulse train. The PEF system can connect to the user's Wi-Fi or be a Wi-Fi host; thus, the system is accessed by the network IP number. The arbitrary wave system was evaluated using Tektronix DPO2012B. The process was the same as datalogging of the biological samples (see section 3.1.2). Its pulse performance and frequency were measured under load stress (10 Ω). We consider signals that may be used during the development of this thesis. Nevertheless, other waveforms may be used in additional work.

Figure 12 – Arbitrary generator system and the data logging. There are three tasks divided into the cores. A 'Pulse Manager' task commands the two DACs. DAC 0 was connected to internal cosine generator, and DAC 1 produce the arbitrary waveforms. The DAC signals feed the high-power linear amplifier. An oscilloscope is used to measure the DUT voltage (V_t and V_b probes). The current is calculated using the shunt resistor parameters (Z_{shunt}). The shunt resistor impedance 1.78 ∠3.18º Ω (at 100 kHz) and 1.9 Ω (at DC).
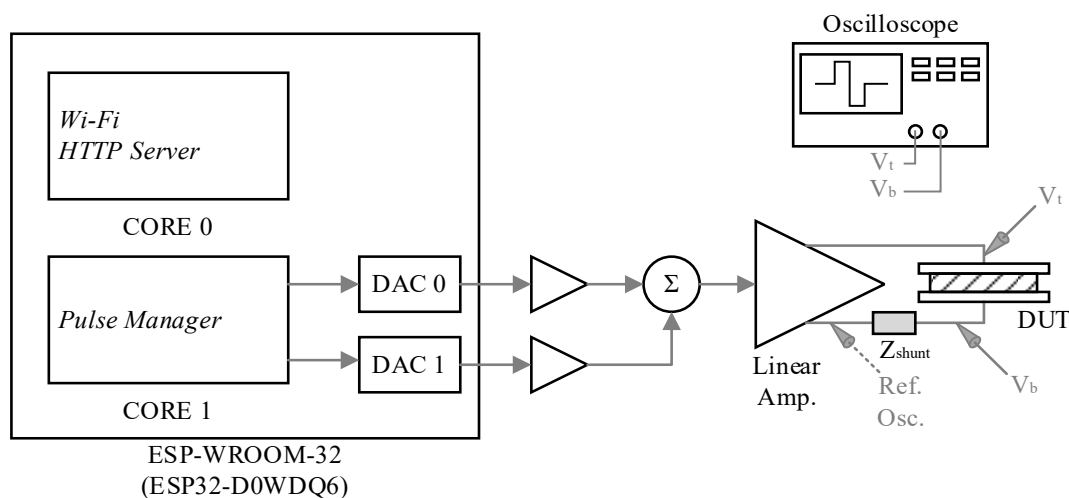
Source: Author.

Figure 13 – The PEF system control interface. This figure was recorded using Google Chrome at an Android Smartphone. Sliders are the PEF related configuration.
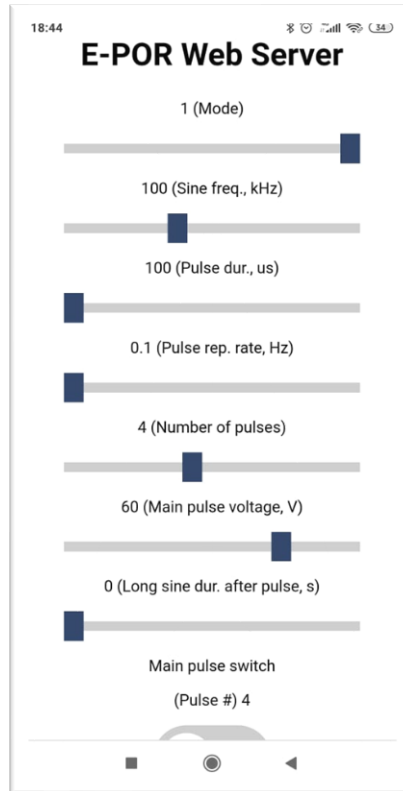
Source: Author.

3.1.2 Data logging

All acquisition were made using Tektronix DPO2012B 100 MHz 8-bits oscilloscope and two probes 1:10 model Tektronix TPP0200 200 MHz (Tektronix, Inc., EUA). The probes were calibrated according to the manufacture's manual. The sampling frequency was set to 1 GHz (maximum). Probes capacitance were adjusted according to the oscilloscope manual (TEKTRONIX, 2008). We used a shunt resistor (Z_{shunt}) model RX21-5W 1R8J ceramic to measure current. The measuring circuit and oscilloscope connections are shown in Figure 12 (see the V_t and V_b probes). We measured the shunt impedance spectrum (1 kHz to 1 MHz) with Keysight 4294A and DC impedance with Fluke 179. Its 100kHz impedance is 1.78 ∠3.18º Ω and DC impedance is 1.9 Ω. The frequency spectrum is shown in Figure 14. The Z_{shunt} phase shift was compensated in the signal processing. The oscilloscope input impedance (1 MΩ) and oscilloscope 1:10 probe parasitic capacitance (13 pF) were considered not significant.

Figure 14 – Shunt impedance spectrum.
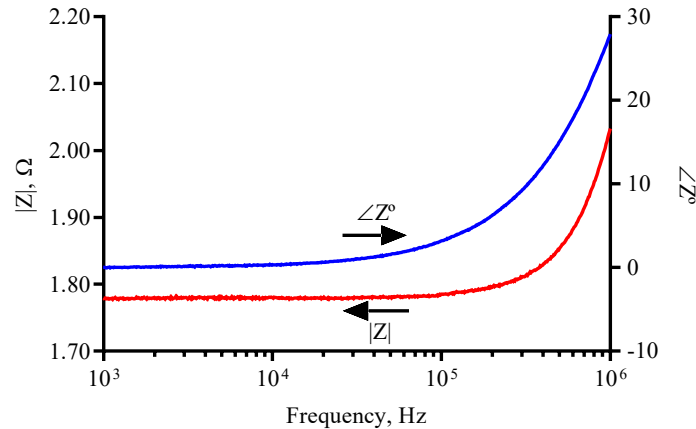
Source: Author.

All sampling precedes and succeeds an impedance analysis using HP 4294A. The setup is described by Figure 8. The switching between the PEF system and the impedance analyser was done manually, which is important to remove any relay or extra connections from the circuit (these devices are not designed to operate at 100 kHz). All DUT cables were kept at a maximum of 30 cm. The time between the impedance readings was 2 minutes, this time is required for unplugging and plugging cables and the measurement recording.

3.1.3 Data processing

All data were processed offline. Measurements were saved in a USB flash drive and loaded into the computer. To extract the AC impedance, we made a script in MATLAB 2018b (Massachusetts, EUA), which estimates the AC voltage and current based on individual discrete sine wave samples. The processing mains steps are shown in Figure 15. The first step is a low pass IIR[12] zero-phase filter[13] (DC to 300 kHz passband and 600 kHz -60dB stopband). Despite the oscilloscopes' top-notch sampling frequency (1 GSamples/s on all channels) and bandwidth (100 MHz), it lacks resolution (8-bits); thus, we trade the bandwidth

---

[12] The main differences between IIR and FIR is in its implementation. As we are processing the signals off-line it is possible to project both to behave similarly and meet our requirements. Thus, we opted for the IIR due to the reduced number of computations.

[13] Zero phase delay or no group delay is achieved by forward-backward processing technique, *i.e.* first: filter the signal forward in time, second: time reverse (*i.e.* 'flipped signal') to filter backwards in time, third: time reserve the whole result. This operation is mathematically equivalent to the squared filter response which gives only real values, thus zero phase. This technique can only be done offline or at quasi real-time, *i.e.*, with a sufficient delay.

for resolution, and our second processing step is downsampling. All signals were oversampled at 1 GHz to be downsampled in sixteen-fold (*i.e.* oversampling ratio equals 16)[14], this is equivalent of a four times resolution enhancement (or 2 bits), thus improving the digital signal resolution to 10-bits and lowering sampling frequency to 62.5 MHz (OPPENHEIM; SCHAFER, 2010). We used the deep memory oscilloscope configuration (1 MPoint record length on all channels). Each channel acquisition file has approximately 25 MB (.CSV converted file). The acquisition time base was 1 ηs, the record window was 1 ms, and number of samples was 10^6. The third step is finding the superposed sinewave top and bottom peaks by using derivates and zero crossings. Lastly, the peaks and zero-crossing values are used to calculate DUT AC and DC voltage and current, respectively. We emphasize that the calculated DC impedance is not the 'true' DC impedance, but the apparent impedance since the DC is subject to dispersive effects. Ten 100 kHz sine cycles were acquired on each signal stage (before, during and after PEF). The surrounding PEF sines cycles were discarded due distortions caused by the PEF rising and falling times. Thus, we processed nine individual sines before and after the PEF and eight sines' cycles during the PEF. The 100 kHz impedance data was analysed in terms of time. All data were analysed as means and 95% confidence interval (95% CI). The 95% CI corresponds to the significance level of 0.05 (equivalent of t-test of two groups using p=0.05). All this thesis data was processed in this way, as it facilitates data analysis. If there is no overlap of confidence intervals for two groups, there is a significant difference.

Figure 15 – MATLAB script main steps.
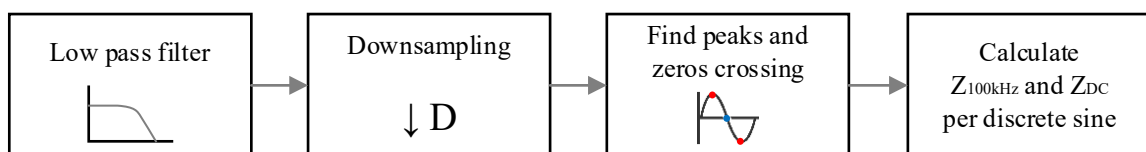
Source: Author.

3.1.4 PEF Protocol

The PEF settings with superposing sine that are used in this thesis are eight rectangular pulses train at a repetition rate of 0.1 Hz (10 s pulse interval), each pulse has 100 μs duration, each pulse is previously superposed by a 5 V_{pp} (*i.e.* 1.75 V_{RMS}) 100 kHz sine.

---

[14] For each 'additional' bit of resolution, the signal must be oversampled by a factor of four.

The 100 μs pulses are monopolar (100 μs rectangular) and bipolar (50 μs positive rectangular + 50 μs negative rectangular). The PEF protocols were described by the top and bottom DC outputs values. We used 1, 15, 30 and 60 V (see Figure 16). A sawtooth wave (*i.e.* ramp) PEF was also used, the sawtooth ware duration (ranging from 0 to 60 V) was 150 μs (400 V/ms) and 1 ms (60 V/ms). This PEF protocol was applied in vegetal tissue. The electric field at sample are approximately $E = V/\ell$. All the measurement recording using oscilloscope were at the first and last (eight) pulse.

The PEF settings without superposing sine that are used in this thesis are eight rectangular-shaped pulses of 100 μs and a repetition rate of 1 Hz (1-second pulses interval). This protocol is similar to the ESOPE (GEHL *et al.*, 2018). All pulse data was acquired using a custom system. It has been assessed the effect of 200 to 600 kV/m PEF at yeasts. Averages were made based on 20 instant readings (200 kHz sampling rate system) (PINTARELLI, 2018; PINTARELLI; ANTÔNIO JR; SUZUKI, 2019).

Figure 16 – PEF pulse train. Pulse 1 (P1) to pulse 8 (P8). (a) Monopolar, and (b) Bipolar.
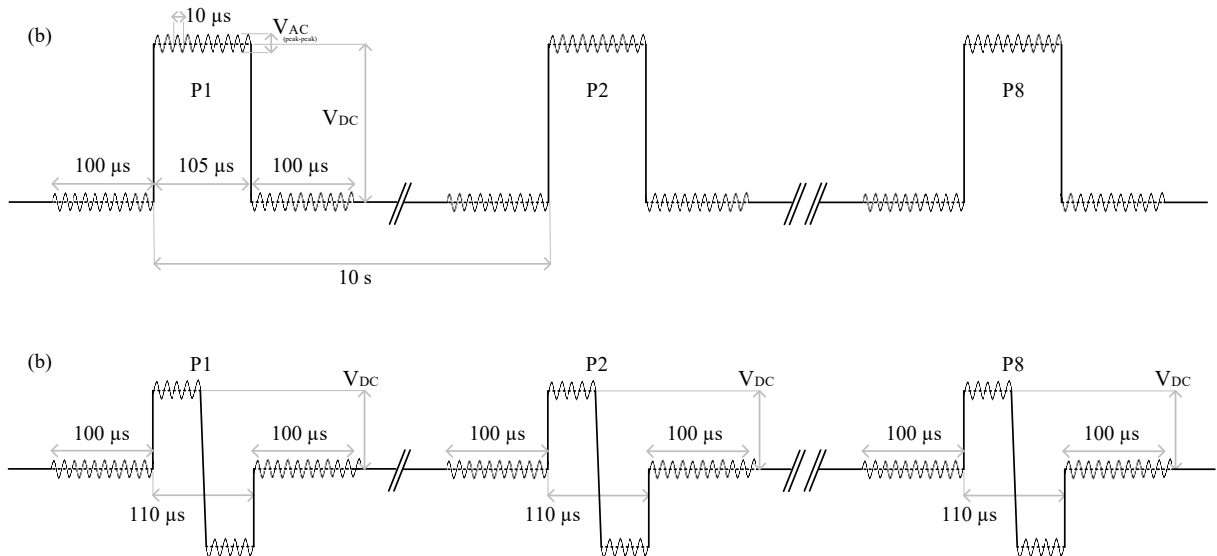
Source: Author.

3.1.5 Measurement Error

We design two experiments to test our measurement capabilities: a static electrical and an electrolytic phantom load. We tested those loads using the same PEF protocol used in the *in vitro* cases.

3.1.5.1 Stationary Electrical load

Data was collected using static impedances (see Figure 17a). The static impedances were designed no simulate a dispersion centred near 100 kHz, and approximately 0 to -80° phase shift. The impedance models are shown in Table 1. Those were measured (N = 3) with Keysight 4294A and Fluke 179. Theoretical frequency spectrums are shown in Figure 17 (b and c). The objective of the static load was to evaluate the measurement errors of the AC measurement under the PEF circumstances (*i.e.* 100 µs, 15, 30 and 60 V generator outputs).

Figure 17 – (a) Static impedance model. Theorical impedance spectrum of the test loads: (b) R = 200 Ω, R1 = 25 Ω, C = 100 ηF; (c) R = 10 Ω, R1 = 10 Ω, C = 100 ηF.
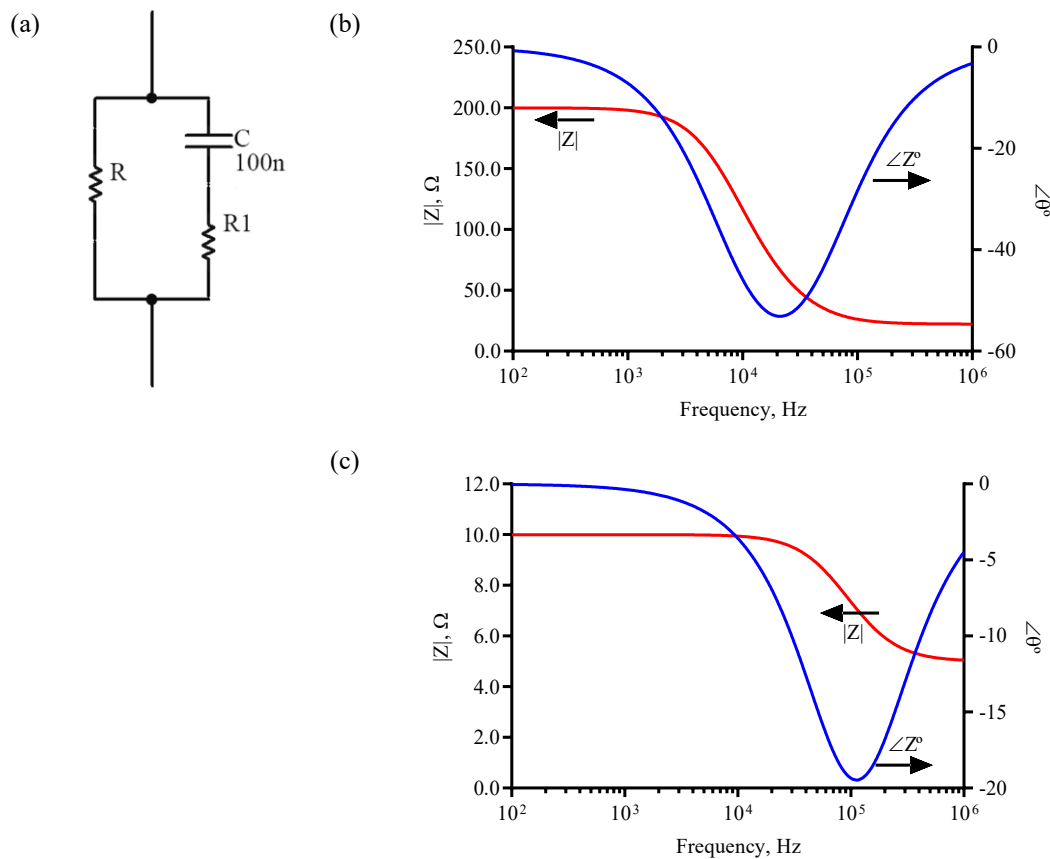
Source: Author.

Table 1 – Test impedances measure (mean ± SD). The DC impedance SD were less than 0.1.

Test load	Theoretical Z at 100 kHz, Ω	Measured Z at 100 kHz, Ω	DC Impedance, Ω
R = 200 Ω, R1 = 25 Ω, C = 100 ηF	26.3 ∠-28.1°	23.13±0.01 ∠-21.98±0.01° Ω	206.5
R = 10 Ω, R1 = 10 Ω, C = 100 ηF	7.4 ∠-19.4°	7.22±0.01 ∠-16.77±0.16	10.1

Source: Author.

3.1.5.2 Phantom Electrolyte Load

We use Carbogel ECG® placed between parallel electrodes as our electrolyte load (PINTARELLI, G.B. *et al.*, 2019). The objective of the phantom load was to evaluate PEF effects on the measurements. The electrolyte load was placed between parallel plate disc electrodes with 29.7 mm diameter at 1 mm distance, as shown in Figure 18.

Figure 18 – Electrolyte phantom.
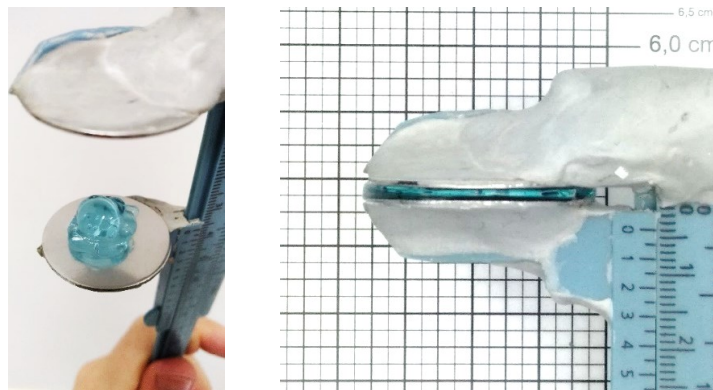
Source: Author.

3.1.6 Electrodes

Electrodes were Stainless steel 316 L discs (diameter of 29.7 mm and thickness of 1.0 mm) as Figure 19. We assembled the electrodes in calipers when the sample is not solid (as the phantoms). Electrodes cables were less than 30 cm.

3.1.7 Impedance Analysis Methods

We used the Keysight 4294A impedance analyser and Keysight 16047E test fixture for measuring $|Z|\angle\theta$. The equipment operation and calibration were done according to the operation manual (KEYSIGHT TECHNOLOGIES, 2003). The fixture compensation was executed using the two equipment functions ('open' and 'short'). The 'open' function calibrates the open circuit parasite capacitance (*i.e.* open electrodes with 1mm separation as Figure 20a). The 'short' function calibrates the series inductance (*i.e.* bound electrodes as Figure 20b). A plastic clamp was used as auxiliary tool to ensure electrodes positioning. The

biological material measurements were taken after setting the fixture (*i.e.* plate electrodes) compensation. We also set the impedance analyser to frequency point average of 3, single pass reading mode and voltage controlled (0.5 mV), those configurations were used during all measurement of this thesis.

Figure 19 – Electrodes used in the thesis.
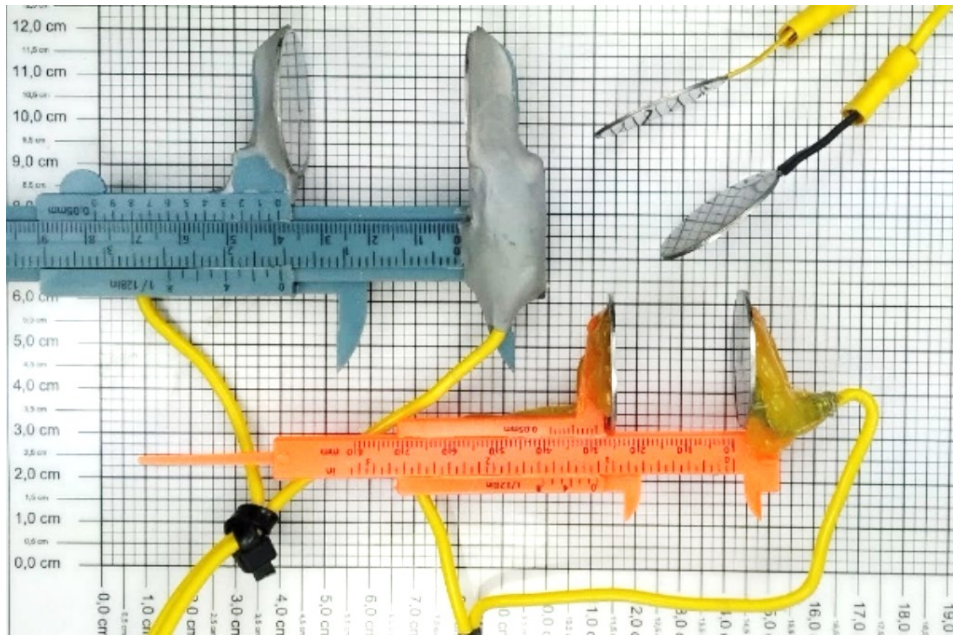
Source: Author.

Figure 20 – (a) Open circuit calibration. (b) Short circuit calibration. Example of a sample reading.
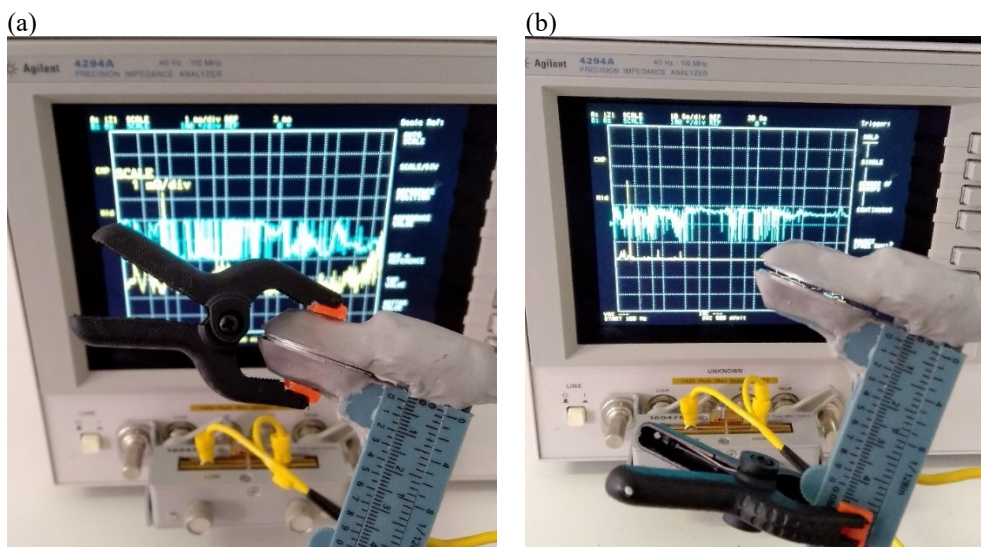
Source: Author.

The electrodes parasitic effects were also measured and compensated. In this case, we used the default 16047E settings (4294A default calibration). The chamber frequency spectrum is as Figure 21. Those are the reference values are the parasite parallel capacitance and series inductance.

Figure 21 – (a) Short circuit and (b) open circuit electrodes response.

(a)   (b)
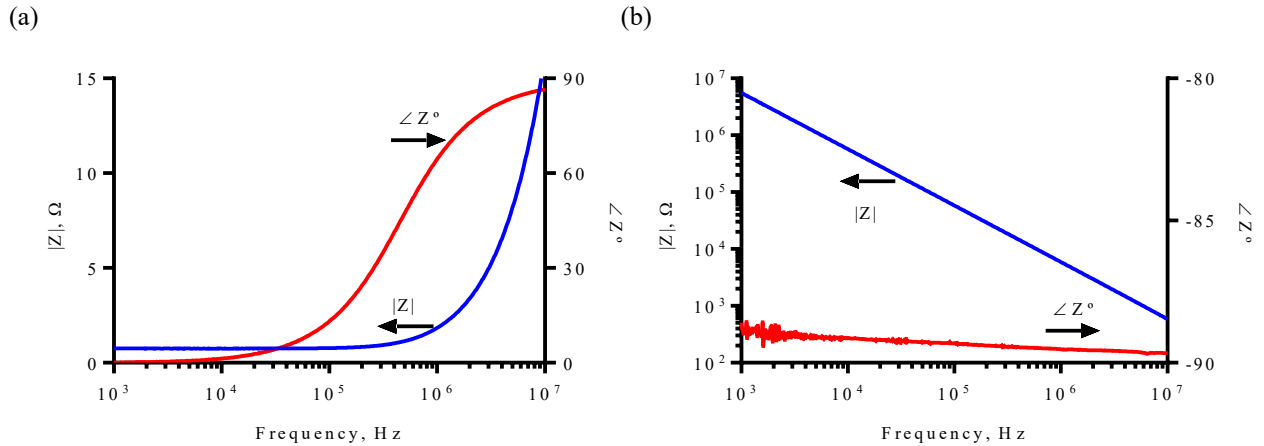
Source: Author.

3.2 RESULTS

3.2.1 System Performance Using Static Load

The PEF generator system frequency response was as Figure 22. The -3dB frequency is over 250 kHz. Although the -3dB frequency is one of the parameters to specify amplifiers (mainly in audio areas), this frequency is not so relevant since amplifier's frequency response is not linear near -3dB frequency (regarding both gains and phase). It would not be appropriate to use this amplifier to generate signals with multiple frequency components if some are above 20 kHz. Based on this, our amplifier is an arbitrary signal generator up to 20 kHz. However, as we only generate a single frequency above 20 kHz, we compensate the group delay and gain non-linearity in the MCU. We observe that after 250 kHz, we are no longer able to produce satisfactory sine waves using our DAC.

There are several prospects with our PEF generator. Figure 23 shows a compilation of some waveforms that will be used throughout this work, *i.e.* mixed rectangular with sine and sawtooth. The DC and AC wave parameters can be modified according to the experiment

(see Figure 13, *e.g.* sine wave frequency, DC duration and AC and DC amplitudes can be configured). The system switching performance is listed in Table 2. Some of the data which was used to evaluate the system's characteristics are available in Appendix A.

Figure 22 – Frequency response of the designed amplifier under resistive 10 Ω load. The gain was the measured load output and DAC output ratio.
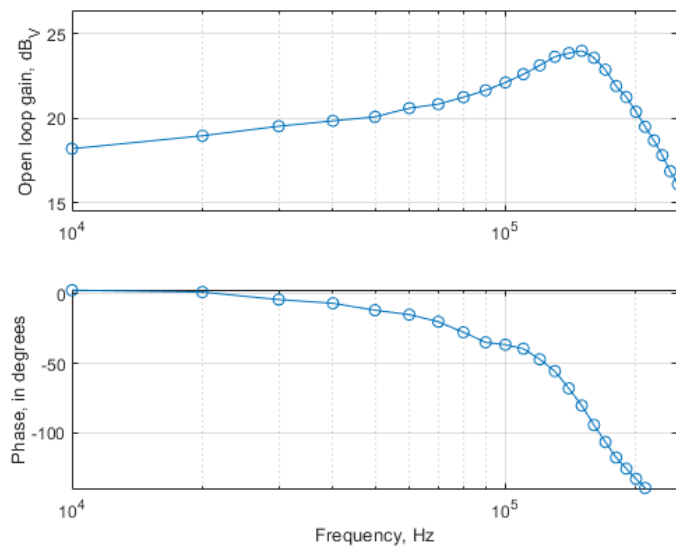
Source: Author.

Table 2 – Designed system characteristics. Tested under resistive 10 Ω load.

Type	Value
t_{rise} (0-80V)	< 5 μs
t_{fall} (80-0V)	< 10 μs
Slew rate	22 V/μs
Total harmonic distortion (THD) (at 30Vpp, 100 kHz)[1]	2,5 %

[1]We observe that this includes the DAC THD, which was 1,5 %.

Source: Author.

The PEF measurements over of the stationary loads (see section 3.1.5.1) are shown in Figure 24: 'a' is 200 Ω // 25 Ω + 100 ηF and 'c' 10 Ω // 10 Ω + 100 ηF. The circle dots reference measurements, *i.e*, AC and DC analysis using the impedance analyser and multimeter, respectively. The error is less than 5% for $|Z|_{100kHz}$, less than 15% for $\angle Z_{100kHz}$, and less than 5% for Z_{DC}. The impedance spectrum of the static loads are 'b' (200 Ω // 25 Ω + 100 ηF) and 'd' (10 Ω // 10 Ω + 100 ηF).

51

Figure 23 – Waveforms and its Fast Fourier Transform (FFT) compilation (a) 100 kHz sine burst, (b) DC rectangular monopolar with 100 kHz sine super positioning and (c) bipolar, (d) sawtooth. The test load was 10 Ω.
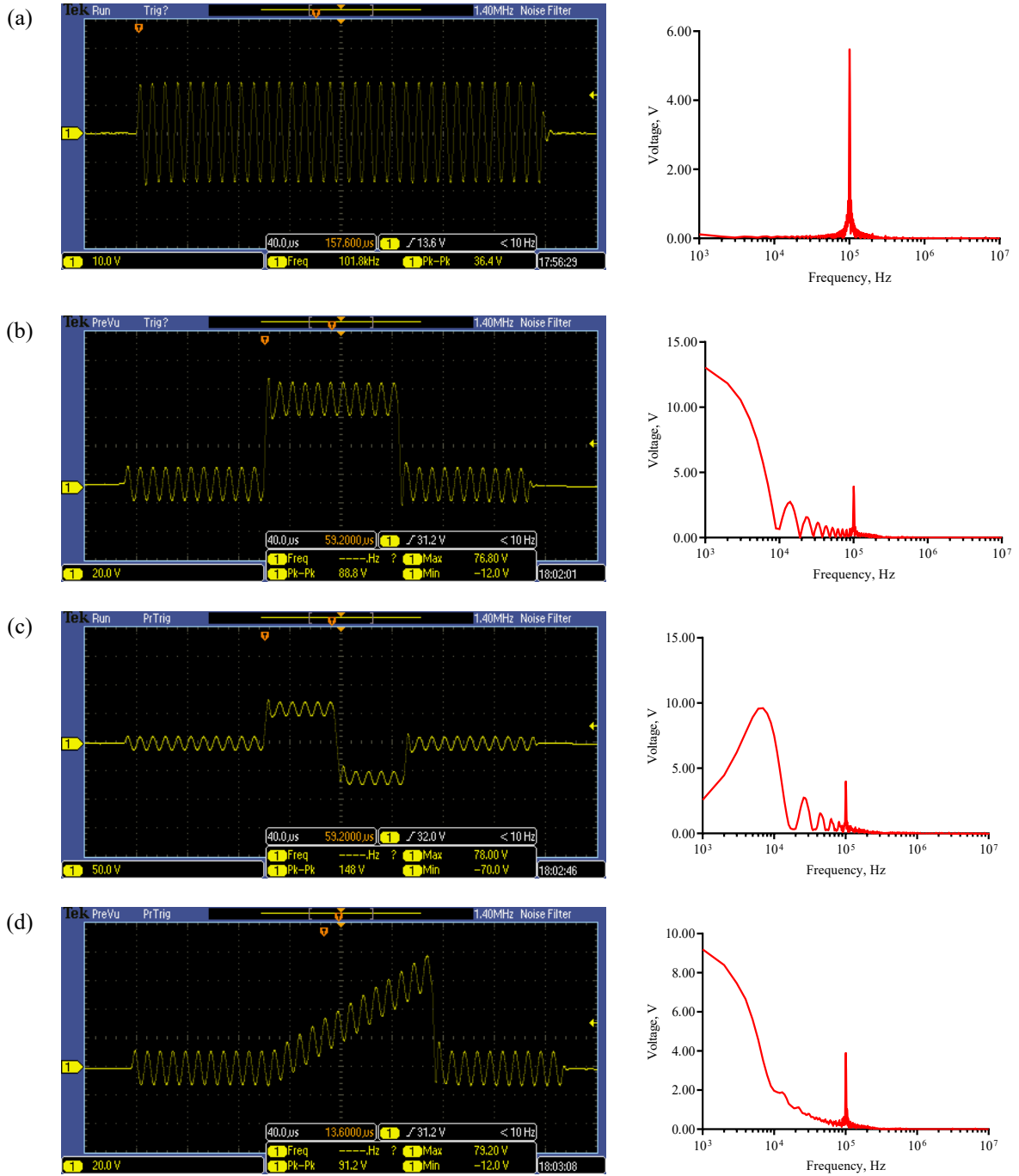
Source: Author.

Figure 24 – Measurements over static loads. The '⊗' symbols are the reference values. Measurement over: (a) 200 Ω // 25 Ω + 100 ηF, and (c) 10 Ω // 10 Ω + 100 ηF. Impedance analyser measurent: (b) 200 Ω // 25 Ω + 100 ηF and (d) 10 Ω // 10 Ω + 100 ηF.
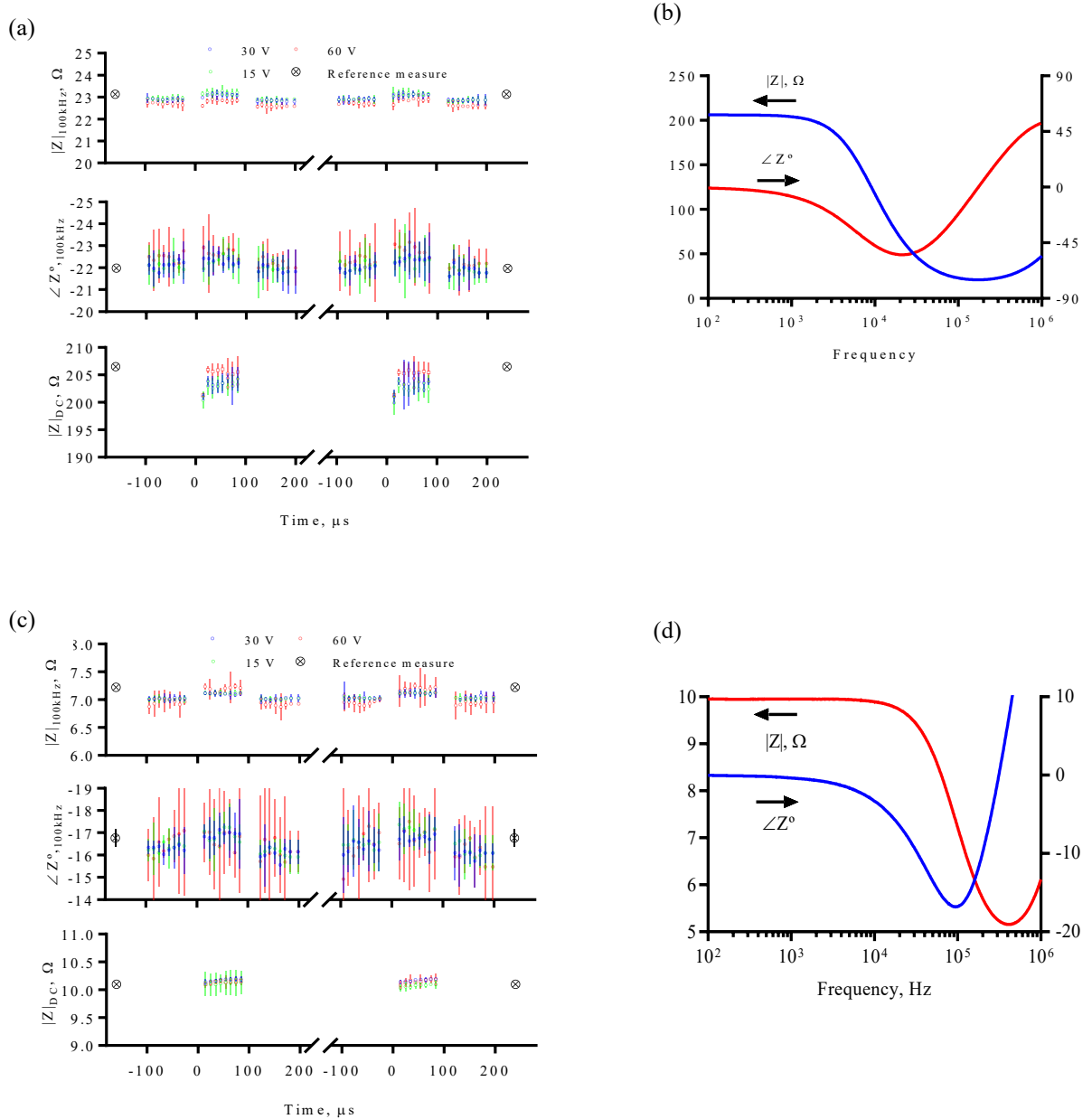
Source: Author.

3.2.2 System Performance Using Phantom Load

The impedance measurements of the phantom electrolyte load are shown in Figure 25. The Z_{100kHz} is less susceptible to interfere with polarization as its impedance does not significantly change during time (see Figure 25a and b). The DC impedance increase does

show significant difference (see Figure 25c). On the other hand, the electrical double layer (EDL) charging occurred at Z_{DC}, as the individual sample analysis shows a capacitive charging and discharging current profile (see Figure 25e and f). The phantom double layer is not stable as there are no changes in the impedance analyser study (see Figure 25d).

Figure 25 – Measurements over the phantom. The AC (a) absolute and (b) phase measurements, and (c) DC measurement. (d) The frequency spectrum before and after the PEF (60 V case). Single (e) oscilloscope sample and (f) its voltages and currents.

(a)

(b)

(c)

(d)
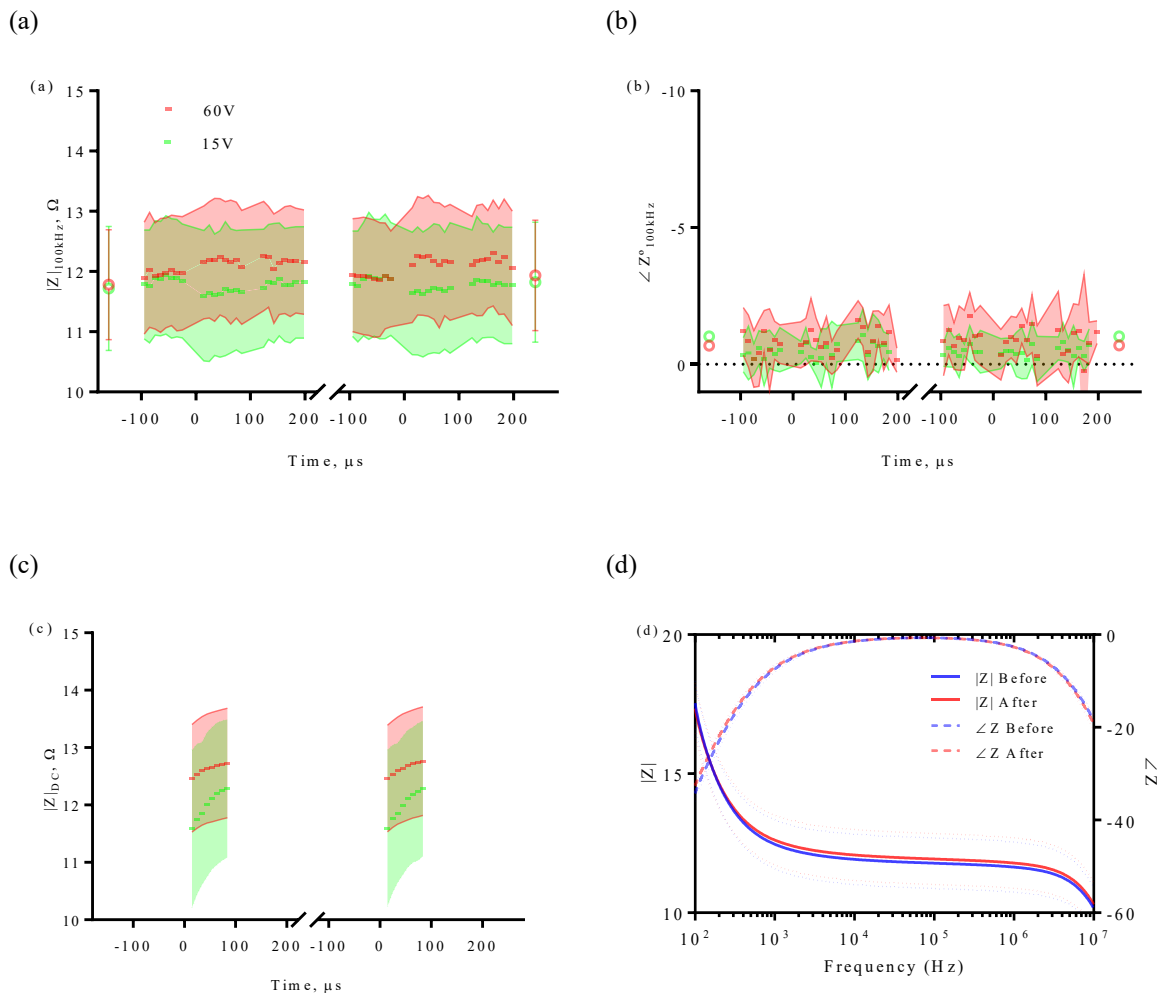
(e)
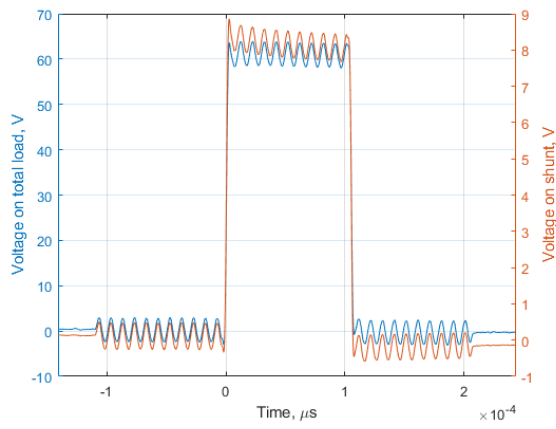
(f)
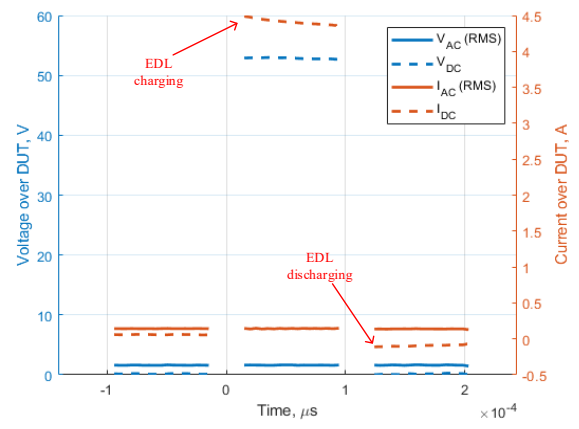
Source: Author.

4 SENSING OF YEAST INACTIVATION BY ELECTROPORATION

Yeast contamination is a problem in the industry, as their contamination can cause financial loss. In wine production, yeast control is challenging and of high importance as yeasts rapid grow can significantly alter grapes pH and flavor, thus, compromising wine quality and causing significant economic losses. The International Organization of Vine and Wine (OIV), the benchmark for vine-based products standards, establishes the maximum acceptable limits for oenological practices; this includes the maximum values for viable yeasts load. Therefore, to obtain adequate wines that are safe for consumption and with preserved palatable aspects, yeasts should be removed or inactivated. In this regard, controlling yeast number in the food processing environment is made necessary. In wines, the *Saccharomyces cerevisiae* yeast is the most frequent contaminant and spoilage species (LOUREIRO, 2003). In other types of foods, other microorganisms may be relevant. Those that can cause foodborne illnesses and can even become lethal. If contaminated yeast is injected into a human body, it can cause health problems. Thermal pasteurization, sterile filtration, and chemical treatment affect food's nutrients composition and sensory characteristics (*e.g.,* color, texture, aroma and flavor). Yeast control in different food can be reached by electroporation while maintaining its pre-processing properties. In the case of wines, pasteurization is avoided as it damages organoleptic properties. Final customers are continuously looking forward to those characteristics, as they are often related to freshness and authenticity (CHARLES-RODRÍGUEZ *et al.*, 2007; COUTO *et al.*, 2005; PUÉRTOLAS *et al.*, 2009).

In this section we will discuss some of latest experimental results that were published at (PINTARELLI *et al.*, 2021). **The paper is reprinted at Appendix B with permission.** We used *in vitro Saccharomyces cerevisiae* ATCC®36900™, low suspension fraction 2.5×10^7 cells/mL[15], to investigate PEF effects on the cell viability (using Methylene blue method, 0.2% $C_{16}H_{18}N_3SCl$), cell morphology (using scanning electronic microscope), media conductivity (using current-voltage measurements and impedance spectroscopy) and estimating absorbed energy. The PEF protocol were 8 rectangular-shaped pulses of 100 μs and a repetition rate of 1 Hz (*i.e.*, 1-second pulses interval). Also, we did *in silico* study to

---

[15]Suspension fraction typically found on wines is $<10^8$ cell/mL. The 2.5×10^7 cells/mL fraction represents a volumetric fraction or weight concentration (weight of yeast cells/total weight of suspension) is 0.43 % in water.

evaluate number of pores at cell membrane, transmembrane voltage, and differential voltage in the cell wall. We investigated the effects of amplitude changes as the electroporation mainly depends on it. It has been assessed the effect of amplitude applying protocols of 200 to 600 kV/m. We show that it is possible to eliminate yeast using irreversible electroporation and detect inactivation (cell breakage) by macroscopic instantaneous current measurements. A 15% in pulse current increase is expected when reducing yeast numbers to 10^5 cells/ml by 500 kV/m irreversible electroporation PEF.

Figure 26a shows the current during the PEF protocols. The absorbed energy is higher when there are cells in the media. Dozens to thousands kJ/L are expected for microbial inactivation (PUÉRTOLAS *et al.*, 2009). Due to the short burst (8 pulses of 100 µs), the theoretical temperature rise at the end of the 600 kV/m protocol is 3,5 ºC (EL ZAKHEM *et al.*, 2006). In practice, the temperature increase should be lower since there is thermal dissipation during the inter-pulse intervals (1 second). At 600 kV/m we observed a conductivity plateau. This may indicate the maximum ion exchange due electroporation in our experiments. Other work reported similar conductivity saturation (EL ZAKHEM *et al.*, 2006; NEAL *et al.*, 2012; PAVLIN *et al.*, 2005). We analyzed the current changes in terms of in pulse current rate. We define in pulse current rate as the average increase of current between last (eight) and first pulse. Figure 26b shows the in pulse current rate as function of PEF amplitude. The YPD media were directly compared to the cell suspensions. At 200 kV/m there are non-significant difference (ns). Over 300 kV/m we detected significant differences (when comparing equal kV/m magnitudes). When comparing in pulse current increase at similar delivered energy, 22-25 kJ/L has no significant difference, and 40-42 kJ/L has significant difference. The phenomenon that changes current is related to the presence of cells and it is not associated with temperature.

The compiled result of the current change in function of cellular viability is shown in Figure 27a. There is correlation between cell viability reduction and current change. SEM images are shown in Figure 27b. Using SEM, we observed that some cells were physically PEF-damaged, and others were not. Zakhem *et al.* reported similar results (EL ZAKHEM *et al.*, 2006). Those are PEF triggered damage and not the actual PEF pores. The physical damage may be correlated to the changes in the surface which changed the cell drying process or intracellular drain out due electroporation membrane destruction. We focused in showing the damaged cells as shown in Figure 27 (c to f). At 200 and 300 kV/m SEM provided details

of physical damage to the cell associated to electroporation. Notwithstanding, neither cell viability nor macroscopic electrical properties readings provided this type of detailing.

Figure 26 – (a) Electrical currents at PEF protocol. The '⬤' means the cell suspensions data, and '◯' means the YPD data. (b) YPD and cell suspension ('Cell S.') conductivity change as a function of PEF protocol amplitude in kV/m. The significance levels are given upper the box plots. 'ns' means not significant (p>0.05), '*' means p<0.05 and '***' means p<0.001. Oscillations below zero at 200 and 300 kV/m are not shown.

Source: Autor.
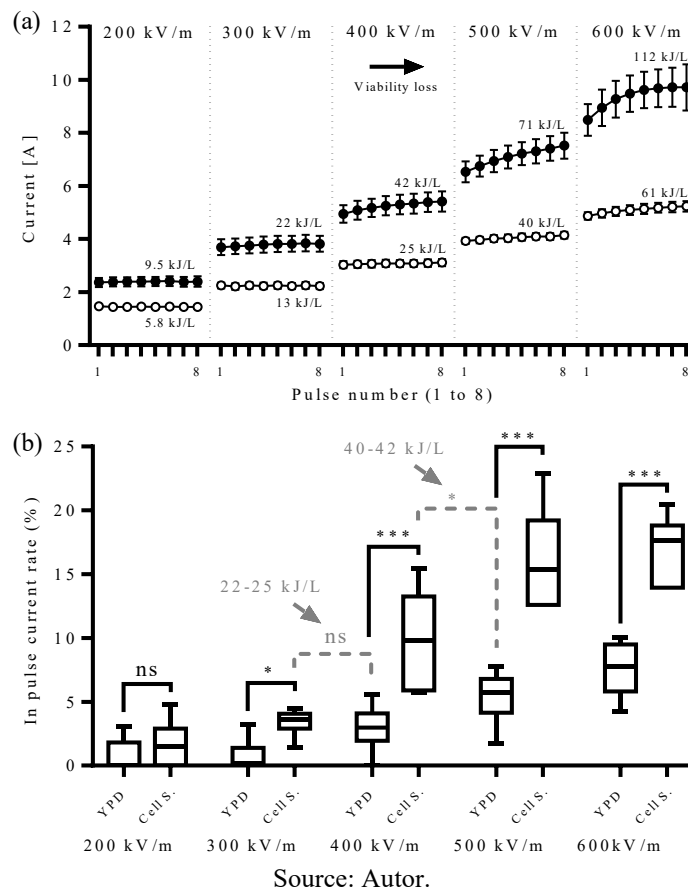
At 500 kV/m we detected yeast viability within the standard limits (LOUREIRO, 2003). The yeast PEF-damage starts at 300 kV/m (GÁŠKOVÁ *et al.*, 1996), and irreversible electroporation threshold at dense cell suspension is reported to be 750 kV/m (EL ZAKHEM *et al.*, 2006). The 500 kV/m threshold we observed may be due the lower cell density. At high cell density solutions yeast clusters are formed, thus a larger field is needed for electroporation (MOLINARI; PILOSOF; JAGUS, 2004). The electroporation threshold may shift in the 300 to 800 kV/m range as it is also dependent on the external buffer (EMANUEL; ROMAN; CAHAN, 2019; PUÉRTOLAS *et al.*, 2009), yeast phase (MOLINARI; PILOSOF;

JAGUS, 2004), temperature (GOLBERG; FISCHER; RUBINSKY, 2010) and cell concentration (EMANUEL; ROMAN; CAHAN, 2019). Moreover, the cell geometry and distribution of cell sizes interfere (LEBOVKA; VOROBIEV, 2004). At 500 kV/m (*i.e.,* when the loss of viability is greater than 90%), it is possible to differentiate the current change between the electroporation protocol, *i.e.*, 400 and 500 kV/m. In our results the current change method is not sensitive to small loss of viability (less than 10 %) or detection of changes in the cell wall.

Figure 27 – (a) Cell viability and conductivity increase due to electroporation protocol amplitude. The errors bars are shorter than the height of the symbol in viability when 0, 200, 300 kV/m. Yeast maximum limit described as clear bottled white wine (LOUREIRO, 2003), unit adequation was realized with (MAYER; GOIN; ZIMMERMANN, 1986). (b) SEM image of yeast cell without electroporation pulses. (c) 200 kV/m, (d) 300 kV/m, (e) 400 kV/m and (f) 500 kV/m. White arrows indicate surface damage.
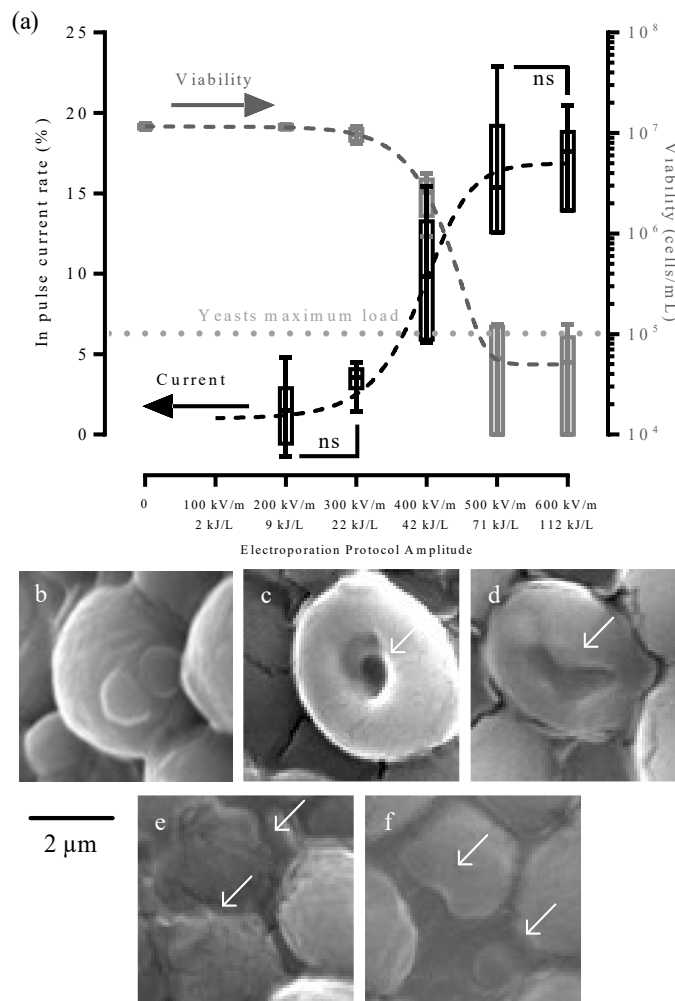
Source: Autor.

5 DIELECTRIC DISPERSION MODULATED SENSING OF YEAST SUSPENSION ELECTROPORATION

In this section we will discuss some of latest experimental results that were published at (PINTARELLI *et al.*, 2022). **The paper is reprinted at Appendix C with permission.** We evaluated the effects of electroporation on the dielectric spectrum of cell suspensions. This evaluation can provide insights into the development of electroporation/PEF high frequency (>10 kHz) sensors. New sensors can be designed to operate in a frequency range adequate for detecting membrane changes while avoiding sub-10 kHz PEF direct current polarization disturbances. This technique provides more accurate readings of electroporation mechanisms to control and optimize industrial processes. To demonstrate the feasibility of supervising electroporation, we propose a numerical study on the sensing of the cell suspension dielectric dispersion.

Yeast cell suspension is known to have well-defined β-dielectric dispersion in the frequency range of 0.1–1 MHz due to the cell membrane, and the yeast *Saccharomyces cerevisiae* have detailed electrical properties literature and their ellipsoidal shape are often approximated as a two-shell sphere (ASAMI; YONEZAWA, 1996; HÖLZEL; LAMPRECHT, 1992; RAICU; RAICU; TURCU, 1996). The electroporation model is used to calculate changes in the membrane conductivity (σ_m) during electroporation. A two-shell model is used to represent the yeast cell under 50 µs (10 to 60 µs) and 1 µs (2 to 3 µs), 400 kV/m PEF. We used low yeast concentration ratio (1% yeast concentration ratio which is approximately 2×10^8 cells/mL). This is a typical yeast concentration from the experimental point of view (EL ZAKHEM *et al.*, 2006). The volumetric model containing one cell is shown in Figure 28. Three external buffers were studied: σ_{Low}, σ_{Med}, and σ_{High} buffer (1 mS/m, 50 mS/m, and 0.1 S/m). The σ_{High} medium is more typical for liquid foods (see Appendix D). We use a useful simplification to model the system's frequency response, which is the assumption that the system is time-invariant on a small scale; thus, all variations occur as sinusoidal signals, and the suspension dielectric spectrum is calculated. A computer model is used to calculate the system dielectric dispersion changes due to the cells' membrane and their interaction with the extracellular media and electroporation. COMSOL Multiphysics® version 4.4 software (COMSOL, Inc., Stockholm, Sweden) is used for FEM modeling and 2D electric currents application ('ec', from the COMSOL's AC/DC Module) (COMSOL, 2018). COMSOL was executed on a laptop running Windows 10 (64-bits) (Microsoft Corporation,

WA, USA), with Core i7-4700HQ processor (Intel Corporation, CA, USA), 16 GB RAM and Nvidia GeForce GTX 870M (Nvidia Corporation, CA, EUA).

Figure 28 – Whole-cell model using two shell model. (a) 2D axisymmetric view. (b) Zoomed membrane view. (c) Half-cut 3D cylindrical model derived from the 2D shaft rotation. The colour scheme is yellow = intracellular media, magenta = cell's membrane, purple = cell's wall, and grey = extracellular media (electroporation buffer). Figures show the case of a single cell with 4 μm external radius.

Source: Author.
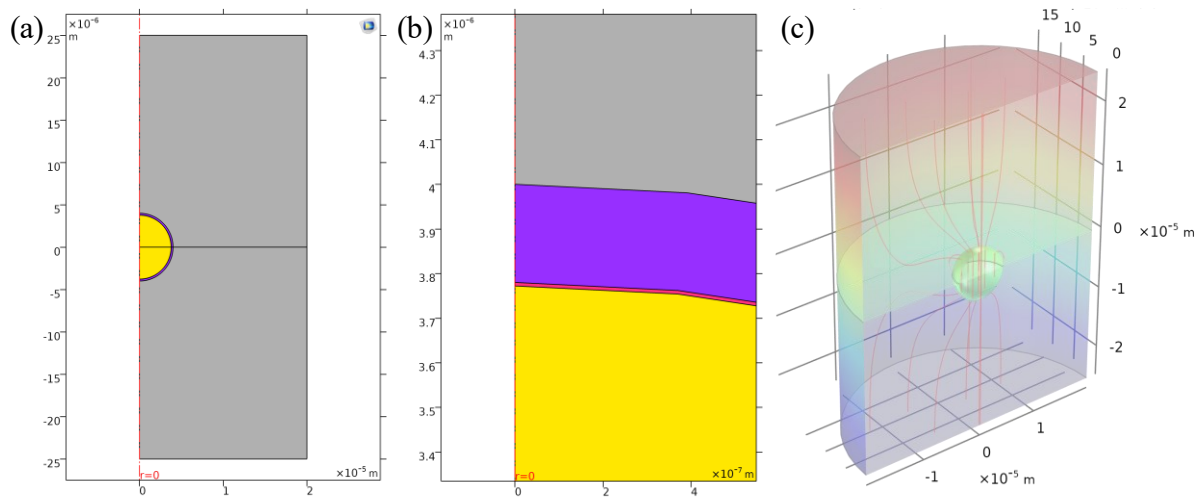
A custom mesh is designed for this study as shown in Figure 29. The mesh is edge mapped for bilateral symmetry and mapped as 10 per 1000 quadratic elements for each cell's membrane and wall. Other elements are made using COMSOL's free triangular semiconductor 'fine' pre-set. The maximum element size is set as 3.3×10^{-7} m. The mesh consists of 171,416 (single cell) to 478,398 (three cells) elements. The transmembrane voltage due to PEF can be analytically calculated using the Laplace equation (SUZUKI *et al.*, 2011). We validated the numerical calculations by comparing them to the analytical solution proposed by (GIMSA; WACHNER, 2001). The maximum relative error between the analytical solution and the computer simulation was 5.18%. Therefore, we considered our model to be sufficiently accurate for our study.

The membrane is always more insulating than the medium, hence it obstructs the low-frequency current passage. The membrane causes the main β-dispersion. If the electrical characteristics of the interfaces change, it is expected that the dispersion will shift. The dispersion shifting and plateau amplitude are correlated to the interfaces electrical property's

ratio $\left(\frac{\sigma_1+j\varepsilon_1}{\sigma_2+j\varepsilon_2}\right)$. We evaluate the equipotential and current density lines. The contour plots of equipotential lines (horizontal) and current density lines (vertical) are shown in Figure 30, Figure 31 and Figure 32 for σ_{Low}, σ_{Med}, and σ_{High} buffer, respectively. The plots are useful to check how the electromagnetic wave sinusoidal signal is distorted by the cell. More 'current lines' means denser electric currents. At σ_{Low} medium, the 100 kHz current mostly passes through the cell. The same effect occurs at proximately 1 MHz for other media. If a signal is supposed to sense changes in the cell wall and membranes, it must be in a frequency at which there is a voltage drop in those components. Figure 33 shows the 'electric profile', *i.e.* the local voltage at cell's Y-axis (vertical). Gradient voltages are possible in the cell membrane for all media. On the other hand, the σ_{Med} buffer is the most susceptible medium for wall voltage drop. Over 100 MHz there is no voltage drop across neither cell components. We also evaluate the voltage drop for the arc lengths step of 800 ηm. The results are shown in Figure 34. There is a voltage drop on a vast part of the cell. Another perspective of the same data is the differential voltage evaluation at membrane and wall due frequency, as shown in Figure 48. The 100 kHz is the upper limit to sense membrane at σ_{Med} and σ_{High} buffers. The σ_{Med} buffer is less susceptible to sense the wall. Using the σ_{High} buffer, it is possible to discern the membrane and wall individually. On the other hand, for sensing membrane, we must use over 10 kHz as lower frequency may be contaminated with dispersion due to electrode-solution interface.

Figure 29 – Detail of the whole-cell mesh. Zoom at (a) whole cell (b) wall zoomed and (c) membrane.
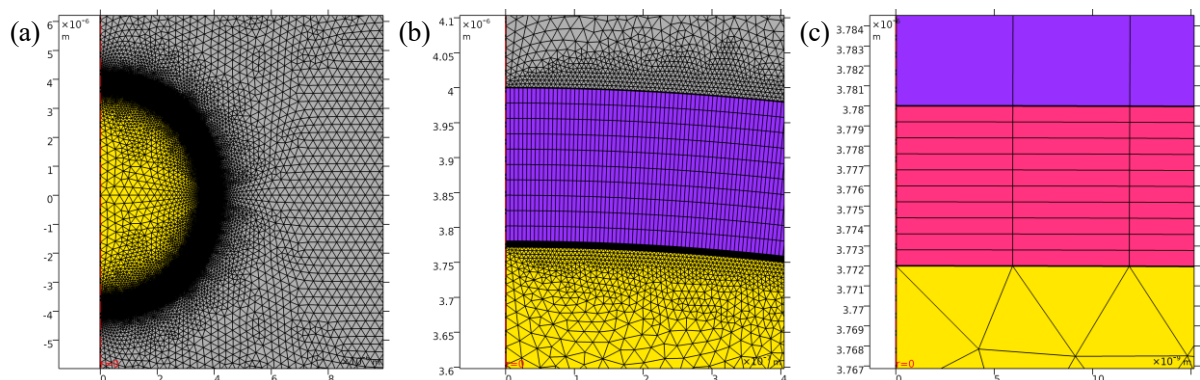
Source: Author.

Figure 30 – Contour plots of electric potential (horizontal black lines) and current density (grey vertical lines) from 1 kHz to 100 MHz with σ_{Low} buffer. (a) 1 kHz, (b) 10 kHz, (c) 100 kHz, (d) 1 MHz, (e) 10 MHz, and (f) 100 MHz.
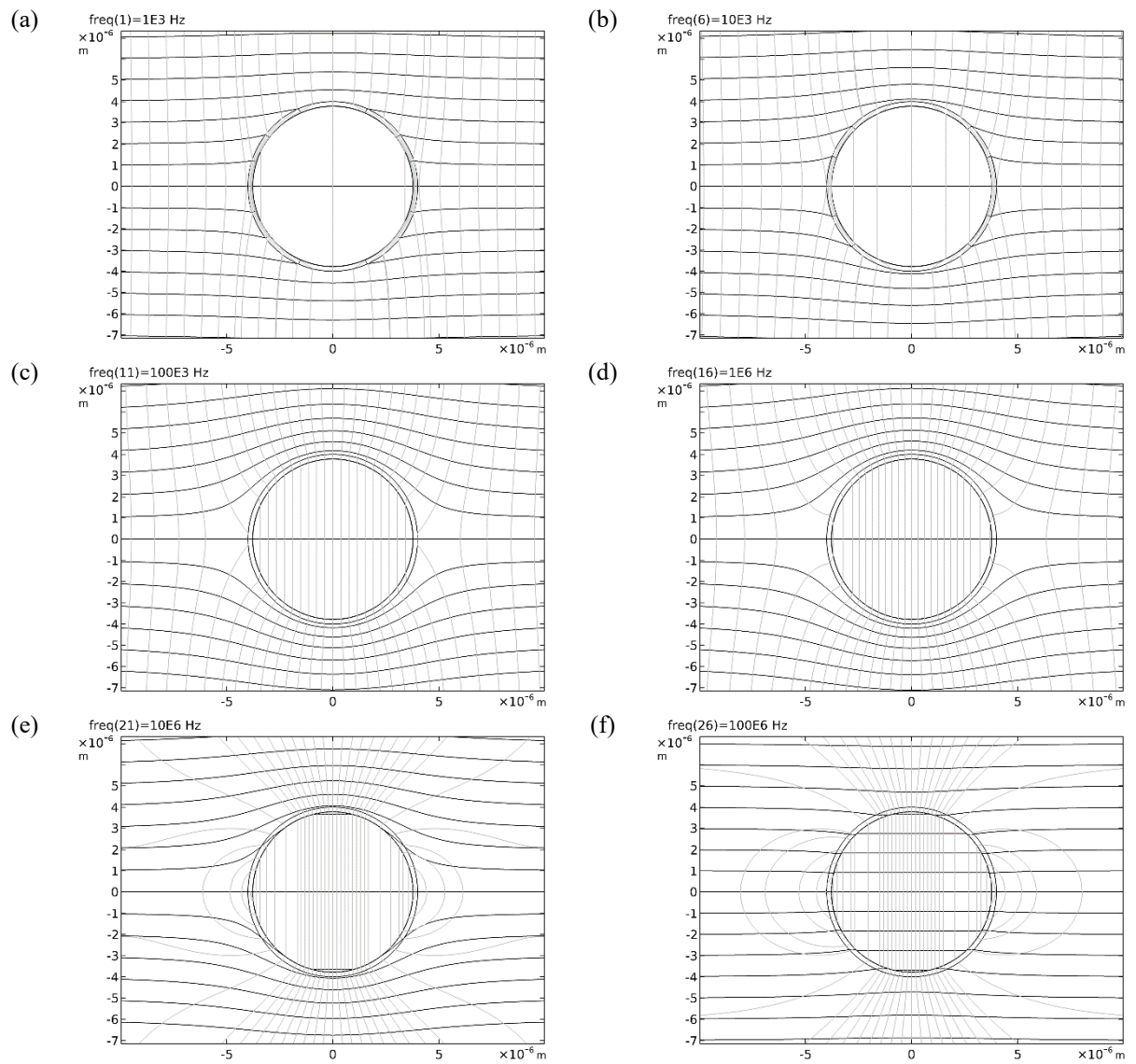
Source: Author.

Figure 31 – Electric equipotential lines (horizontal black lines) and current density (grey vertical lines) from 1kHz to 100 MHz with σ_{Med} buffer. (a) 1 kHz, (b) 10 kHz, (c) 100 kHz, (d) 1 MHz, (e) 10 MHz, and (f) 100 MHz.
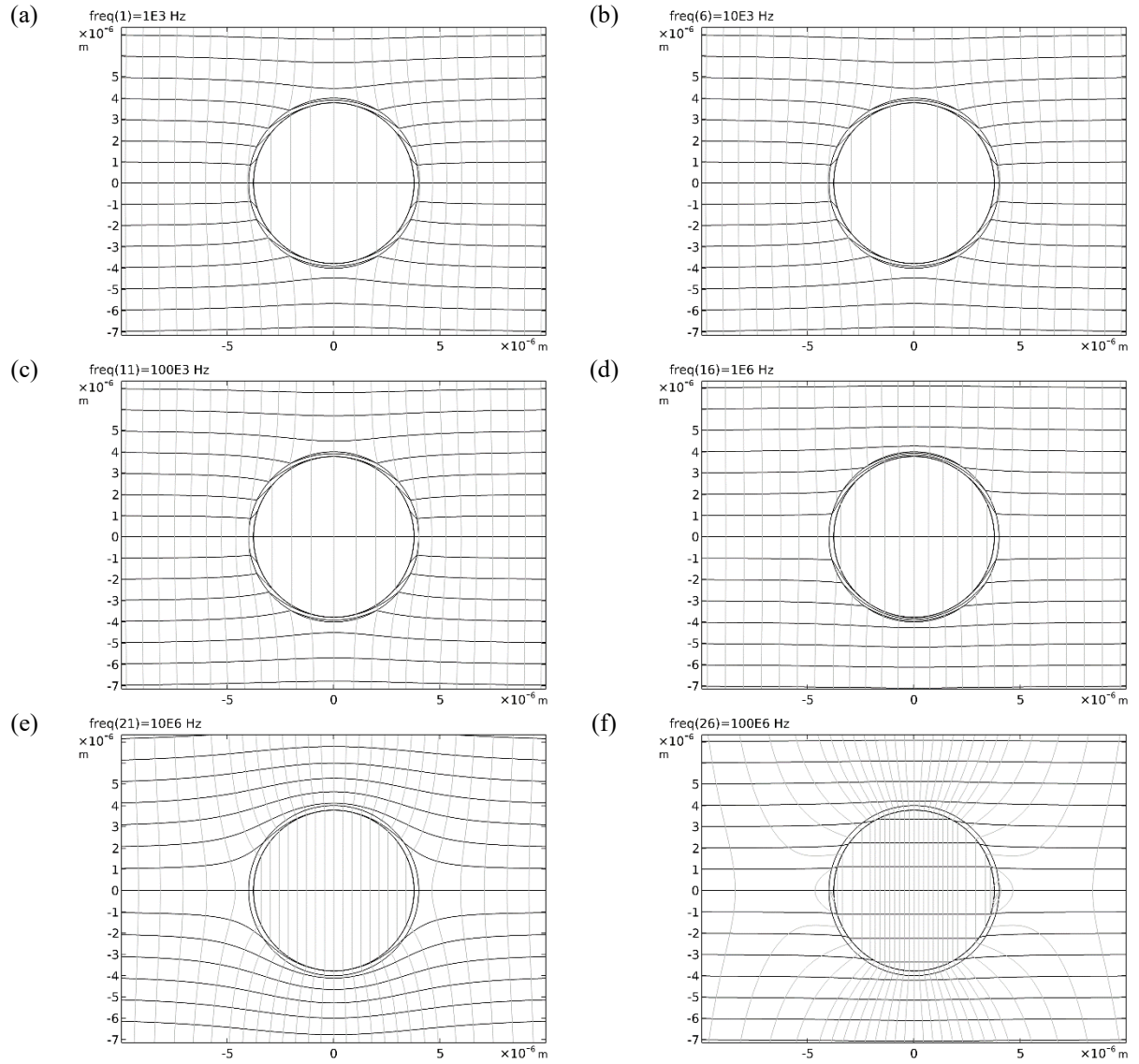
Source: Author.

Figure 32 – Contour plots of electric potential (horizontal black lines) and current density (grey vertical lines) from 1kHz to 100 MHz with σ_{High} buffer. (a) 1 kHz, (b) 10 kHz, (c) 100 kHz, (d) 1 MHz, (e) 10 MHz, and (f) 100 MHz.
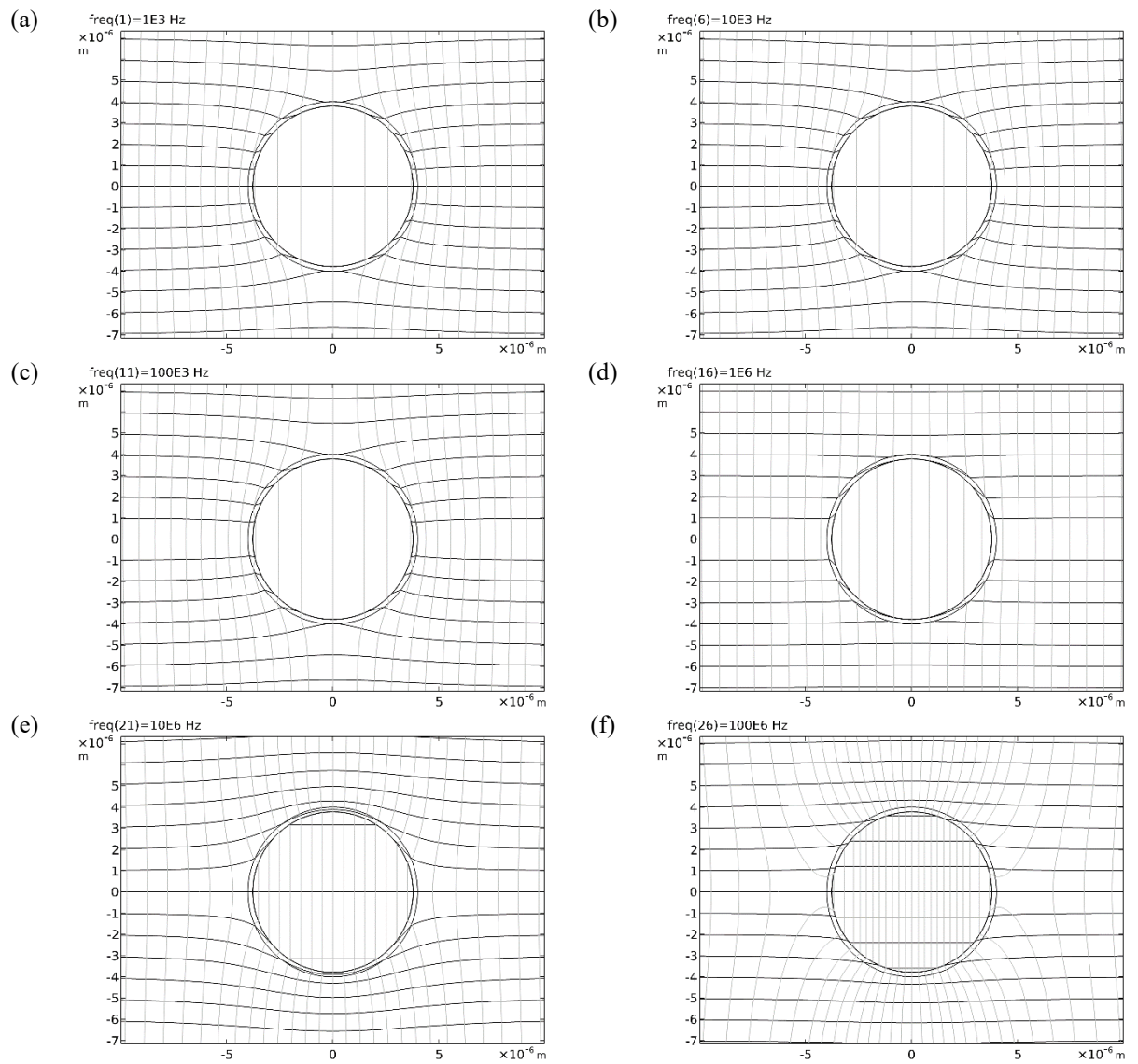
Source: Author.

Figure 33 – Electric potential profiles across the longitudinal axis (line AB) and its zoom (at cell's wall and membrane) for (a and b) σ_{Low} buffer, (c and d) σ_{Med} buffer, and (e and f) σ_{High} buffer. The dotted lines used in the zooms demarcates the cell's wall and membrane.
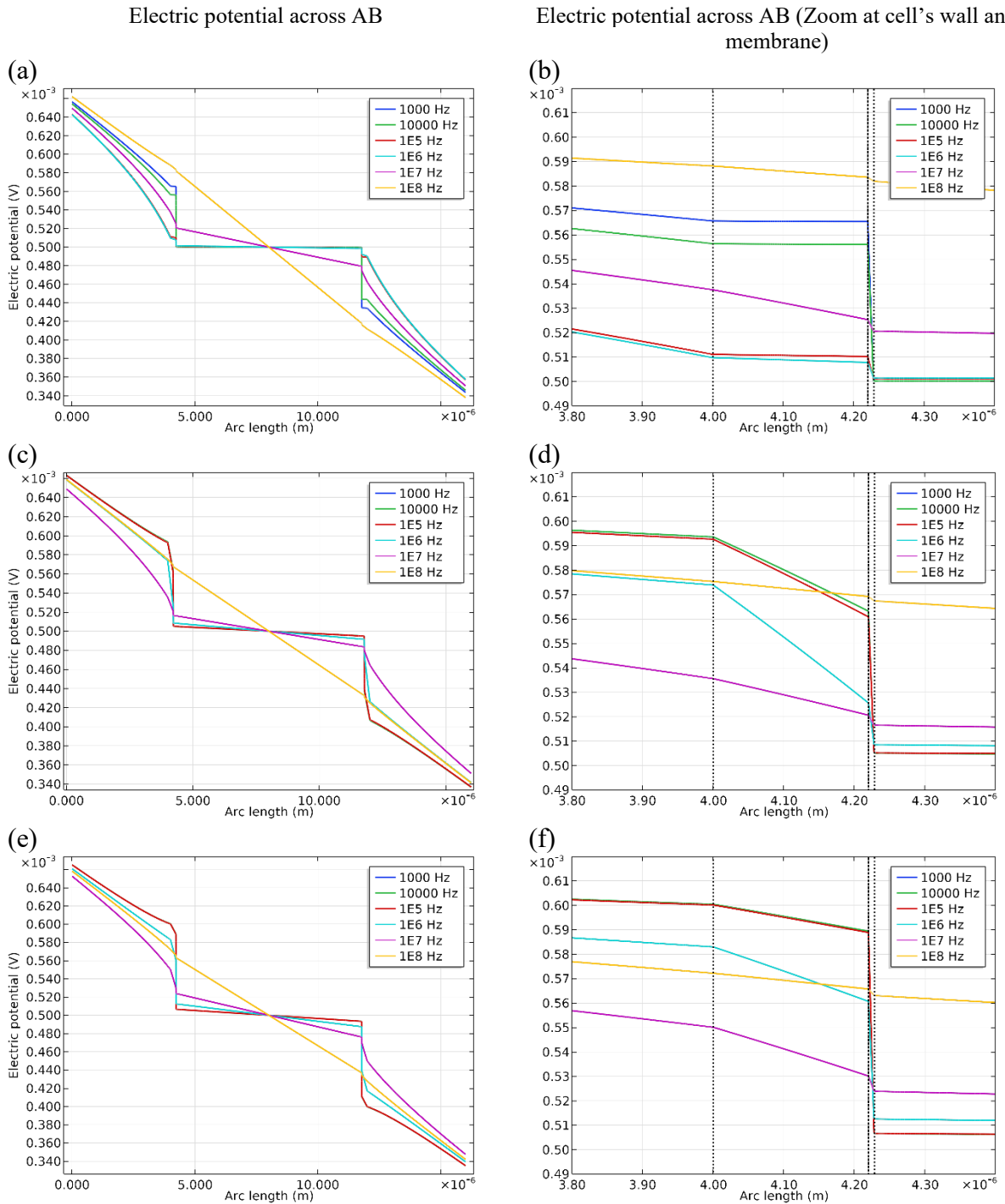
Source: Author.

Figure 34 – Electric potential profiles across the diverse longitudinal axis for (a) σ_{Low} buffer, (b) σ_{Med} buffer, and (c) σ_{High} buffer. The dotted lines used in the zooms demarcates the cell's wall and membrane. (d) The location of the lines to study electrical potential profiles (800 ηm steps).

(a)

(b)

(c)

(d)
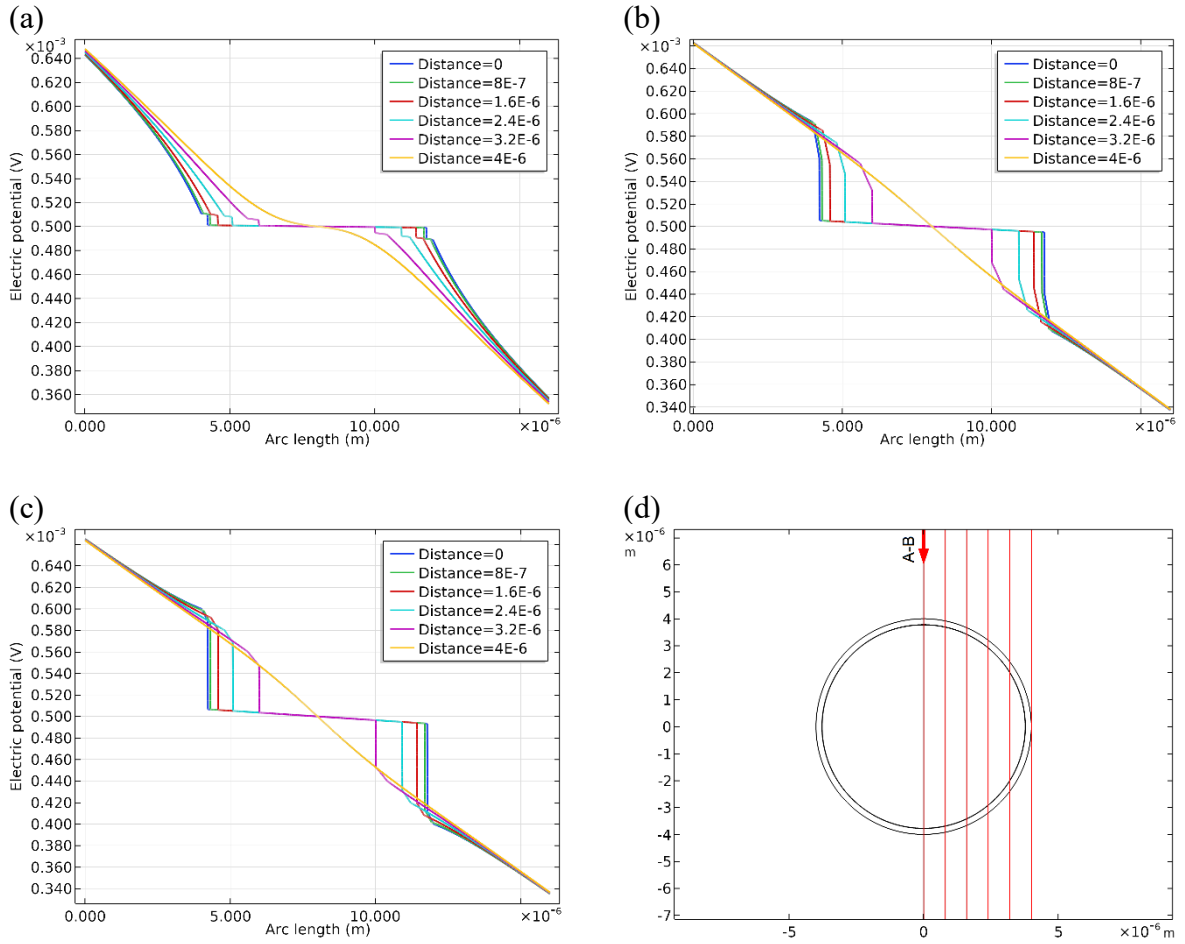
Source: Author.

Figure 35 – Voltage difference at cell membrane and wall. Measurements at the cell pole. (a) 1e-3 S/m, (b) 50e-3 S/m and (c) 0.1 S/m buffer.
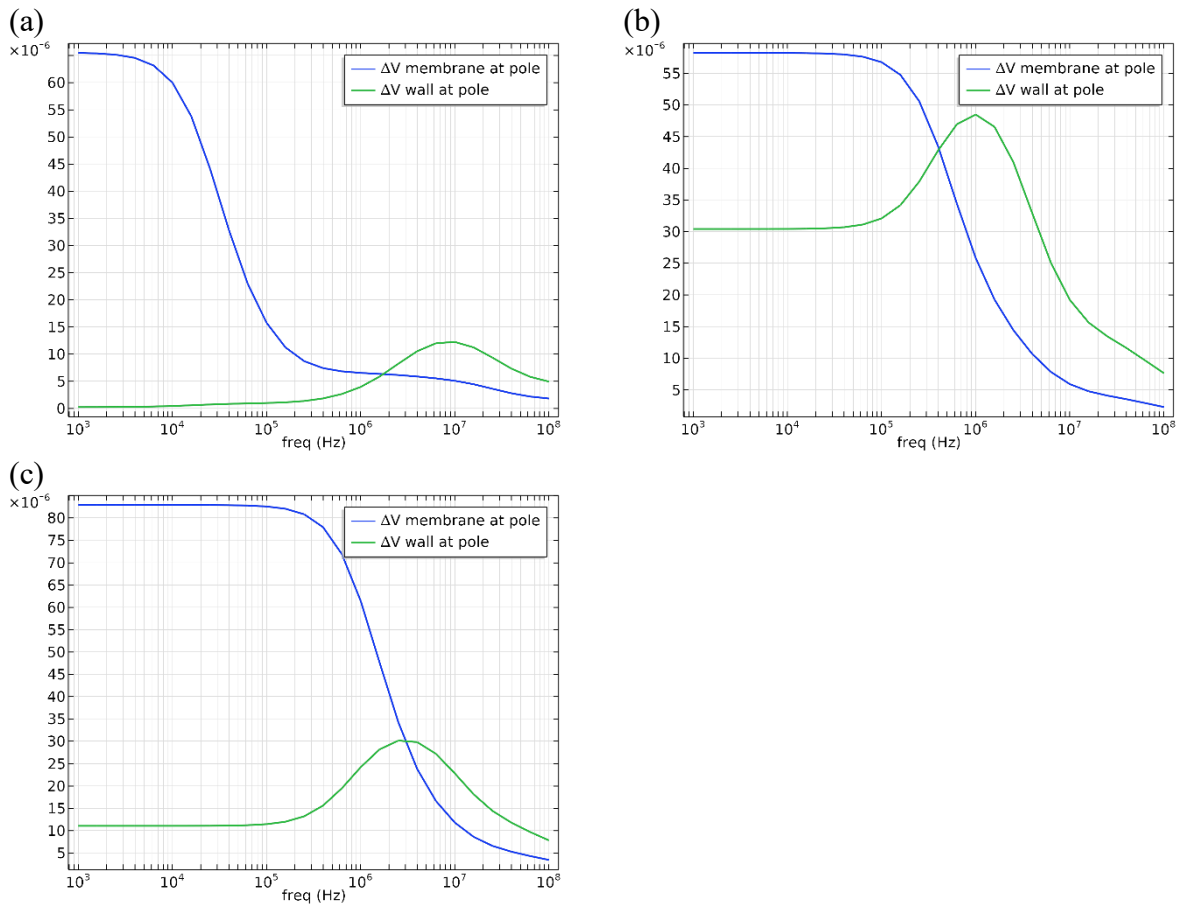
Source: Author.

When the transmembrane voltage reaches a certain value (~0.2 – 1 V) (TEISSIÉ; ROLS, 1993), membrane permeability increases as a consequence of the formation of hydrophilic pores in the lipid bilayer leading to an increase in membrane conductivity. The membrane conductivity, transmembrane voltage, and solution's relative permittivity when using 50 µs PEF is shown in Figure 36. During 10 to 60 µs, the PEF is enabled. All buffers are adequate to induce electroporation transmembrane voltages. The σ_{Low} buffer has the slowest time dynamics (see the post-60 µs dynamism of membrane conductivity and transmembrane voltage). This occurs due to the poor buffer-cell-interface conductive coupling, which leads to slower capacitive charging and discharging processes. The membrane state change is practically instantaneous when using σ_{Med} and σ_{High} buffers. Also, the extent of membrane area affected by electroporation is higher when σ_{High} buffer is used (approximately $-\pi/2$ to $\pi/2$). The dispersion centre depends on the system's characteristics; the dispersion centre is approximately 10 kHz for σ_{Low} buffer and 500 kHz for σ_{Med} and σ_{High}

buffer (see the solution's relative permittivity at Figure 36). Frequencies higher than 1 MHz are not suitable for sensing the membrane dispersion as the displacement current can flow through the cell (membrane impedance is negligible), which is called 'electrically invisible'. This work, as well as others in the literature, have demonstrated that to sense the cell's primally barrier (*i.e.* cell membrane), we should not exceed approximately 1-100 MHz (ASAMI; YONEZAWA, 1996; GOWRISHANKAR; WEAVER, 2003).

Figure 36 - Results of 50 µs PEF: Membrane conductivity, transmembrane voltage and solution equivalent relative permittivity. The horizontal axis is the time in µs. The PEF starts at 10 µs, and ends at 60 µs. The vertical axis of the membrane conductivity and transmembrane voltage figures represent the angle location in the membrane. The vertical axis of solution relative permittivity figures is the sensing frequency (1 kHz to 100 MHz range).
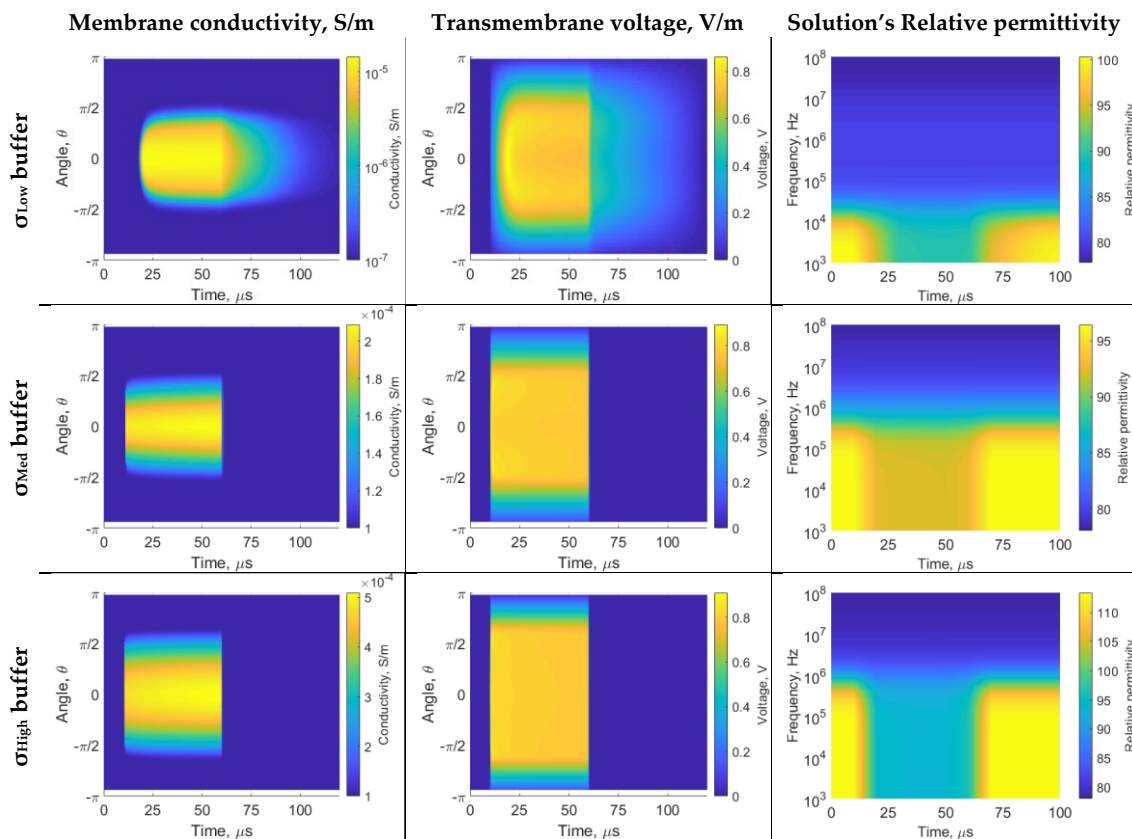
Source: Author.

The 1 µs PEF results are shown in Figure 37. During 2 to 3 µs, the PEF is enabled. The σ_{Low} buffer slow dynamic cannot charge the membrane sufficiently for electroporation (the membrane charges up to 200 mV). Thus, the membrane conductivity change is negligible, and the spectrum does not change significantly (*i.e.*, unsuccessful electroporation).

The σ_{Med} buffer can charge the membrane sufficiently for electroporation. However, the 1 µs does not saturate conductivity as seen in 50 µs PEF (Figure 36). Thus, σ_{Med} buffer β-dispersion decays only at the end of the 1 us pulse.

Figure 37 **-** Results of 1 µs PEF: Membrane conductivity, transmembrane voltage and solution equivalent relative permittivity. The axis description is used within Figure 3. The PEF starts at 2 µs, and ends at 3 µs. When using σ_{Low}, the membrane conductivity changes are lower than 0.1%.
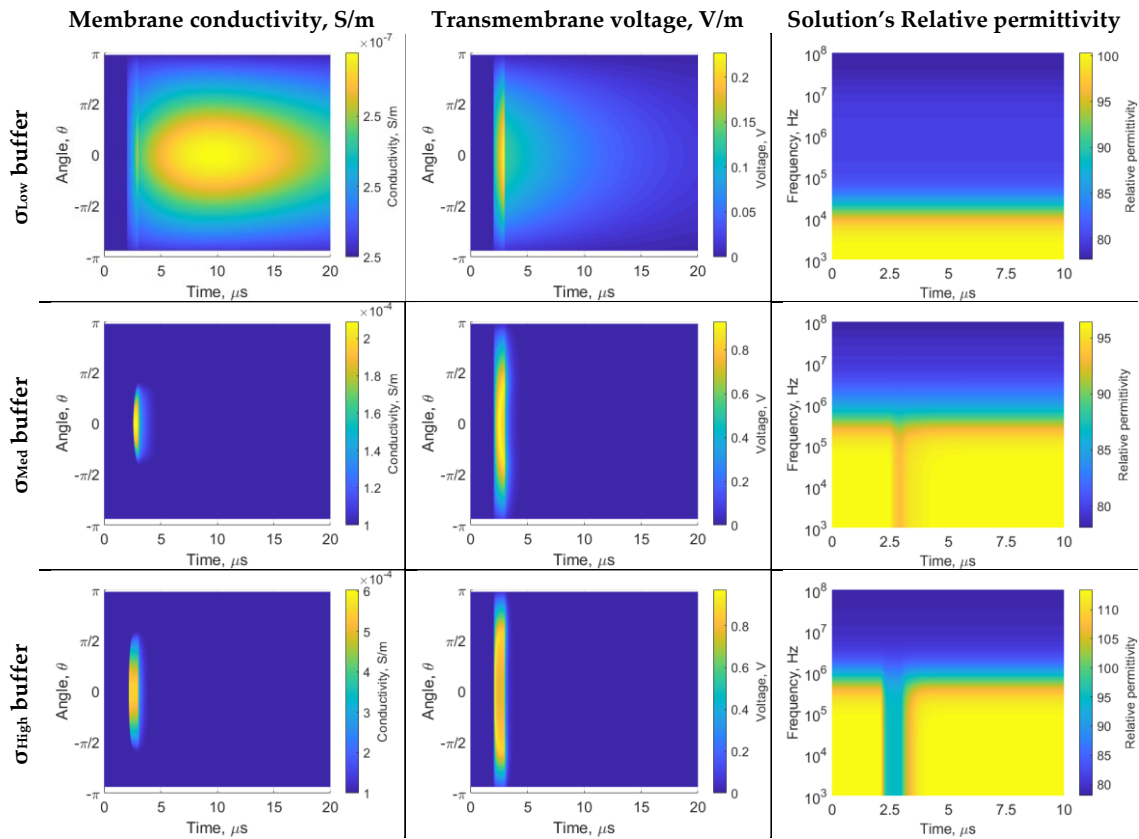
Source: Author.

[blank page]

6 SENSING THE DYNAMICS OF COMPLEX ELECTRICAL PROPERTIES UNDER PEF: *IN VITRO* VEGETAL STUDY

In this chapter, we evaluate the 'DC' and 100 kHz impedance reading due to the PEF amplitude and DC pulse polarity. We will use *in vitro* vegetal tissue to show the feasibility of using the proposed sensing method in tissues. Also, tissues may be able to demonstrate the effects of the electroporation in a higher extend comparing to the cell suspension. The PEF equipment and measurement system is described in the previous chapter. We also propose a simple 2D geometry model that describes the vegetal β-dispersion.

6.1 MATERIALS AND METHODS

6.1.1 *In vitro* experiments

Potato tubers (*Solanum tuberosum*) were purchased from local stores. The producer (Rio Bonito Orgânicos, Itatinga, Brazil) is certified by the Brazilian Ministry of Agriculture, Livestock and Food Supply (MAPA) audit for organically grown products. The Organic Conformity Assessment Organization accredited by MAPA provides the traceability of the product at https://conecta.paripassu.com.br (traceability code PQV98MD1WM64AEOJ). This study complies with relevant institutional, national, and international guidelines and legislation on experimental research and field studies on plants or plant material (ANDRADE *et al.*, 2022).

Each one of the groups had seven to nine samples. Potatoes were not peeled and were individually cut before the experiment using regulable stainless steel vegetable mandolin model Benriner K91 (Benriner Co., Japan). Our potato discs (slices) were 1 ± 0.1 mm height (see Figure 38a). Our cuts were orthogonal to the proximal-distal axis. We discarded the 20 % of the proximal and distal portions to avoid using tissues from the bud and stem end. We used the centre vegetable portion, which is composed by the parenchyma tissue (uniform shaped cells in all directions), and pith tissue with its medullary rays (see Figure 38b) (GROMMERS; VAN DER KROGT, 2009; OEY *et al.*, 2016). We used parallel plate disc electrodes with 29.7 mm diameter (see section 3.1.6 for electrodes characteristics), which covered those tissue portion (see Figure 38c). The electrode embraced and held the samples with plastic pressure claws at 1 mm distance (d = 1 mm). The millimetre electrode distance facilitates obtaining high electric fields compatible with electroporation. The electrodes were cleaned with 70%

ethyl alcohol and dried before the sample insertion. All samples were submitted to the same process (insertion and removal of the electrode system); this includes the control samples. We monitored the potatoes temperature using an infrared thermometer; the temperatures were 20 $\pm$ 1.5 ºC.

Electric pulse protocols were generated by custom made generator (see Figure 16, monopolar and bipolar). Protocols were eight pulses of 100 µs and a repetition rate of 0.1 Hz. The low repetition rate was used to corroborate that the DUT discharged and mitigate interference from electroporation memories and electric double layer charging. This protocol is similar to European Standard Operating Procedures of Electrochemotherapy (ESOPE) (GEHL *et al.*, 2018). Amplitudes (voltage output of the electroporator, V) were varied as the electroporation mainly depends on it. The magnitude was estimated as the voltage applied divided by the distance between the electrodes. It has been assessed the effect of amplitude applying protocols of 12.5, 25 and 50 kV/m. A sawtooth (*i.e.* ramp) wave study was used to measure the sample dependence on the voltage. We used a 150 µs and 1 ms single triangular wave. We user each sample only once (one PEF application only). The electric field (E) value was estimated using E = V/d. An electroporation measurement system with pre and post impedance analysis and voltage and current measurements was configured for this experiment as described in chapter 4. In this chapter we will call the apparent impedance as 'DC resistance' to facilitate comparison with current literature. Current-voltage measurements were acquired in the first and last (eight) pulse of the protocol at 1 GHz using a digital oscilloscope Tektronix DPO 2012B with two Tektronix TPP0200 200 MHz (Tektronix, Inc., Oregon, United States). A MATLAB R2018b script was used to calculate the sample's impedance at DC and 100 kHz. The acquisition equipment errors were diagnosed, and the worst-case error equals to 12 %. The electrical impedance study before and after PEF was performed with 4294A and 16047E adapter (Agilent Technologies, California, United States). We used a 100 Hz to 1 MHz frequency range analysis, as this is the main β-dispersion range. The impedance measurements occurred 120 seconds before and after the electroporation protocol.

Figure 38 – (a) Potato slices used (1 mm slices). (b) Longitudinal diagram of a potato tuber. (c) Electrodes position at the sample.

(a)

(b)

(c)
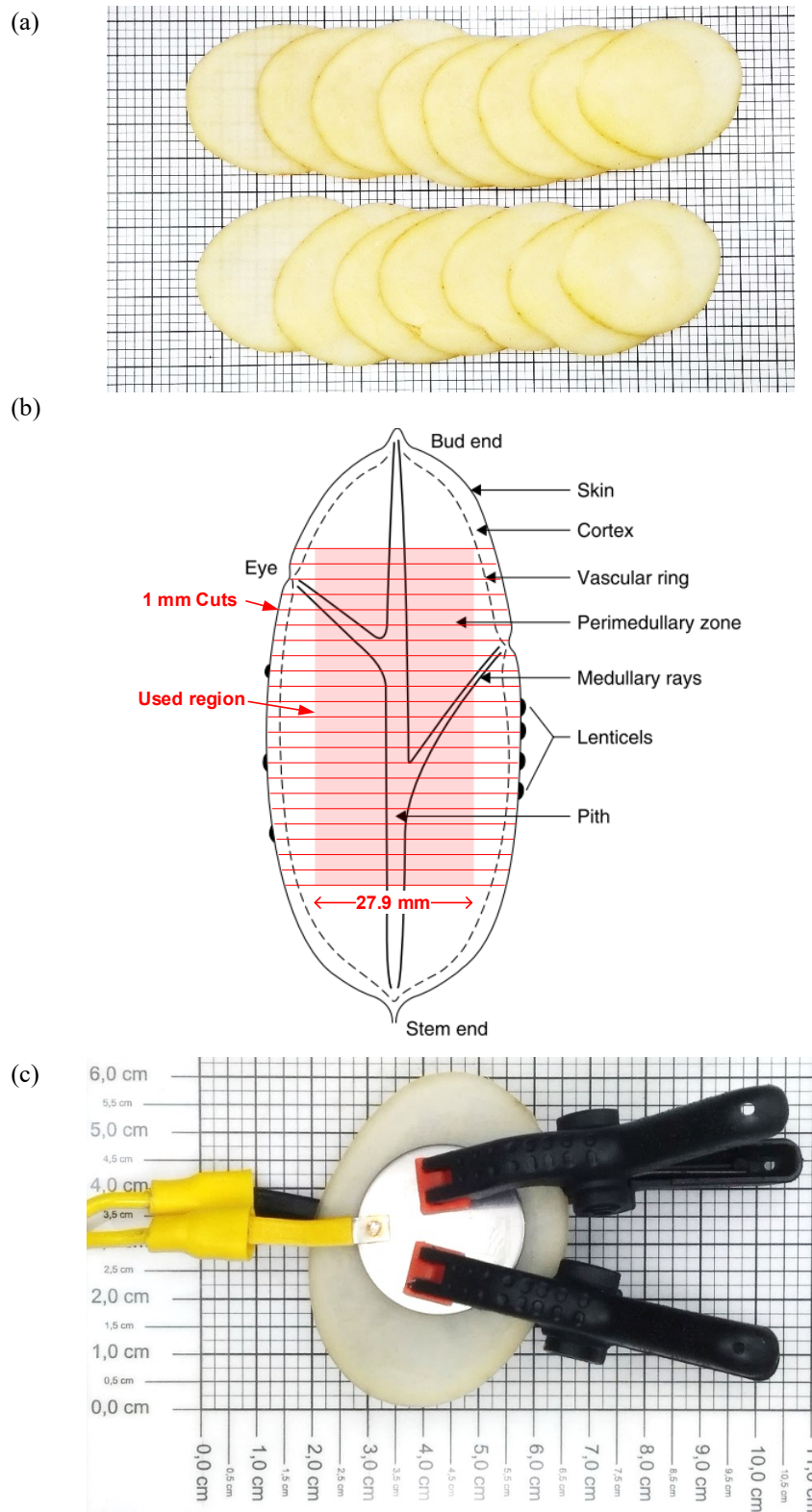
Source: (b) is Adapted from (GROMMERS; VAN DER KROGT, 2009). (a) and (c) from the author.

We execute a histology study to verify for cell destruction. The tissue slice was cut using a sharp razor blade, a drop of Methylene blue (0.2% $C_{16}H_{18}N_3SCl$) was placed to mark cell walls, and the tissue is observed in the optical microscope Biofocus (BIO1600BA) (see Figure 39). Dead cells typically show rupture of the membrane and lose their natural morphological formation. Moreover, as potato tubers are known to show dark staining due electroporation. The 'dark staining' is the effect of the oxidation due to decompartmentalization of certain enzymes and substrates. The samples were stored in a sealed place with room temperature at 25 °C and in an acid environment (sealed environment with wet paper towel with 2.5 ml of citric acid 4% diluted in deionized water) for a period of 24 h. Electroporation technique overly extracts polyphenol oxidase enzyme which reacts with the oxygen, this reaction leads to a darkening of the vegetable tissue (BERKENBROCK *et al.*, 2019; IVORRA; MIR; RUBINSKY, 2009).

Figure 39 – Histological study at microscope slice.
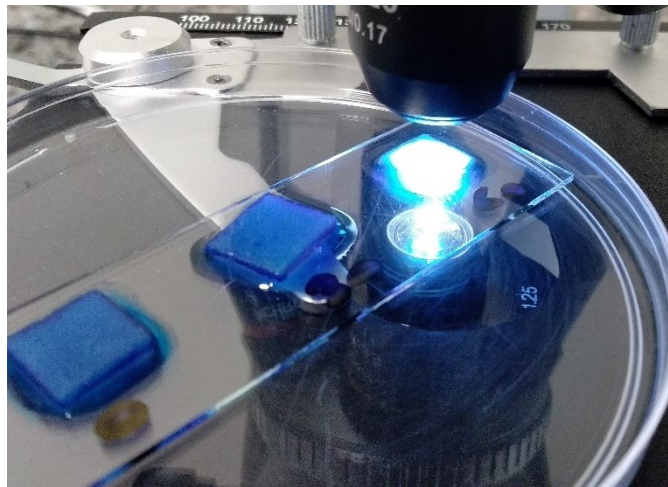
Source: Author.

6.1.2 Vegetal tissue model

Similarly to Chapter 5, we use a useful simplification to model the system's frequency response which is the assumption that all variations in time occur as sinusoidal signals. Thus, solving methods will consider this problem as time-harmonic, and it can be formulated as stationary. A frequency range from 10 kHz to 1 MHz is employed, as those are one decade from the 100 kHz membrane sensing frequency. This approach applies to all

periodic signals applied to linear systems. Furthermore, we can use Fourier analysis to study the system's frequency response.

The vegetal tissue model is a novel 2D 'honeycomb' infinitesimal geometry of hexagonal cells containing intracellular fluid, membrane, wall, and intracellular space. The model represents the parenchyma tissue, which is the most uniform tissue of the potato tuber (GROMMERS; VAN DER KROGT, 2009; OEY *et al.*, 2016). The geometry is shown at Figure 40a. The vertical side boundaries are periodic. We used an analysis area to compensate the 'natural' current diffraction that happen at an 'infinite' tissue (see the voltage measurement location at Figure 40a). There is a current bias of 1×10^{-3} A between the top and bottom boundaries used for small signal analysis. We suppose that our simulation volume behaves as an infinitesimal volume. Cell structural parameters of potato tuber tissue are described by literature (KONSTANKIEWICZ *et al.*, 2002; REEVE; TIMM; WEAVER, 1971). However, we did not find previous reports on the cell parts electrical characteristics. We used some parameters measured in yeast (HÖLZEL; LAMPRECHT, 1992), and changed the extracellular, cytoplasm's, and membrane's conductivity to approach our *in vitro* measurements. We used the Appendix D data, N = 69, to calculate *in vitro* equivalent permittivity and conductivity (we used the dimensional chamber parameters to obtain the permittivity and conductivity). The used electrical parameters are given in Table 3.

COMSOL Multiphysics® version 4.4 software (COMSOL, Inc., Stockholm, Sweden) is used for FEM modeling and 2D electric currents application ('ec', from the COMSOL's AC/DC Module) (COMSOL, 2018). COMSOL was executed on a laptop running Windows 10 (64-bits) (Microsoft Corporation, WA, USA), with Core i7-4700HQ processor (Intel Corporation, CA, USA), 16 GB RAM and Nvidia GeForce GTX 870M (Nvidia Corporation, CA, EUA). The mesh was generated using the COMSOL free triangular semiconductor 'fine' pre-set selecting a piece of the model as the Figure 40b. This piece was mapped to the other seven similar objects. The total element number was approximately 4 million. The detail of the membrane and wall are show in Figure 40c and Figure 40d.

Figure 40 – (a) Hexagonal model of potato tuber tissue. The analysis area (dashed orange) is used to compute the equivalent electrical properties. Voltage is measured at a point on top and bottom of the analysis area. Top and bottom boundaries are the current sources. The vertical boundaries are periodic. The mesh is generated using COMSOL at the dashed blue area. This mesh is mapped to other seven consecutive areas. (b) Detail of the mesh of piece of the hexagonal model. (c) Detail of the membrane. (d) Detail of the wall. Yellow is the intracellular content, pink is the membrane, purple is the wall, and grey is the extracellular media.
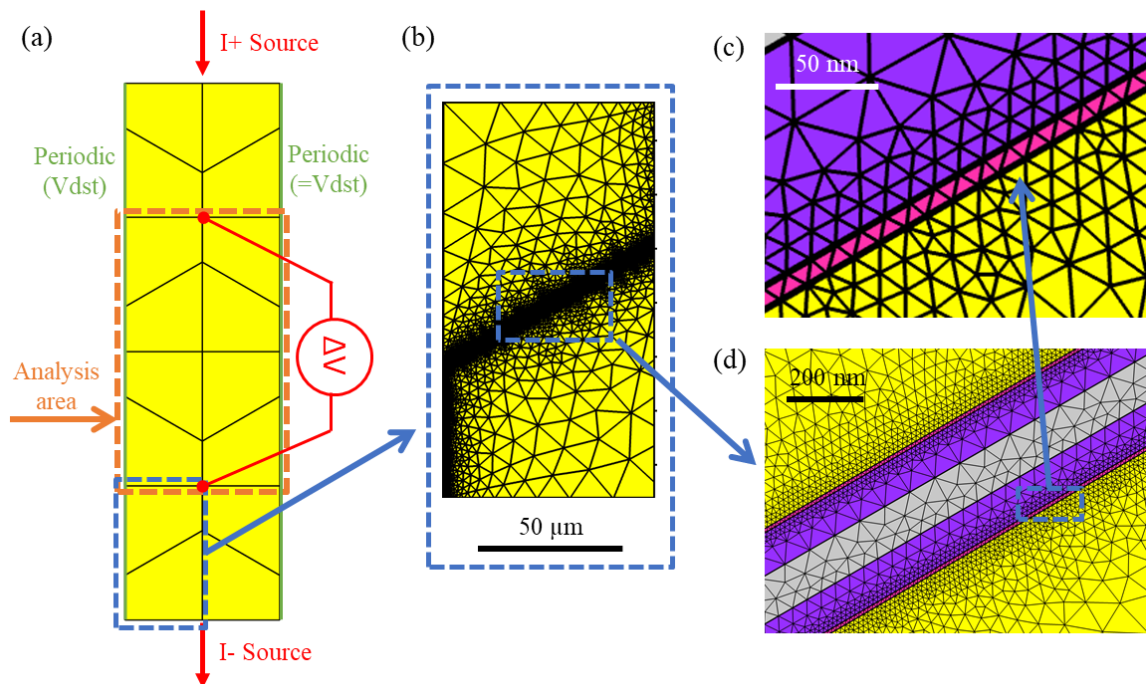
Source: Author.

Table 3 – Geometry parameters for potato tuber tissue modelling.

Description	Value
Extracellular conductivity	0.4 S/m
Extracellular relative permittivity	78
Cytoplasm's conductivity	0.8 S/m
Cytoplasm's relative permittivity	50
Membrane's conductivity	1e-6 S/m
Membrane's relative permittivity	7.6
Cell wall's conductivity	1e-3 S/m
Cell wall's relative permittivity	60

Source: Author.

6.2 RESULTS

Electroporation is generally explained in terms of electric conductivity, thus, the increase in pores increases the conductivity of the membrane. This is equally as worsening the dielectric characteristic of the membrane. In this chapter we use AC frequency superposing the PEF, this approach can sense electroporation. Also, it can introduce further insight in the electroporation modelling detailing as the conductivity can be explained as a complex number, in other words, we may introduce another degree of freedom to analyse electroporation and other voltage dependant phenomena. The nature of electromagnetic waves is explained using imaginary space-time (frequency), therefore using the complex variable to study PEF may give another degree of freedom in terms of PEF sensing and modelling. The use of the instantaneous current and voltage readings on the equipment output has a competitive advantage since its electronic topologies use transistors as on/off switches (*i.e.* operating in saturation and not allowing arbitrary shapes). However, in treatments with high added value, it is possible to more design complex equipment with PEF and small signal generators. Thus, further detailing of the state of electroporation would be possible.

The impedance during the eight pulse 100 μs monopolar PEF is accordingly to Figure 41, and the bipolar PEF is accordingly to Figure 42. The PEF at electroporation levels (> 12.5 kV/m) decreases the apparent impedance (called $|Z|_{DC}$). The 100 kHz show a decrease in the phase during electroporation. The absolute 100 kHz impedance increases during PEF at reversible electroporation (12.5 kV/m) and decreases at irreversible electroporation. The COMSOL calculated equivalent permittivity and conductivity is shown in Figure 43, the model is a good approach specially at 100 kHz. The before and after the frequency spectrum is as Figure 44. The > 25 kV/m PEF changes the spectrum in an irreversible way. The 95% CI deviations are because the tissue is not entirely homogenous, and some variations in the electrode insertion process and delays in the measurement time (see Appendix D). The tissue histology and staining after 24 h is shown in Figure 45 (control data did not stain, data not shown).

Figure 41 – The impedance monitoring during the 8 pulse 100µs monopolar PEF. The dots are the mean. The before and after 'ọ̆' symbol at Z_{100kHz} plots are taken using the impedance analyser. Values are means and 95 % CI.
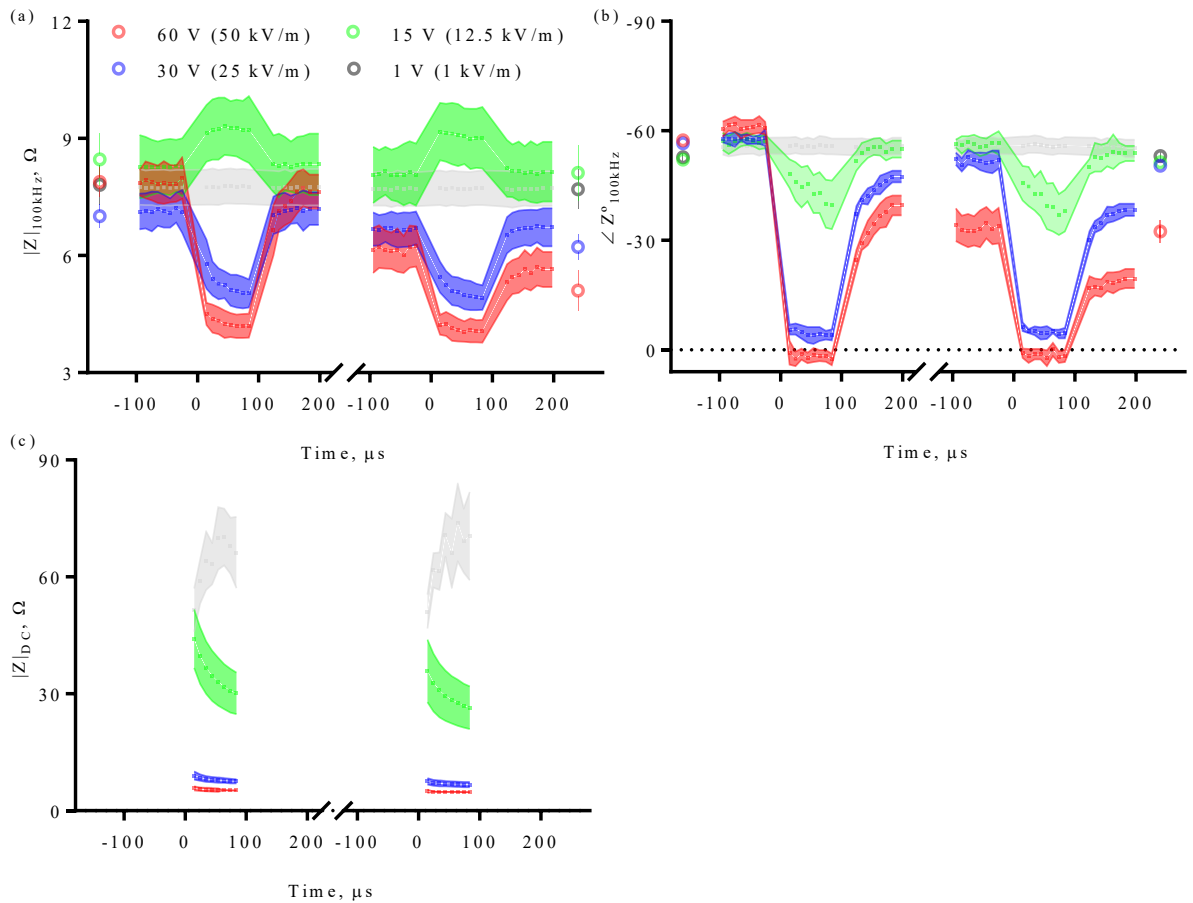
Source: Autor.

Figure 42 – The impedance monitoring during the 8 pulse 100µs bipolar PEF.
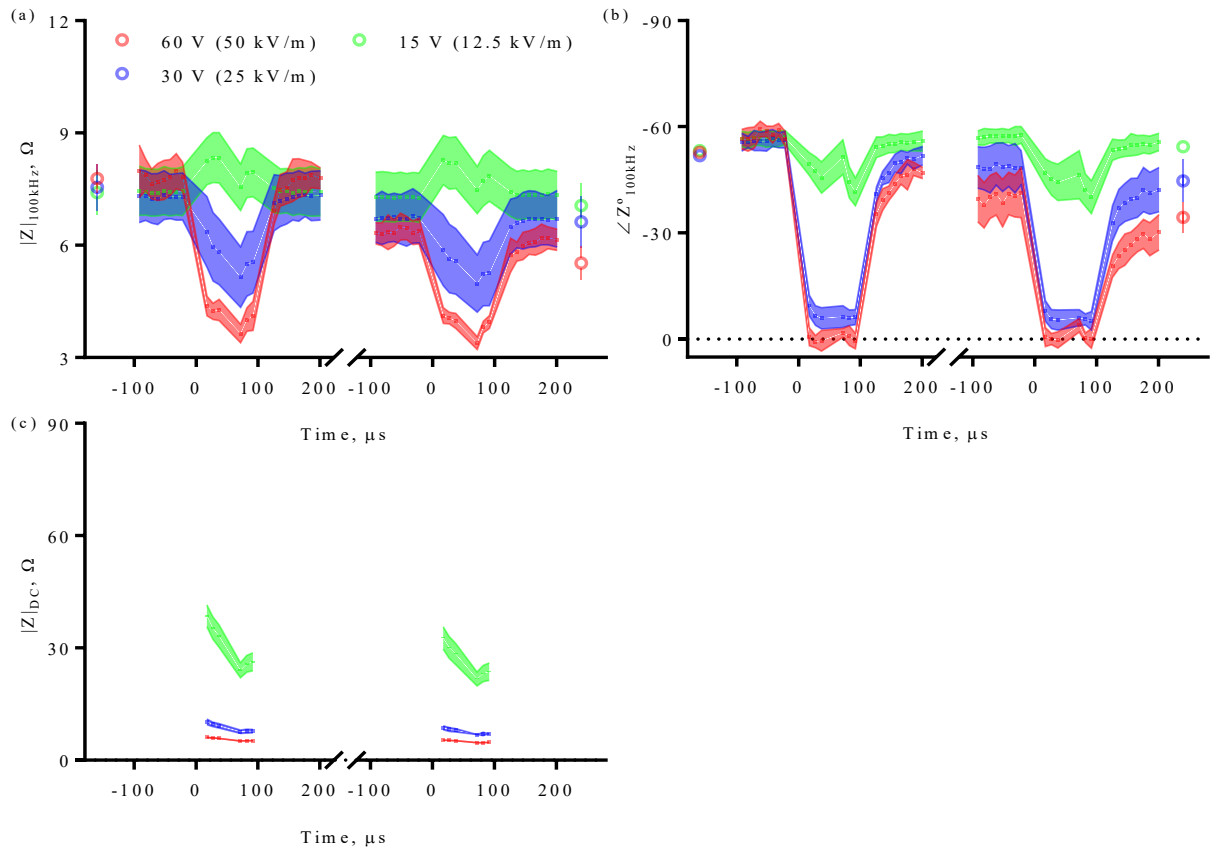
Source: Autor.

Figure 43 – The equivalent permittivity and conductivity of the 2D COMSOL model (dotted lines) and *in vitro* (areas are 95% CI).
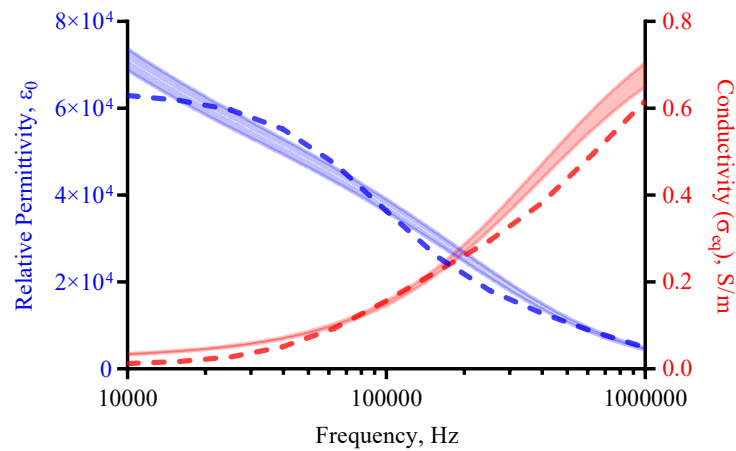
Source: Autor.

Figure 44 – Impedance measurements before and after the PEF. The monopolar protocols are (a) 1 V, (b) 15 V, (c) 30 V and (d) 60 V. The bipolar protocols are (e) 15 V, (f) 30 V and (g) 60 V.
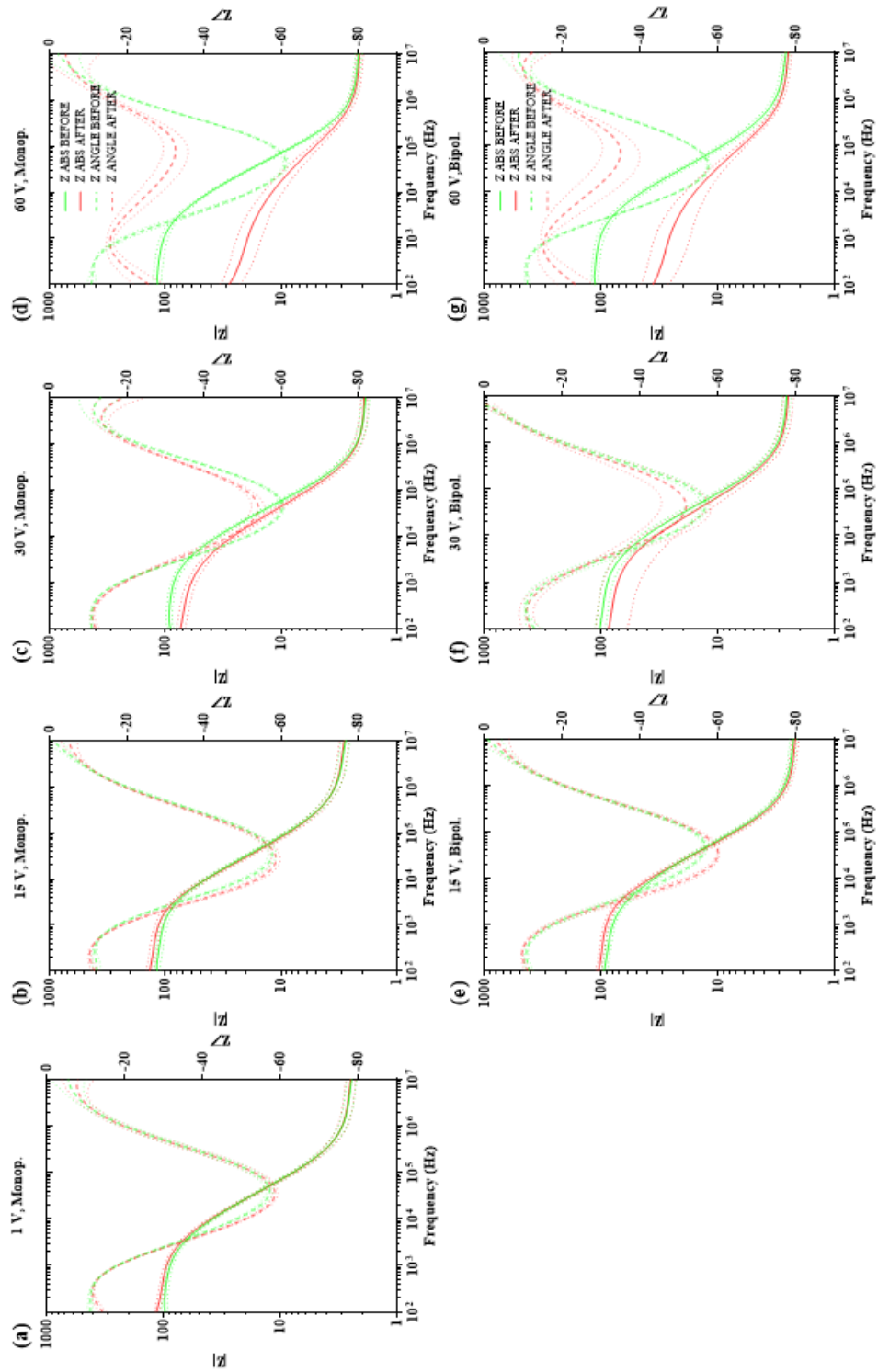
Source: Autor.

Figure 45 – Potato tissue staining due PEF and respective histological study. Control data did not stain (like the 12.5 kV/m).
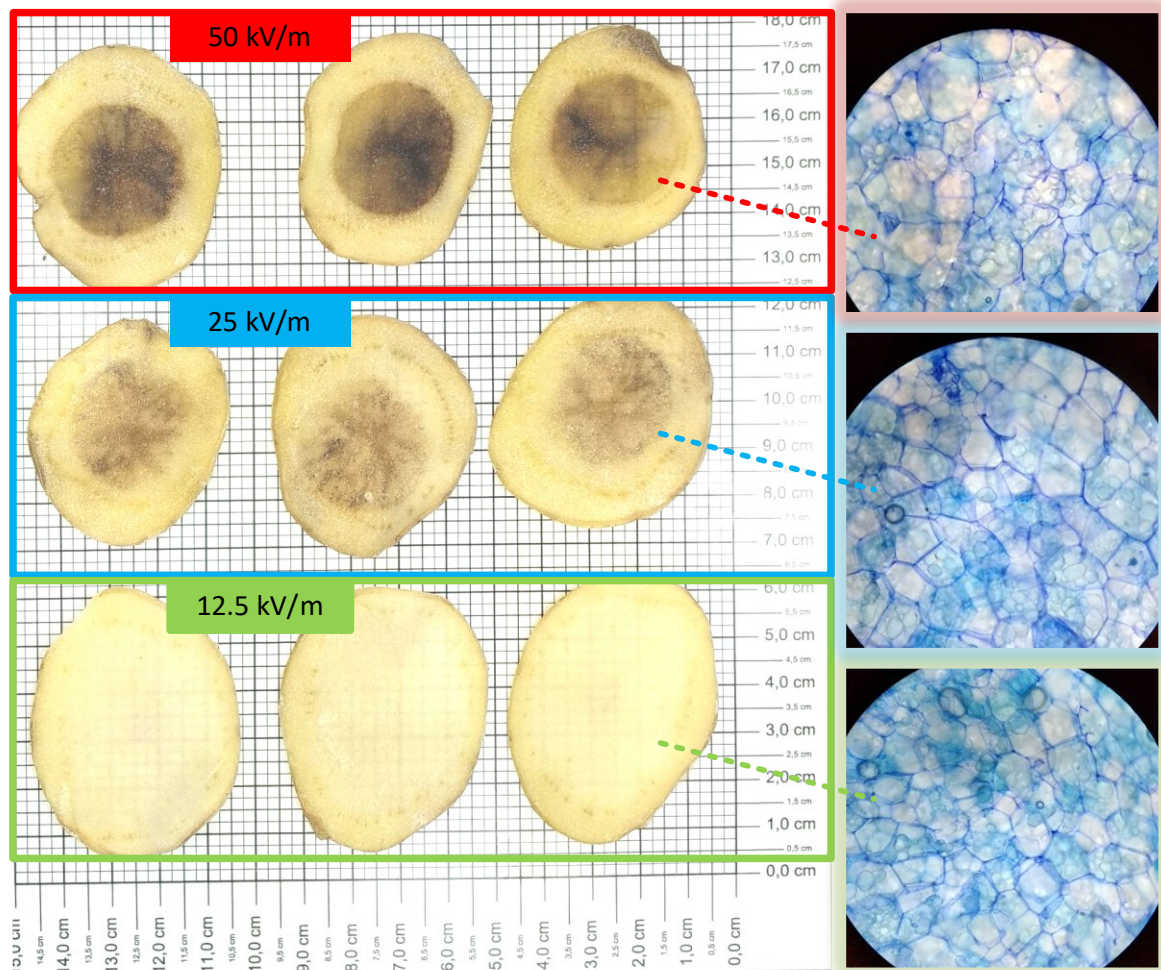
Source: Autor.

6.2.1 Electroporation Threshold

The nonlinear increase of the sample's conductivity ('instantaneous' current-voltage measurement) during PEF is often attributed mostly to the rise and expansion of pores due to electroporation or cell destruction (WEAVER; VERNIER, 2017). The 50 kV/m (60 V_{PEF}) and 12.5 kV/m (15 V_{PEF}) are reported to be the approximate irreversible and reversible electroporation thresholds for potato tissue. The 25 kV/m partly execute an irreversible electroporation, as can be seen by the weaker staining (see Figure 45) (BERKENBROCK *et al.*, 2019; IVORRA; MIR; RUBINSKY, 2009). It is known that the tissue staining does not completely correspond to the electroporation threshold (indirect measurement). However, it is

likely that the 50 kV/m is broadly irreversible threshold. The $Z_{DC,60V}$ and $Z_{DC,30V}$ immediately decreases during the pulse, this type of data is usually used for detect the electroporation or modelling the conductivity as function of the absolute PEF amplitude ($\sigma(E)$) (BERKENBROCK *et al.*, 2019). The $Z_{100kHz,60V}$ and $Z_{100kHz,30V}$ does not return to the original (before PEF) state probably due irreversible electroporation which the cells are destroyed (see histology in Figure 45). This information may be used to sense irreversible electroporation. Those results are very similar to (ZHAO(B) *et al.*, 2018) report using PEF and potatoes and other fruit damaged by cryotherapy (OCHANDIO FERNÁNDEZ *et al.*, 2019), particularly the impedance analyser results (phase shift at 60 V_{PEF} and 25 V_{PEF} in the Figure 45).

Considering that 12.5 kV/m is the reversible electroporation threshold, the $Z_{DC,15V}$ decrease may be explained by electroporation of some cells and ion efflux. However, the $|Z|_{100kHz,15V}$ increase does not correlate with the DC decrease and $\angle Z_{100kHz,15V}$ loss. It may be possible that the $|Z|_{100kHz,15V}$ increase is explained (without direct evidence) by the active membrane response of some cells (membrane 'closing' state due induced V_m), and the $\angle Z_{100kHz,15V}$ and $Z_{DC,15V}$ changes consequence of electroporation. We cannot prove (yet) the dynamics of the $Z_{100kHz,15V}$. Nevertheless, electroporation may have a more complex frequency response due to PEF amplitude. Thus, more experiments using other PEF amplitudes are necessary. We observe that the current electroporation models based on experiments of instantaneous current and voltage readings do not foresee this type of change. External ionic concentrations (as an PEF induced V_m) can alter the sample conductivity (HÖLZEL; LAMPRECHT, 1992). In tissues, it is not appropriate to discuss the 'external conductivity', since the external media is neighbours' adjacent cells connected through cell-cell junctions (we observe that the animal cells junctions are called the gap junctions, and the plant cells junctions are called plasmodesmata).

The $Z_{DC,1V}$ overall increase can be explained by the double-layer electrode-electrolyte charging and electrolysis (the 1 kV/m was only executed in the monopolar analysis); however, the double-layer charging is not stable as there are no differences in the impedance analyser. The 1 kV/m (1 V_{PEF}) has no significant changes during the $Z_{100kHz,1V}$. This evidence may indicate that there are no expressive phenomenon occurring. Thus, the 100 kHz measurement is not affected by double-layer electrode-electrolyte charging and electrolysis.

6.2.2 The 100 kHz Phase Analysis

The $\angle Z_{100kHz}$ rises (less capacitive effect) at 12.5, 25 and 50 kV/m (15, 30 and 60 V_{PEF}). The rising of $\angle Z_{100kHz}$ also could be explained by a series inductance, however, biological media or water electrolysis do not have inductive behaviour.

The $\angle Z_{100kHz}$ change may be partly explained by the increase in the membrane conductivity (losses its permittivity, *i.e.* due electroporation) as a 'porated' dielectric (*i.e.* cell membrane) losses its capacitive properties. In other words, if the Z_{DC} change due membrane permeability increase, the $\angle Z_{100kHz}$ will rise as consequence. The $|Z|_{100kHz,60V}$ and $|Z|_{100kHz,30V}$ changes are due respective $\angle Z_{100kHz}$, as the real part of does not substantially change. The electroporation may change the phase of the AC during the pulse. However, we did not find reports regarding the lessening of the capacitive effect in PEF papers or other high voltage stress. Our report on phase shift may be one of the most significant contributions of this work to the current electroporation and PEF knowledge. We also must consider that the biological media dielectric polarization may bound (and saturates over 25 kV/m) to the direction of the electric field (*i.e.* paraelectric dielectric, as the biological material is a dielectric subjected to ionic polarization and molecules orientational polarization, this type of dielectric is also known as paraelectric (LOIDL *et al.*, 2008)). This effect occurs in some high dielectrics under DC stress (*e.g.* ceramic dielectrics).

6.2.3 The Monopolar and Bipolar Comparison

The monopolar $\angle Z_{100kHz,60V}$ and $\angle Z_{100kHz,30V}$ (Figure 39b) take more time to stabilise to a plateau after the PEF (we considered the impedance analysis after 2 minutes to be the plateau) than the bipolar (Figure 42b). The 100 µs recording after the pulse is insufficient to evaluate the returning time. During the bipolar, the angle stabilises faster, this may be the fewer charges which accumulate in the instable double layer or may indicate a late electroporation pore closure. The bipolar impedance data has a transient, after the transient it was not possible to observe differences in impedance between monopolar and bipolar protocols. The Z_{DC} decrease followed by an increase (Figure 42c) which is not observed in the monopolar PEF (Figure 39c) which may indicate the (partially) charging and unchanging of the electrode interface. A monopolar and bipolar sample measurement are shown in Figure 46.

Figure 46 – Sample current measurement. (a) a monopolar PEF and its processing (b). (c) a bipolar PEF and its processing (d).
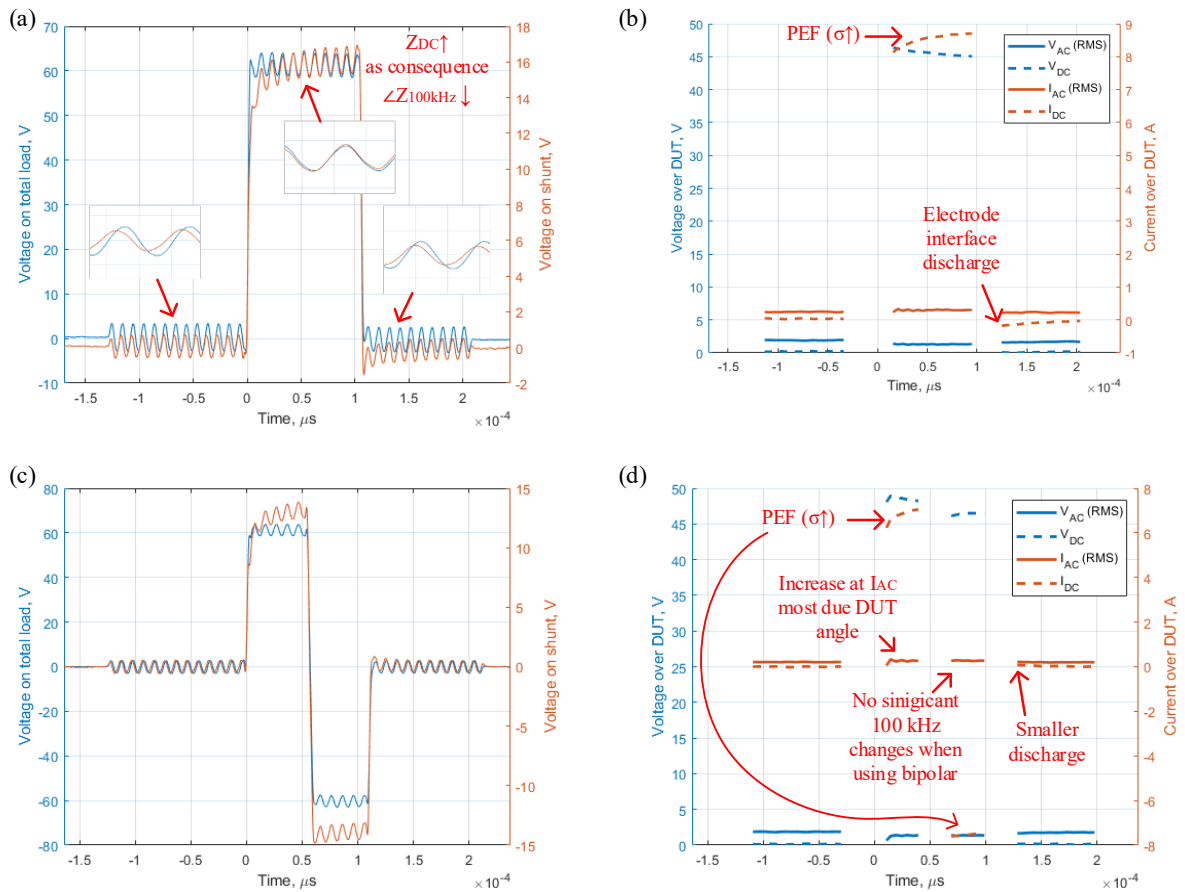
Source: Autor.

The use of monopolar pulses means a reduction in the cost of the electroporator's power electronics. From the electrical and electronic engineering point of view, the bipolar pulses mean four transistor switches at least and its drivers and may require extra isolated supplies. On the other hand, monopolar pulses require simpler topology, *i.e.* four times less transistor switches and much more simpler driver circuit. From the point of view of impedance, we have not seen results that would justify the use of bipolar pulses. Further studies of molecule uptake (in the case of reversible electroporation) or cell viability (in the case of irreversible electroporation), and electrode wear due metal dissociation, are required to access the need of bipolar pulses.

6.2.4 Impedance due DC ΔV/Δt Using Sawtooth Wave

The impedance due the sawtooth wave (*i.e.* ramp DC bias) are shown in Figure 47. The ramp can deliver more detailed levels of the electroporation thresholds. In the ramp beginning (low DC voltages) the electrical current from the electrode's charges may predominate. Using two ΔV/Δt (60 V/ms and 400 V/ms) the electrode charging time varies. Both Z_{DC} and $\angle Z_{100kHz}$ may be used to evaluate the electroporation thresholds, which we believe is approximately 15 kV/m and 25 kV/m in the potato tissue. The ramp has a different ΔV/Δt than a rectangular pulse, which can be a limiting factor in its comparison with rectangular pulses. A further reversed sawtooth wave (decreasing ramp) can be used to study ramp effects. The irreversible electroporation (IRE) evaluation (> 25 kV/m) may have extra timing dynamics (in the order of minutes, see the last impedance measurements from Figure 41 and Figure 42), this behaviour is not described by Figure 47, as the cells death may not occur in the ramp time, still the impedance change during the reversible and irreversible electroporation. Thus, it may be possible to sense the electroporation during the PEF pulse. The fact that during irreversible electroporation the DC impedance approaches the impedance read at 100 kHz indicates that the β distribution has decreased (on its plateau, or it was shifted to higher frequencies).

Figure 47 – Impedance measurement during the sawtooth (*i.e.* ramp) pulse. Measurement using (a) 1 ms (60 V/ms) and (b) 150 µs (400 V/ms).

(a)
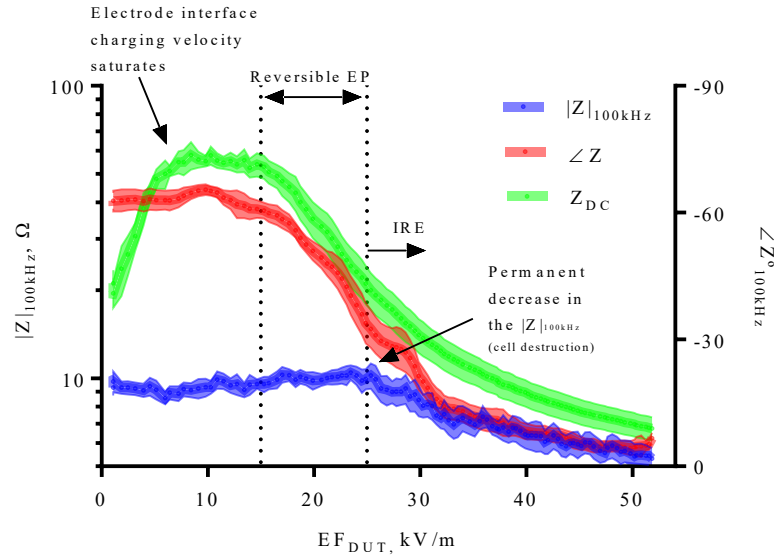
(b)
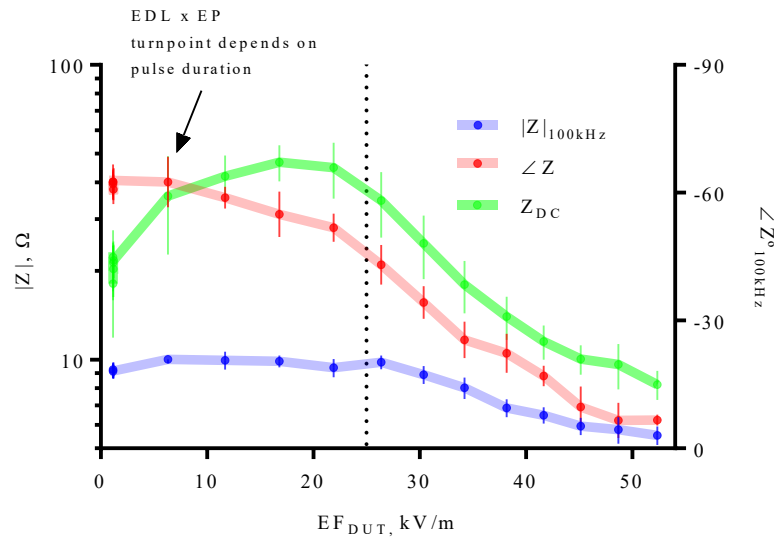
Source: Autor.

7 DISCUSSION & FUTURE WORK

Pulsed energy technology is relatively new (~1980s) and under active research. It is known that conductivity increases due to electroporation. As discussed at section 2.5, the conductivity increase phenomenon was observed in high cell fraction suspensions of animal cells (KINOSITA; TSONG, 1979; PAVLIN *et al.*, 2005; SUZUKI *et al.*, 2011), bacteria (EMANUEL; ROMAN; CAHAN, 2019) and yeast (EL ZAKHEM *et al.*, 2006; PINTARELLI *et al.*, 2021; RAMOS; FARIAS D., 2013), and tissues (CASTELLVÍ; MERCADAL; IVORRA, 2017; LANGUS *et al.*, 2016; NEAL *et al.*, 2012; SUÁREZ *et al.*, 2014). However, PEF is usually delivered in the signature of rectangular pulses burst. PEF contains a broad spectrum of frequencies, which are subject to dispersive effects which interfere in the electroporation measurement & sensing. Current models use instantaneous current-voltage measurements to describe the PEF electrical current (LOPES *et al.*, 2021; PAVLIN *et al.*, 2005; SEL *et al.*, 2005; ZHAO *et al.*, 2018), which is a sum of conduction current, dispersive effects (due to sample reactance), electrode-biological-media polarization, and electroporation. Those phenomenon dynamics have not been completely understood, interfering in the electroporation direct current measurement & sensing.

The purpose of this thesis is to develop electroporation detection methods based on the electrical current and impedance measurement. Ultimately, we propose using alternate current as an alternative to avoid the dispersive effects. We believe that the work is innovative because the literature lacks an approach to sensing electroporation during PEF while avoiding other PEF effects. **Here we briefly show and discuss the major innovations of this thesis to current PEF technology:**

1) We started the thesis by showing that it is possible to sense irreversible electroporation using *in vitro* wine low fraction yeast suspension ATCC®36900™ (2.5×10^7 cells/mL) using direct current measurement. To demonstrate the electroporation is taking place, we show cell damage using Scanning Electronic Microscope (SEM) and viability loss due to PEF. **This is the first report to sense irreversible electroporation using low cell fraction.** The techniques of measurement of current-voltage and impedance used in this part are similar to others reported in the literature (CASTELLVÍ; MERCADAL; IVORRA, 2017; PAVLIN *et al.*, 2005). The yeast PEF-damage is reported to start at 300 kV/m (GÁŠKOVÁ *et al.*, 1996), and irreversible electroporation is reported to be at 750 kV/m (EL ZAKHEM *et al.*, 2006). We observed a 500 kV/m irreversible electroporation threshold. The value may be due

the lower cell density. At high cell density solutions yeast clusters are formed, thus a larger field is needed for electroporation (MOLINARI; PILOSOF; JAGUS, 2004). Also, this deviation is partly explained by the cells distribution of sizes (LEBOVKA; VOROBIEV, 2004). At 500 kV/m it is possible to differentiate the current change and detect irreversible electroporation while meeting the yeast load standards, *i.e.*, 90% viability reduction (OIV suggests at least 5×10^6 cells/mL for fermenting wines (CASTELLUCCI, 2010)). This part also shows data from SEM which show physical changes and yeast breakdown detail (those were not perceived by the electrical current measurement). Zakhem *et al.* reported similar results (EL ZAKHEM *et al.*, 2006). Cell-wall architecture also may be involved with the yeast inactivation. We show numerical calculation of transmembrane and wall voltages. The electric field in the cell wall is above 1 MV/m for 400 kV/m, and transmembrane voltage is higher to the 'typical' 1 V irreversible electroporation threshold. The cellulose dielectric breakdown strength is about 9 MV/m (FERNÁNDEZ *et al.*, 2016). Our numerical findings support the evidences of Pillet *et al.* (PILLET *et al.*, 2016) that lost integrity of cell wall and membrane plasmatic permeability were the causes of yeast inactivation. In this first part, however, it is not possible to sense reversible electroporation, and the direct current is affected by other effects rather electroporation. Probably, the effect superposing electroporation is the polarization of the electrode-media interface (double layer charging). The double layer charging does not affect the 100 kHz impedance measurement.

2) We did a numerical model (*in silico*) investigation of the usage of alternate current frequency during PEF to sense electroporation using yeast suspension. The transmembrane voltage due to PEF can be analytically calculated using the Laplace equation (SUZUKI *et al.*, 2011). We validated the numerical calculations by comparing them to the analytical solution proposed by Gimsa and Wachner (GIMSA; WACHNER, 2001). The maximum relative error between the analytical solution and the computer simulation was 5.18%. Therefore, we considered our model to be sufficiently accurate for our study. The electroporation model is solved in the time domain (as described previously (COSTA *et al.*, 2021; PINTARELLI *et al.*, 2021)). We show that we can simulate the β-dispersion and the electroporation model simultaneously. **This is the first report combining those models.** We propose using hypotheses that the electroporation dynamics is faster than the kHz-MHz analysis, thus, we can suppose the system is linear. **This is the first report that proposes this assumption.** It is known that the optimal cell sensing range is 10 kHz to 100 kHz (ARNDT *et al.*, 2004; KRINKE *et al.*, 2009; XU *et al.*, 2016). We show that it is possible to detect electroporation

using the shift of the β-dispersion in a range of 10 kHz to 1 MHz. **This is the first report to demonstrate the β-dispersion behaviour during electroporation.** Frequencies lower than 10 kHz are known to be affected by electrodes polarization, and frequencies higher than 1 MHz cannot sense the membrane as it become electrically invisible (CHIAPPERINO *et al.*, 2019; GOWRISHANKAR; WEAVER, 2003; LI; CHEN; HAN, 2018). This proposed sensor technology may be used to industrial irreversible electroporation or in lab on a chip electroporation device (ZHANG *et al.*, 2020).

      3) We finished the thesis building and using a custom PEF that overlaps the PEF with a 100 kHz sine. We tested the theory using *in vitro* vegetal tissue (potato tuber). The tissue was used as it mostly contains cells; thus, the effects of electroporation are more expressive. The tissue is trackable, and we used the centre vegetable portion, which is composed by the parenchyma tissue (uniform shaped cells in all directions), and pith tissue with its medullary rays (GROMMERS; VAN DER KROGT, 2009; OEY *et al.*, 2016). We used two PEF protocols: one similar to European Standard Operating Procedures of Electrochemotherapy (ESOPE) (GEHL *et al.*, 2018) and other is a ramp (two $\Delta V/\Delta t$ tested). We execute a histology study to verify for cell destruction and tissue staining to detect tissue electroporation. We also propose a vegetal tissue model which is a novel 2D 'honeycomb' infinitesimal geometry of hexagonal cells containing intracellular fluid, membrane, wall, and intracellular space. We detect the irreversible electroporation threshold similar to the current literature (approximately 25 kV/m) (BERKENBROCK *et al.*, 2019; IVORRA; MIR; RUBINSKY, 2009). We also show that the impedance data does not return to the original due irreversible electroporation cell destruction (destruction is show using cell histology). Those results are very similar to (ZHAO(B) *et al.*, 2018) report using PEF and potatoes and other fruit damaged by cryotherapy (OCHANDIO FERNÁNDEZ *et al.*, 2019). We show that the at exceptionally low voltages (1 V) the direct current apparent impedance can increase which indicates the electrode charging. We also show that the system's 100 kHz complex impedance can be used to detect reversible and irreversible electroporation, in other words, this means the shift of β-dispersion. **This is the first report that lights the behaviour of β-dispersion during PEF. We show evidence that we can use a frequency 'evades' the undesired and intrinsic PEF effects (electrode-media dielectric double layer charging) and is partially affected by the membrane (conduction and displacement current).** The information can be used to improve electroporation sensing. The sensor can enhance electroporation modelling, control, and systems.

Our reports measuring the β-dispersion shift during PEF (*in silico* and *in vitro*) may be the most significant contribution of this work to the current electroporation and PEF knowledge. Yet, we believe that this thesis could trigger further research. We hope this thesis spark new papers, new patents, and other thesis. Future work may get us closer to our goal which is to improve methods and equipment for electroporation. Here it is a list of ideas for future work:

1. Apply this thesis methods to sense electroporation using *in vitro* or *in vivo* animal biological samples.

2. Use the AC sensor information to describe a model of electroporation using equivalent circuits.

3. Use diverse AC frequencies do understand the dispersion shift at PEF. It is known that the entire spectrum is interdependent; this, this is important to understand the C_{DL} and C_β dynamics.

4. Improve the voltage level of the PEF system to get data of pasteurization at industrial level with flow system (cm chamber using tens of kV).

The author intends to continue the PEF research and is available for the development of the above and other projects.

8 CONCLUSION

This thesis shows sensing methods for PEF-based treatment. We propose using the current reading of the protocol itself to get feedback on the treatment. Our sensing method is non-invasive and was implemented in parallel to the PEF signature, using the same application electrodes and overlapping the primary PEF protocol. This thesis contributes to the sensing of irreversible electroporation using low cell fraction and direct current measurement; proposes a numerical model of β-dispersion behaviour during PEF to sense electroporation using yeast suspension; and reports behaviour of β-dispersion during tissues electroporation. Ultimately the proposed sensing methods can be used to better understand (*e.g.* modelling) and control electroporation.

We used *in vitro* yeast to show that irreversible electroporation can be used to eliminate yeast to meet wines standards, and the in the pulse current measurements can be used to detect the elimination. The in pulse current measurement lacks to show damage details and it is affected to other effects rather electroporation. We used computer simulation with yeast and electroporation model to show that the impedance measurement at certain frequencies could be used to detect the occurrence of electroporation, *i.e.*, dielectric dispersion modulated sensing, while mitigating unwanted electrode polarization noises. We show changes in the frequency spectrum due to electroporation. We used an *in vitro* tissue study using PEF protocols with a 100 kHz superposed sine to show a detection method based on the impedance measurement centered on the frequency of 100 kHz as an alternative to avoid the dispersive effects of the electrodes. Our results show that certain levels of PEF induce a reduction in the sample's capacitive effect, and the capacitance may be no longer the main characteristic of the sample at irreversible electroporation experiments.

[blank page]

REFERÊNCIAS

ADLER, Andy; BOYLE, Alistair. Electrical Impedance Tomography: Tissue Properties to Image Measures. **IEEE Transactions on Biomedical Engineering**, [*s. l.*], v. 64, n. 11, p. 2494–2504, 2017. Disponível em: https://ieeexplore.ieee.org/document/7982758/.

ANDRADE, Daniella L. L. S. *et al.* Electrochemotherapy treatment safety under parallel needle deflection. **Scientific Reports**, [*s. l.*], v. 12, n. 1, p. 2766, 2022. Disponível em: https://doi.org/10.1038/s41598-022-06747-x.

ARNDT, Silke *et al.* Bioelectrical impedance assay to monitor changes in cell shape during apoptosis. **Biosensors and Bioelectronics**, [*s. l.*], v. 19, n. 6, p. 583–594, 2004. Disponível em: http://linkinghub.elsevier.com/retrieve/pii/S0956566303002690.

ASAMI, K.; YONEZAWA, T. Dielectric behavior of wild-type yeast and vacuole-deficient mutant over a frequency range of 10 kHz to 10 GHz. **Biophysical Journal**, [*s. l.*], v. 71, n. 4, p. 2192–2200, 1996. Disponível em: https://linkinghub.elsevier.com/retrieve/pii/S0006349596794201.

BARBA, Francisco J. *et al.* Current applications and new opportunities for the use of pulsed electric fields in food science and industry. **Food Research International**, [*s. l.*], v. 77, p. 773–798, 2015. Disponível em: http://dx.doi.org/10.1016/j.foodres.2015.09.015.

BASTOS, João Pedro A.; SADOWSKI, Nelson. **Magnetic Materials and 3D Finite Element Modeling**. [*S. l.*]: CRC Press, 2017-. ISSN 0883-7694.v. 40 Disponível em: https://www.cambridge.org/core/product/identifier/S0883769415000226/type/journal_article.

BATISTA NAPOTNIK, Tina; MIKLAVČIČ, Damijan. In vitro electroporation detection methods – An overview. **Bioelectrochemistry**, [*s. l.*], v. 120, p. 166–182, 2018. Disponível em: https://linkinghub.elsevier.com/retrieve/pii/S156753941730395X.

BERKENBROCK, José Alvim *et al.* Verification of Electroporation Models Using the Potato Tuber as In Vitro Simulation. **Journal of Medical and Biological Engineering**, [*s. l.*], v. 39, n. 2, p. 224–229, 2019. Disponível em: https://proceedings.cmbes.ca/index.php/proceedings/article/viewFile/616/610.

CASTELLUCCI, Federico. **OIV (2010) Organisation International de la Vigne et du Vin. Resolution OIV/OENO 206/2010. Microbiological Analysis of Wines and Musts — Revision of Resolution OENO 8/1995.** Tbilisi, Georgia.: [*s. n.*], 2010.

CASTELLVÍ, Quim *et al.* Avoiding neuromuscular stimulation in liver irreversible electroporation using radiofrequency electric fields. **Physics in Medicine & Biology**, [*s. l.*], v. 63, n. 3, p. 035027, 2018. Disponível em: https://iopscience.iop.org/article/10.1088/1361-6560/aaa16f.

CASTELLVÍ, Quim. Bioimpedance Measurements and the Electroporation Phenomenon. [*s. l.*], n. January, 2014. Disponível em: http://berg.upf.edu/system/files/biblio/QuimCastellvi_Bioimpedance.pdf.

CASTELLVÍ, Quim; MERCADAL, Borja; IVORRA, Antoni. Assessment of Electroporation by Electrical Impedance Methods. *In*: HANDBOOK OF ELECTROPORATION. Cham: Springer International Publishing, 2017. p. 671–690. *E-book*. Disponível em: http://link.springer.com/10.1007/978-3-319-26779-1_164-1.

CHANG, Donald C. **Guide to electroporation and electrofusion**. [*S. l.*]: Academic Press, 1992. *E-book*. Disponível em: https://www.sciencedirect.com/science/book/9780080917276. Acesso em: 10 abr. 2018.

CHANG, D.C.; REESE, T.S. Changes in membrane structure induced by electroporation as revealed by rapid-freezing electron microscopy. **Biophysical Journal**, [*s. l.*], v. 58, n. 1, p. 1–12, 1990. Disponível em:

https://www.ncbi.nlm.nih.gov/pmc/articles/PMC1280935/pdf/biophysj00125-0013.pdf. Acesso em: 14 jan. 2018.

CHARLES-RODRÍGUEZ, A.V. *et al.* Comparison of Thermal Processing and Pulsed Electric Fields Treatment in Pasteurization of Apple Juice. **Food and Bioproducts Processing**, [*s. l.*], v. 85, n. 2, p. 93–97, 2007. Disponível em: http://www.sciencedirect.com/science/article/pii/S0960308507705813. Acesso em: 22 maio 2017.

CHEN, C. *et al.* Membrane electroporation theories: a review. **Medical and Biological Engineering and Computing**, [*s. l.*], v. 44, n. 1–2, p. 5–14, 2006. Disponível em: https://link.springer.com/content/pdf/10.1007%2Fs11517-005-0020-2.pdf. Acesso em: 9 nov. 2017.

CHIAPPERINO, Michele Alessandro *et al.* Electroporation modelling of irregular nucleated cells including pore radius dynamics. **Electronics (Switzerland)**, [*s. l.*], v. 8, n. 12, p. 1–12, 2019.

COMSOL. **AC/DC Module User's Guide 5.4**. [*S. l.: s. n.*], 2018.

COROVIC, Selma *et al.* Modeling of electric field distribution in tissues during electroporation. **BioMedical Engineering OnLine**, [*s. l.*], v. 12, n. 1, p. 16, 2013. Disponível em: http://biomedical-engineering-online.biomedcentral.com/articles/10.1186/1475-925X-12-16. Acesso em: 5 abr. 2018.

COSTA, Jorge A. *et al.* Sensitivity Analysis of a Nuclear Electroporation Model—A Theoretical Study. **IEEE Transactions on Dielectrics and Electrical Insulation**, [*s. l.*], v. 28, n. 6, p. 1850–1858, 2021. Disponível em: https://ieeexplore.ieee.org/document/9679728/.

COUTO, José António *et al.* Thermal inactivation of the wine spoilage yeasts Dekkera/Brettanomyces. **International Journal of Food Microbiology**, [*s. l.*], v. 104, n. 3, p. 337–344, 2005. Disponível em: https://linkinghub.elsevier.com/retrieve/pii/S0168160505002680.

DAVALOS, Rafael V.; RUBINSKY, Boris. Temperature considerations during irreversible electroporation. **International Journal of Heat and Mass Transfer**, [*s. l.*], v. 51, n. 23–24, p. 5617–5622, 2008. Disponível em: https://ac.els-cdn.com/S0017931008002706/1-s2.0-S0017931008002706-main.pdf?_tid=39e609ce-ff97-11e7-892e-00000aab0f27&acdnat=1516641244_cfe541d58eb6495be8d0d6141b6ae492. Acesso em: 22 jan. 2018.

DELEMOTTE, Lucie; TAREK, Mounir. Molecular Dynamics Simulations of Lipid Membrane Electroporation. **The Journal of Membrane Biology**, [*s. l.*], v. 245, n. 9, p. 531–543, 2012. Disponível em: http://link.springer.com/10.1007/s00232-012-9434-6.

DI BIASIO, A.; AMBROSONE, L.; CAMETTI, C. The Dielectric Behavior of Nonspherical Biological Cell Suspensions: An Analytic Approach. **Biophysical Journal**, [*s. l.*], v. 99, n. 1, p. 163–174, 2010. Disponível em: http://dx.doi.org/10.1016/j.bpj.2010.04.006.

EL ZAKHEM, H. *et al.* The early stages of Saccharomyces cerevisiae yeast suspensions damage in moderate pulsed electric fields. **Colloids and Surfaces B: Biointerfaces**, [*s. l.*], v. 47, n. 2, p. 189–197, 2006. Disponível em: https://linkinghub.elsevier.com/retrieve/pii/S0927776505003620.

EMANUEL, Efrat; ROMAN, Pogreb; CAHAN, Rivka. Influence of the current density in moderate pulsed electric fields on P. putida F1 eradication. **Bioelectrochemistry**, [*s. l.*], v. 126, p. 172–179, 2019. Disponível em: https://linkinghub.elsevier.com/retrieve/pii/S156753941830375X.

ESCOBAR-CHÁVEZ, José Juan. *et al.* **Current Technologies To Increase The Transdermal Delivery Of Drugs**. [*S. l.*]: BENTHAM SCIENCE PUBLISHERS, 2012. *E-book*. Disponível em: https://ebooks.benthamscience.com/book/9781608051915/. Acesso em:

12 jan. 2018.

ESPRESSIF SYSTEMS. **ESP32 Datasheet**. [*S. l.: s. n.*], 2017.

FERNÁNDEZ, Inmaculada *et al.* Thermal degradation assessment of Kraft paper in power transformers insulated with natural esters. **Applied thermal engineering**, [*s. l.*], v. 104, p. 129–138, 2016.

FERNÁNDEZ, M. Laura; RISK, Marcelo R. Lipid Electropore Stabilization. *In*: HANDBOOK OF ELECTROPORATION. Cham: Springer International Publishing, 2017. p. 77–93. *E-book*. Disponível em: http://link.springer.com/10.1007/978-3-319-32886-7_83.

FLORES-COSÍO, G. *et al.* Application of dielectric spectroscopy to unravel the physiological state of microorganisms: current state, prospects and limits. **Applied Microbiology and Biotechnology**, [*s. l.*], v. 104, n. 14, p. 6101–6113, 2020. Disponível em: http://link.springer.com/10.1007/s00253-020-10677-x.

GANEVA, V; GALUTZOV, B; TEISSIÉ, J. High yield electroextraction of proteins from yeast by a flow process. **Analytical Biochemistry**, [*s. l.*], v. 315, n. 1, p. 77–84, 2003. Disponível em: http://linkinghub.elsevier.com/retrieve/pii/S0003269702006991. Acesso em: 23 abr. 2018.

GÁŠKOVÁ, D. *et al.* Effect of high-voltage electric pulses on yeast cells: factors influencing the killing efficiency. **Bioelectrochemistry and Bioenergetics**, [*s. l.*], v. 39, n. 2, p. 195–202, 1996. Disponível em: http://linkinghub.elsevier.com/retrieve/pii/0302459895018921. Acesso em: 23 abr. 2018.

GEHL, Julie *et al.* Updated standard operating procedures for electrochemotherapy of cutaneous tumours and skin metastases. **Acta Oncologica**, [*s. l.*], v. 57, n. 7, p. 874–882, 2018. Disponível em: https://www.tandfonline.com/doi/full/10.1080/0284186X.2018.1454602.

GIMSA, Jan; WACHNER, Derk. Analytical Description of the Transmembrane Voltage Induced on Arbitrarily Oriented Ellipsoidal and Cylindrical Cells. **Biophysical Journal**, [*s. l.*], v. 81, n. 4, p. 1888–1896, 2001. Disponível em: https://linkinghub.elsevier.com/retrieve/pii/S0006349501758407.

GOLBERG, Alex; FISCHER, Judith; RUBINSKY, Boris. The Use of Irreversible Electroporation in Food Preservation. *In*: [*S. l.*]: Springer Berlin Heidelberg, 2010. p. 273–312. *E-book*. Disponível em: http://link.springer.com/10.1007/978-3-642-05420-4_13. Acesso em: 28 abr. 2017.

GOWRISHANKAR, Thiruvallur R.; WEAVER, James C. An approach to electrical modeling of single and multiple cells. **Proceedings of the National Academy of Sciences**, [*s. l.*], v. 100, n. 6, p. 3203–3208, 2003. Disponível em: http://www.pnas.org/cgi/doi/10.1073/pnas.0636434100.

GRIMNES, S.; MARTINSEN, O. G. **Bioimpedance and Bioelectricity Basics**. 3rd. ed. [*S. l.*]: Academic Press, 2014.

GROMMERS, Hielko E.; VAN DER KROGT, Do A. Potato Starch. *In*: STARCH. Third Edited. [*S. l.*]: Elsevier, 2009. p. 511–539. *E-book*. Disponível em: http://dx.doi.org/10.1016/B978-0-12-746275-2.00011-2.

HEILEMAN, Khalil; DAOUD, Jamal; TABRIZIAN, Maryam. Dielectric spectroscopy as a viable biosensing tool for cell and tissue characterization and analysis. **Biosensors and Bioelectronics**, [*s. l.*], v. 49, p. 348–359, 2013. Disponível em: http://dx.doi.org/10.1016/j.bios.2013.04.017.

HOLMES, David *et al.* Leukocyte analysis and differentiation using high speed microfluidic single cell impedance cytometry. **Lab on a Chip**, [*s. l.*], v. 9, n. 20, p. 2881, 2009. Disponível em: http://xlink.rsc.org/?DOI=b910053a.

HÖLZEL, Ralph; LAMPRECHT, Ingolf. Dielectric properties of yeast cells as determined by

electrorotation. **Biochimica et Biophysica Acta (BBA) - Biomembranes**, [*s. l.*], v. 1104, n. 1, p. 195–200, 1992. Disponível em: https://linkinghub.elsevier.com/retrieve/pii/000527369290150K.

HÜCKEL, E. Zur Theorie der Elektrolyte. *In*: ERGEBNISSE DER EXAKTEN NATURWISSENSCHAFTEN. Berlin, Heidelberg: Springer Berlin Heidelberg, 1924. p. 199–276. *E-book*. Disponível em: http://link.springer.com/10.1007/978-3-642-94260-0_9.

IBBA, Pietro *et al.* Bio-impedance and circuit parameters: An analysis for tracking fruit ripening. **Postharvest Biology and Technology**, [*s. l.*], v. 159, n. September 2019, p. 110978, 2020. Disponível em: https://doi.org/10.1016/j.postharvbio.2019.110978.

ISHAI, Paul Ben *et al.* Electrode polarization in dielectric measurements: a review. **Measurement Science and Technology**, [*s. l.*], v. 24, n. 10, p. 102001, 2013. Disponível em: https://iopscience.iop.org/article/10.1088/0957-0233/24/10/102001.

IVORRA, A.; MIR, L.M.; RUBINSKY, B. Electric Field Redistribution due to Conductivity Changes during Tissue Electroporation: Experiments with a Simple Vegetal Model. **IFMBE Proceedings**, [*s. l.*], v. 25, n. XIII, p. 59–62, 2009.

JARM, Tomaz; KRAMAR, Peter (org.). **1st World Congress on Electroporation and Pulsed Electric Fields in Biology, Medicine and Food & Environmental Technologies**. Singapore: Springer Singapore, 2016. (IFMBE Proceedings). v. 53 *E-book*. Disponível em: http://link.springer.com/10.1007/978-981-287-817-5.

JIANG, Chunlan; DAVALOS, Rafael V; BISCHOF, John C. A Review of Basic to Clinical Studies of Irreversible Electroporation Therapy. **IEEE Transactions on Biomedical Engineering**, [*s. l.*], v. 62, n. 1, p. 4–20, 2015. Disponível em: http://ieeexplore.ieee.org/document/6949110/. Acesso em: 26 jul. 2017.

JORDAN, C.A.; NEUMANN, E.; SOWERS, A.E. **Electroporation and Electrofusion in Cell Biology**. 1. ed. Boston, MA: Springer US, 1989. *E-book*. Disponível em: http://link.springer.com/10.1007/978-1-4899-2528-2.

KEMPKES, Michael A. Industrial Pulsed Electric Field Systems. *In*: HANDBOOK OF ELECTROPORATION. Cham: Springer International Publishing, 2017. p. 881–901. *E-book*. Disponível em: http://link.springer.com/10.1007/978-3-319-32886-7_211.

KEYSIGHT TECHNOLOGIES. **4294A Precision Impedance Analyzer Operation Manual**. [*S. l.: s. n.*], 2003. Disponível em: https://literature.cdn.keysight.com/litweb/pdf/04294-90060.pdf?id=1000002189-1:epsg:man.

KINOSITA, Kazuhiko; TSONG, Tian Yow. Voltage-induced conductance in human erythrocyte membranes. **Biochimica et Biophysica Acta (BBA) - Biomembranes**, [*s. l.*], v. 554, n. 2, p. 479–497, 1979. Disponível em: http://www.sciencedirect.com/science/article/pii/0005273679903869. Acesso em: 19 jan. 2018.

KLEIN, Nina *et al.* In vitro study on the mechanisms of action of electrolytic electroporation (E2). **Bioelectrochemistry**, [*s. l.*], v. 133, p. 107482, 2020. Disponível em: https://doi.org/10.1016/j.bioelechem.2020.107482.

KONSTANKIEWICZ, K. *et al.* Cell structural parameters of potato tuber tissue. **International Agrophysics**, [*s. l.*], v. 16, n. 2, p. 119–127, 2002.

KOTNIK, Tadej *et al.* Cell membrane electroporation- Part 1: The phenomenon. **IEEE Electrical Insulation Magazine**, [*s. l.*], v. 28, n. 5, p. 14–23, 2012. Disponível em: http://ieeexplore.ieee.org/document/6268438/. Acesso em: 8 nov. 2017.

KOTNIK, Tadej *et al.* Membrane Electroporation and Electropermeabilization: Mechanisms and Models. **Annual Review of Biophysics**, [*s. l.*], v. 48, n. 1, p. 63–91, 2019. Disponível em: https://www.annualreviews.org/doi/10.1146/annurev-biophys-052118-115451.

KOTNIK, Tadej; MIKLAVČIČ, Damijan; MIR, Lluis M. Cell membrane

electropermeabilization by symmetrical bipolar rectangular pulses. **Bioelectrochemistry**, [*s. l.*], v. 54, n. 1, p. 91–95, 2001. Disponível em: http://linkinghub.elsevier.com/retrieve/pii/S1567539401001153.

KOTNIK, Tadej; PUCIHAR, Gorazd; MIKLAVČIČ, Damijan. Induced Transmembrane Voltage and Its Correlation with Electroporation-Mediated Molecular Transport. **The Journal of Membrane Biology**, [*s. l.*], v. 236, n. 1, p. 3–13, 2010. Disponível em: http://citeseerx.ist.psu.edu/viewdoc/download?doi=10.1.1.175.9772&rep=rep1&type=pdf. Acesso em: 17 jan. 2018.

KRINKE, Dana *et al.* A microelectrode-based sensor for label-free in vitro detection of ischemic effects on cardiomyocytes. **Biosensors and Bioelectronics**, [*s. l.*], v. 24, n. 9, p. 2798–2803, 2009. Disponível em: https://linkinghub.elsevier.com/retrieve/pii/S0956566309000967.

LANGUS, J. *et al.* Dynamic finite-element model for efficient modelling of electric currents in electroporated tissue. **Scientific Reports**, [*s. l.*], v. 6, n. 1, p. 26409, 2016. Disponível em: http://www.nature.com/articles/srep26409. Acesso em: 11 abr. 2018.

LAUFER, Shlomi *et al.* Electrical impedance characterization of normal and cancerous human hepatic tissue. **Physiological Measurement**, [*s. l.*], v. 31, n. 7, p. 995–1009, 2010. Disponível em: https://iopscience.iop.org/article/10.1088/0967-3334/31/7/009.

LEBOVKA, N. I.; VOROBIEV, E. On the origin of the deviation from the first-order kinetics in inactivation of microbial cells by pulsed electric fields. **International Journal of Food Microbiology**, [*s. l.*], v. 91, n. 1, p. 83–89, 2004.

LI, Shudong; CHEN, Xiaoyan; HAN, Fengze. Simulation of Cell Dielectric Properties Based on COMSOL. **Proceedings of International Conference on Artificial Life and Robotics**, [*s. l.*], v. 23, n. 4, p. 603–606, 2018. Disponível em: http://alife-robotics.co.jp/LP/2018/OS15-8.htm.

LOIDL, A. *et al.* Bananas go paraelectric. **Journal of Physics: Condensed Matter**, [*s. l.*], v. 20, n. 19, p. 191001, 2008. Disponível em: https://iopscience.iop.org/article/10.1088/0953-8984/20/19/191001.

LOPES, Lucas Bertinetti *et al.* Computer optimization of conductive gels for electrochemotherapy. **Medical Engineering and Physics**, [*s. l.*], v. 98, n. July, p. 133–139, 2021. Disponível em: https://doi.org/10.1016/j.medengphy.2021.10.011.

LOUREIRO, V. Spoilage yeasts in the wine industry. **International Journal of Food Microbiology**, [*s. l.*], v. 86, n. 1–2, p. 23–50, 2003. Disponível em: https://linkinghub.elsevier.com/retrieve/pii/S0168160503002460.

LV, Yanpeng *et al.* A Study on Nonthermal Irreversible Electroporation of the Thyroid. **Technology in Cancer Research & Treatment**, [*s. l.*], v. 18, p. 153303381987630, 2019. Disponível em: http://journals.sagepub.com/doi/10.1177/1533033819876307.

MA, Gege; SOLEIMANI, Manuchehr. A New Label-Free and Contactless Bio-Tomographic Imaging with Miniaturized Capacitively-Coupled Spectroscopy Measurements. **Sensors**, [*s. l.*], v. 20, n. 11, p. 3327, 2020. Disponível em: https://www.mdpi.com/1424-8220/20/11/3327.

MA, Hanbin; SU, Yang; NATHAN, Arokia. Cell constant studies of bipolar and tetrapolar electrode systems for impedance measurement. **Sensors and Actuators B: Chemical**, [*s. l.*], v. 221, p. 1264–1270, 2015. Disponível em: https://linkinghub.elsevier.com/retrieve/pii/S0925400515301465.

MAXWELL, James Clerk. On Action at a Distance. *In*: NIVEN, W. D. (org.). **The Scientific Papers of James Clerk Maxwell**. Reprinteded. Cambridge: Cambridge University Press, 1980. v. 2, p. 311–323. *E-book*. Disponível em: https://www.cambridge.org/core/product/identifier/CBO9780511710377A034/type/book_part .

MAYER, V.W.; GOIN, C.J.; ZIMMERMANN, F.K. Aneuploidy and other genetic effects induced by hydroxyurea in Saccharomyces cerevisiae. **Mutation Research/Fundamental and Molecular Mechanisms of Mutagenesis**, [*s. l.*], v. 160, n. 1, p. 19–26, 1986. Disponível em: https://linkinghub.elsevier.com/retrieve/pii/S0027510796900044.

MESCIA, Luciano *et al.* Modeling of Electroporation Induced by Pulsed Electric Fields in Irregularly Shaped Cells. **IEEE Transactions on Biomedical Engineering**, [*s. l.*], v. 65, n. 2, p. 414–423, 2018. Disponível em: http://ieeexplore.ieee.org/document/8106660/.

MIKLAVCIC, Damijan (org.). **Handbook of Electroporation**. Cham: Springer International Publishing, 2016. *E-book*. Disponível em: http://link.springer.com/10.1007/978-3-319-26779-1.

MIKLAVČIČ, Damijan; PUC, Marko. Electroporation. *In*: WILEY ENCYCLOPEDIA OF BIOMEDICAL ENGINEERING. Hoboken, NJ, USA: John Wiley & Sons, Inc., 2006. *E-book*. Disponível em: http://doi.wiley.com/10.1002/9780471740360.ebs1390. Acesso em: 12 jun. 2017.

MISHRA, K.P. Membrane Electroporation and Emerging Biomedical Applications. *In*: HANDBOOK OF MEMBRANE SEPARATIONS. [*S. l.*]: CRC Press, 2008. p. 741–758. *E-book*. Disponível em: http://www.crcnetbase.com/doi/10.1201/9781420009484.ch26. Acesso em: 12 jun. 2017.

MOLINARI, P.; PILOSOF, A. M.R.; JAGUS, R. J. Effect of growth phase and inoculum size on the inactivation of Saccharomyces cerevisiae in fruit juices, by pulsed electric fields. **Food Research International**, [*s. l.*], v. 37, n. 8, p. 793–798, 2004.

MORGAN, Hywel *et al.* Single cell dielectric spectroscopy. **Journal of Physics D: Applied Physics**, [*s. l.*], v. 40, n. 1, p. 61–70, 2007.

NEAL, Robert E. *et al.* Experimental Characterization and Numerical Modeling of Tissue Electrical Conductivity during Pulsed Electric Fields for Irreversible Electroporation Treatment Planning. **IEEE Transactions on Biomedical Engineering**, [*s. l.*], v. 59, n. 4, p. 1076–1085, 2012. Disponível em: http://ieeexplore.ieee.org/document/6125234/. Acesso em: 23 jan. 2018.

OCHANDIO FERNÁNDEZ *et al.* Freeze-Damage Detection in Lemons Using Electrochemical Impedance Spectroscopy. **Sensors**, [*s. l.*], v. 19, n. 18, p. 4051, 2019. Disponível em: https://www.mdpi.com/1424-8220/19/18/4051.

OEY, Indrawati *et al.* Determination of Pulsed Electric Fields Effects on the Structure of Potato Tubers. *In*: MIKLAVCIC, Damijan (org.). **Handbook of Electroporation**. Cham: Springer International Publishing, 2016. p. 1–19. *E-book*. Disponível em: http://link.springer.com/10.1007/978-3-319-26779-1_151-1.

OPPENHEIM, Alan V; SCHAFER, Ronald W. **Discrete-Time Signal Processing**. 3rd. ed. New Jersey: Prentice-Hall, 2010.

OPPENHEIN, A. V.; WILLSKY, A. S.; NAWAB, S. H. **Signals and Systems**. 2. ed. [*S. l.*]: Pearson, 1996.

PAI, S. T.; ZHANG, Qi. Energy Storage. *In*: CHEN, W. K. (org.). **Introduction to High Power Pulse Technology**. 10. ed. [*S. l.*]: World Scientific, 1995. p. 7–45. *E-book*. Disponível em: http://www.worldscientific.com/doi/abs/10.1142/9789812831934_0002. Acesso em: 21 nov. 2018.

PAKHOMOV, Andrei G.; MARKOV, Marko S.; MIKLAVČIČ, Damijan. **Advanced Electroporation Techniques in Biology and Medicine**. 1. ed. Boca Raton, Florida: CRC Press, 2010.

PAVLIN, Mojca *et al.* Effect of Cell Electroporation on the Conductivity of a Cell Suspension. **Biophysical Journal**, [*s. l.*], v. 88, n. 6, p. 4378–4390, 2005. Disponível em: http://lbk.electroporation.net/pdfs/bj2005.pdf. Acesso em: 23 jan. 2018.

PILLET, Flavien *et al.* Cell wall as a target for bacteria inactivation by pulsed electric fields. **Scientific reports**, [*s. l.*], v. 6, p. 19778, 2016.

PINTARELLI, G.B. *et al.* Computer simulation of commercial conductive gels and their application to increase the safety of electrochemotherapy treatment. **Medical Engineering & Physics**, [*s. l.*], v. 74, n. xxxx, p. 99–105, 2019. Disponível em: https://linkinghub.elsevier.com/retrieve/pii/S1350453319301924.

PINTARELLI, Guilherme B. *et al.* Dielectric Dispersion Modulated Sensing of Yeast Suspension Electroporation. **Sensors**, [*s. l.*], v. 22, n. 5, p. 1811, 2022. Disponível em: https://www.mdpi.com/1424-8220/22/5/1811.

PINTARELLI, G. B. *et al.* Sensing of Yeast Inactivation by Electroporation. **IEEE Sensors Journal**, [*s. l.*], v. 21, n. 10, p. 12027–12035, 2021. Disponível em: https://ieeexplore.ieee.org/document/9378567/.

PINTARELLI, G. B. *et al.* Simulações De Distribuição De Campo E Corrente Elétrica Em Tecidos Biológicos. *In*: AS ENGENHARIAS FRENTE A SOCIEDADE, A ECONOMIA E O MEIO AMBIENTE. [*S. l.*]: Atena Editora, 2019. *E-book*. Disponível em: https://www.atenaeditora.com.br/arquivos/ebooks/as-engenharias-frente-a-sociedade-a-economia-e-o-meio-ambiente-3.

PINTARELLI, G.B. **Técnicas de eletroporação: dispositivo eletrônico e ensaios em leveduras**. 2018. - Universidade Federal de Santa Catarina (UFSC), [*s. l.*], 2018. Disponível em: http://tede.ufsc.br/teses/PEEL1829-D.pdf.

PINTARELLI, G.B.; ANTÔNIO JR, Afrânio C; SUZUKI, D.O.H. **BR 10 2019 018097 8 - Equipamento para aplicação de pulsos de tensão elétrica de amplitude, período e forma de onda variáveis e análise de efetividade para técnicas de eletroporação na transfecção genética e tratamento de neoplasias**. Concessão: 2019.

POTTER, Huntington; HELLER, Richard. Transfection by electroporation. **Current protocols in molecular biology**, [*s. l.*], v. 121, n. 1, p. 3–9, 2018.

PUÉRTOLAS, E. *et al.* Pulsed electric fields inactivation of wine spoilage yeast and bacteria. **International Journal of Food Microbiology**, [*s. l.*], v. 130, n. 1, p. 49–55, 2009. Disponível em: https://linkinghub.elsevier.com/retrieve/pii/S0168160509000038.

RAICU, Valerică; RAICU, Georgeta; TURCU, Grigore. Dielectric properties of yeast cells as simulated by the two-shell model. **Biochimica et Biophysica Acta (BBA) - Bioenergetics**, [*s. l.*], v. 1274, n. 3, p. 143–148, 1996. Disponível em: https://linkinghub.elsevier.com/retrieve/pii/0005272896000242.

RAMOS, Airton *et al.* Sinusoidal Signal Analysis of Electroporation in Biological Cells. **IEEE Transactions on Biomedical Engineering**, [*s. l.*], v. 59, n. 10, p. 2965–2973, 2012. Disponível em: http://ieeexplore.ieee.org/document/6303901/. Acesso em: 22 maio 2017.

RAMOS, Airton; FARIAS D., Heric. Numerical analysis of impedance spectra of yeast suspensions. **Journal of Microwaves, Optoelectronics and Electromagnetic Applications**, [*s. l.*], v. 12, n. 2, p. 647–654, 2013. Disponível em: http://www.scielo.br/scielo.php?script=sci_arttext&pid=S2179-10742013000200032&lng=en&tlng=en. Acesso em: 26 abr. 2018.

RAMOS, Airton; SUZUKI, Daniela O. H. Computational Approach for Electrical Analysis of Biological Tissue Using the Equivalent Circuit Model. *In*: HANDBOOK OF ELECTROPORATION. Cham: Springer International Publishing, 2017. p. 1179–1198. *E-book*. Disponível em: http://link.springer.com/10.1007/978-3-319-32886-7_12.

RANGEL, Marcelo M.M. *et al.* Electrochemotherapy in the treatment of neoplasms in dogs and cats. **Austral journal of veterinary sciences**, [*s. l.*], v. 51, n. 2, p. 45–51, 2019. Disponível em: http://www.scielo.cl/scielo.php?script=sci_arttext&pid=S0719-81322019000200045&lng=en&nrm=iso&tlng=en.

REDONDO, Luís M. S. Basic Concepts of High-Voltage Pulse Generation. *In*: HANDBOOK OF ELECTROPORATION. Cham: Springer International Publishing, 2017. p. 859–879. *E-book*. Disponível em: http://link.springer.com/10.1007/978-3-319-32886-7_209.

REEVE, R. M.; TIMM, Herman; WEAVER, M. L. Cell size in Russet Burbank potato tubers with various levels of nitrogen and soil moisture tensions. **American Potato Journal**, [*s. l.*], v. 48, n. 12, p. 450–456, 1971. Disponível em: http://link.springer.com/10.1007/BF02862060.

RHOADES, J. D.; VAN SCHILFGAARDE, J. An electrical conductivity probe for determining soil salinity. **Soil Science Society of America Journal**, [*s. l.*], v. 40, p. 5, 1976.

RIOU, M. *et al.* Effect of high frequency field on the electric double layer surrounding a biomolecule in a fluid. *In*: , 2014. **COMSOL Conference Boston 2014**. [*S. l.: s. n.*], 2014. Disponível em: http://arxiv.org/abs/1312.7532.

RISKE, Karin A; DIMOVA, Rumiana. Electro-Deformation and Poration of Giant Vesicles Viewed with High Temporal Resolution. **Biophysical Journal**, [*s. l.*], v. 88, n. 2, p. 1143–1155, 2005. Disponível em: https://www.ncbi.nlm.nih.gov/pmc/articles/PMC1305119/pdf/1143.pdf. Acesso em: 30 jul. 2018.

ROSAZZA, Christelle *et al.* Gene Electrotransfer: A Mechanistic Perspective. **Current Gene Therapy**, [*s. l.*], v. 16, n. 2, p. 98–129, 2016. Disponível em: http://www.eurekaselect.com/openurl/content.php?genre=article&issn=1566-5232&volume=16&issue=2&spage=98.

ROY, Arijit *et al.* An experimental method of bioimpedance measurement and analysis for discriminating tissues of fruit or vegetable. **AIMS Biophysics**, [*s. l.*], v. 7, n. 1, p. 41–53, 2020. Disponível em: http://www.aimspress.com/article/10.3934/biophy.2020004.

RUBINSKY, Liel *et al.* Electrolytic Effects During Tissue Ablation by Electroporation. **Technology in Cancer Research & Treatment**, [*s. l.*], v. 15, n. 5, p. NP95–NP103, 2016. Disponível em: http://journals.sagepub.com/doi/10.1177/1533034615601549.

RUBINSKY, Boris. **Irreversible Electroporation**. Berlin, Heidelberg: Springer Berlin Heidelberg, 2010. (Series in Biomedical Engineering). *E-book*. Disponível em: http://link.springer.com/10.1007/978-3-642-05420-4.

SALE, A. J. H.; HAMILTON, W. A. Effects of high electric fields on microorganismsI. Killing of bacteria and yeasts. **Biochimica et Biophysica Acta (BBA) - General Subjects**, [*s. l.*], v. 148, n. 3, p. 781–788, 1967. Disponível em: http://www.sciencedirect.com/science/article/pii/0304416567900529. Acesso em: 13 nov. 2017.

SAULIS, Gintautas *et al.* Changes of the solution pH due to exposure by high-voltage electric pulses. **Bioelectrochemistry**, [*s. l.*], v. 67, n. 1, p. 101–108, 2005. Disponível em: http://linkinghub.elsevier.com/retrieve/pii/S1567539405000587.

SCHWAN, Herman P. Determination of biological impedances. *In*: ELECTROPHYSIOLOGICAL METHODS. [*S. l.*]: Elsevier, 1963. p. 323–407. *E-book*. Disponível em: http://dx.doi.org/10.1016/B978-1-4831-6743-5.50013-7.

SCHWAN, Herman P. Electrical Properties of Tissue and Cell Suspensions. *In*: [*S. l.: s. n.*], 1957. p. 147–209. *E-book*. Disponível em: https://linkinghub.elsevier.com/retrieve/pii/B9781483231112500080.

SEL, D. *et al.* Sequential Finite Element Model of Tissue Electropermeabilization. **IEEE Transactions on Biomedical Engineering**, [*s. l.*], v. 52, n. 5, p. 816–827, 2005. Disponível em: http://ieeexplore.ieee.org/document/1403998/.

SHIMIZU, Naohiro *et al.* A novel method of hydrogen generation by water electrolysis using an ultra-short-pulse power supply. **Journal of Applied Electrochemistry**, [*s. l.*], v. 36, n. 4, p. 419–423, 2006. Disponível em: http://link.springer.com/10.1007/s10800-005-9090-y.

SIMONIS, Povilas; GARJONYTE, Rasa; STIRKE, Arunas. Mediated amperometry as a prospective method for the investigation of electroporation. **Scientific Reports**, [*s. l.*], v. 10, n. 1, p. 19094, 2020. Disponível em: https://doi.org/10.1038/s41598-020-76086-2.

SUÁREZ, Cecilia *et al.* The Role of Additional Pulses in Electropermeabilization Protocols. **PLoS ONE**, [*s. l.*], v. 9, n. 12, p. e113413, 2014. Disponível em: http://dx.plos.org/10.1371/journal.pone.0113413. Acesso em: 31 jul. 2017.

SUN, TAO; GREEN, NICOLAS G.; MORGAN, HYWEL. Analytical and numerical modeling methods for impedance analysis of single cells on-chip. **Nano**, [*s. l.*], v. 3, n. 1, p. 55–63, 2008. Disponível em: https://www.worldscientific.com/doi/abs/10.1142/S1793292008000800.

SUZUKI, Daniela O. H. *et al.* Theoretical and Experimental Analysis of Electroporated Membrane Conductance in Cell Suspension. **IEEE Transactions on Biomedical Engineering**, [*s. l.*], v. 58, n. 12, p. 3310–3318, 2011. Disponível em: http://ieeexplore.ieee.org/document/5677451/. Acesso em: 22 maio 2017.

SUZUKI, Daniela O.H. *et al.* Tratamento De Cânceres Com Eletroquimioterapia. *In*: NOVAS TECNOLOGIAS APLICADA À SAÚDE: DESENVOLVIMENTO DE SISTEMAS DINÂMICOS - CONCEITOS, APLICAÇÕES E UTILIZAÇÃO DE TÉCNICAS INTELIGENTES. 1. ed. Mossoró, RN: [*s. n.*], 2019.

TEISSIÉ, J.; ROLS, M.P. An experimental evaluation of the critical potential difference inducing cell membrane electropermeabilization. **Biophysical Journal**, [*s. l.*], v. 65, n. 1, p. 409–413, 1993. Disponível em: https://linkinghub.elsevier.com/retrieve/pii/S000634959381052X.

TEKTRONIX. **DPO2000 and MSO2000 Series Oscilloscopes User Manual**. Beaverton, USA: [*s. n.*], 2008.

TOEPFL, S.; HEINZ, V.; KNORR, D. High intensity pulsed electric fields applied for food preservation. **Chemical Engineering and Processing: Process Intensification**, [*s. l.*], v. 46, n. 6, p. 537–546, 2007. Disponível em: https://linkinghub.elsevier.com/retrieve/pii/S0255270106001929.

TOMOV, T.; TSONEVA, I. Are the stainless steel electrodes inert?. **Bioelectrochemistry**, [*s. l.*], v. 51, n. 2, p. 207–209, 2000. Disponível em: http://linkinghub.elsevier.com/retrieve/pii/S0302459800000696.

VOLDMAN, Joel. Electrical Forces for Microscale Cell Manipulation. **Annual Review of Biomedical Engineering**, [*s. l.*], v. 8, n. 1, p. 425–454, 2006. Disponível em: http://www.annualreviews.org/doi/10.1146/annurev.bioeng.8.061505.095739.

WALTZ, Emily. Vaccines Go Electric. **IEEE Spectrum**, [*s. l.*], n. June, 2021.

WEAVER, James C *et al.* A brief overview of electroporation pulse strength–duration space: A region where additional intracellular effects are expected. **Bioelectrochemistry**, [*s. l.*], v. 87, p. 236–243, 2012. Disponível em: https://www.ncbi.nlm.nih.gov/pmc/articles/PMC3423488/pdf/nihms368145.pdf. Acesso em: 22 set. 2017.

WEAVER, James C.; CHIZMADZHEV, Yu.A. Theory of electroporation: A review. **Bioelectrochemistry and Bioenergetics**, [*s. l.*], v. 41, n. 2, p. 135–160, 1996. Disponível em: http://linkinghub.elsevier.com/retrieve/pii/S0302459896050623. Acesso em: 26 abr. 2017.

WEAVER, James C.; VERNIER, P. Thomas. Pore lifetimes in cell electroporation: Complex dark pores?. [*s. l.*], 2017. Disponível em: http://arxiv.org/abs/1708.07478. Acesso em: 30 jul. 2018.

XU, Youchun *et al.* A review of impedance measurements of whole cells. **Biosensors and Bioelectronics**, [*s. l.*], v. 77, p. 824–836, 2016. Disponível em: https://linkinghub.elsevier.com/retrieve/pii/S0956566315304917.

YANG, Wuqiang. Design of electrical capacitance tomography sensors. **Measurement Science and Technology**, [*s. l.*], v. 21, n. 4, p. 042001, 2010. Disponível em: https://iopscience.iop.org/article/10.1088/0957-0233/21/4/042001.

ZAMPAGLIONE, Immacolata *et al.* In vivo DNA gene electro-transfer: a systematic analysis of different electrical parameters. **The Journal of Gene Medicine**, [*s. l.*], v. 7, n. 11, p. 1475–1481, 2005. Disponível em: https://onlinelibrary.wiley.com/doi/10.1002/jgm.774.

ZHANG, Yuanjun *et al.* A Novel Electroporation System for Living Cell Staining and Membrane Dynamics Interrogation. **Micromachines**, [*s. l.*], v. 11, n. 8, p. 767, 2020. Disponível em: https://www.mdpi.com/2072-666X/11/8/767.

ZHANG, Li Li; ZHAO, X. S. Carbon-based materials as supercapacitor electrodes. **Chemical Society Reviews**, [*s. l.*], v. 38, n. 9, p. 2520, 2009. Disponível em: http://xlink.rsc.org/?DOI=b813846j.

ZHAO(B), Yajun *et al.* Ablation outcome of irreversible electroporation on potato monitored by impedance spectrum under multi-electrode system. **BioMedical Engineering Online**, [*s. l.*], v. 17, n. 1, p. 1–13, 2018. Disponível em: https://doi.org/10.1186/s12938-018-0562-9.

ZHAO, Yajun *et al.* Characterization of Conductivity Changes During High-Frequency Irreversible Electroporation for Treatment Planning. **IEEE Transactions on Biomedical Engineering**, [*s. l.*], v. 65, n. 8, p. 1810–1819, 2018. Disponível em: https://ieeexplore.ieee.org/document/8122021/.

ZHUANG, Jie; KOLB, Juergen F. Time domain dielectric spectroscopy of nanosecond pulsed electric field induced changes in dielectric properties of pig whole blood. **Bioelectrochemistry**, [*s. l.*], v. 103, p. 28–33, 2015. Disponível em: http://dx.doi.org/10.1016/j.bioelechem.2014.08.009.

ZIMMERMANN, Ulrich; NEIL, G. A. **Electromanipulation of cells**. [*S. l.*]: CRC Press, 1996.

APPENDIX A – Arbitrary Generator Waveforms

This appendix contains some of our generator input-output waveforms as Figure 48. Those were measured using Tektronix DPO2012B oscilloscope.

Figure 48 – PEF generator frequency response. CH1 (yellow) is the voltage output, CH2 (blue) is the DAC output and the red the output FFT. All data collected using a 10 Ω load. (a) 10 kHz, (b) 100 kHz zoom, (c) 100 kHz, (d) 250 kHz, (e) rise time and (f) fall time.

(d)

(e)

(f)

Source: Author.

APPENDIX B – Sensing of Yeast Inactivation by Electroporation

1

106

Sensing of Yeast Inactivation by Electroporation

G. B. Pintarelli, *Member, IEEE*, C. T. S. Ramos, J. R. da Silva, M. J. Rossi, D. O. H. Suzuki

Abstract—Irreversible electroporation is a treatment to control microorganisms in food without harming food palatable aspects. The treatment by electroporation is dependent on the electric field amplitude, pulse durations and pulse repetitions. This study was carried out as a further investigation on the effects of irreversible electroporation pulse amplitude on *S. cerevisiae* and methods to verify the occurrence of irreversible electroporation, such as cell viability hemocytometer, macroscopic impedance measurements, scanning electron microscopy and numerical simulations. Active yeasts in wine represent a small portion of the volume (< 10^8 cell/mL), which challenges macroscopic impedance analysis. Irreversible electroporation proved to reach active yeast limits established by standards within 500 kV/m. We detected a 15% increase in the in pulse current measurements for a 100-fold yeast viability decrease to 10^5 cells/ml. Scanning electron microscopic images show details of yeast surface damage which may be PEF-triggered. Electric fields above 1 MV/m on the cell wall and release of intracellular substance caused by membrane permeability increase may directly contribu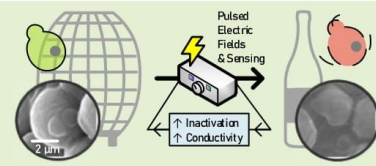te to yeast inactivation. Electroporation combined with instantaneous current-voltage measurements may be an adequate procedure for reducing yeast numbers in the industry.

Index Terms— Pulsed Electric Fields, Yeast, Inactivation, Irreversible Electroporation, Bioimpedance, Biotechnology, Scanning Electron Microscope.

I. Introduction

LIVING microorganisms are commonly part of foods and beverages processing. For instance, yeasts are used in the fermentation process of beer, bread, and wine. Generally, they do not present adverse effects when used with restrictions; however, excessive yeast growth may intensify metabolic decomposition, which depreciates the food quality. This process is called yeast spoilage and can make food inedible for humans or reduce its edible quality. If ingested in non-safe quantities, yeast can provoke infection [1], [2]. Foods with delicate sensory properties, such as wine, a small yeast excess can lead to a difference in its acidity, which causes a significant change to the overall palatable aspects [3]. In any event, the detection of poor quality food can lead to a waste of product and company profit loss [4].

Heat processing of foods is one of the earliest and still one of the most important preservation methods [5]. Thermal pasteurization is the food heating process that aims to kill pathogenic agents and stop yeast fermentation, making food safe to eat and store. Sterile filtration with precipitation agent and chemical treatment (*e.g.,* SO₂) are also options that can achieve similar results of pasteurization. However, it is known that thermal pasteurization, sterile filtration, and chemical treatment affect food's nutrients composition and sensory characteristics (*e.g.,* color, texture, aroma and flavor) [6]–[9]. In the case of wines, pasteurization is avoided as it damages organoleptic properties. Final customers are continuously looking forward to those characteristics, as they are often related to freshness and authenticity [3], [6], [8].

In wine production, yeast control is challenging and of high importance as yeasts rapid grow can significantly alter grapes pH and flavor, thus, compromising wine quality and causing significant economic losses. There is no fine control of the yeasts involved in the wine production process [4]. In wines, the *S. cerevisiae* yeast is the most frequent contaminant and spoilage species [2]. In other types of foods, other microorganisms may be relevant. Those that can cause foodborne illnesses and can even become lethal. For instance, *Listeria monocytogenes*, *Escherichia coli* O157, *Salmonella, Staphylococcus aureus*, *Bacillus cereus*, *Campylobacter*, *Clostridium perfringens* and *Aspergillus niger* [10].

The International Organization of Vine and Wine (OIV), the benchmark for vine-based products standards, establishes the maximum acceptable limits for oenological practices; this includes the maximum values for viable yeasts load [11]. Therefore, to obtain adequate wines that are safe for consumption and with preserved palatable aspects, yeasts should be removed or inactivated. In this regard, controlling yeast number in the food processing environment is made necessary.

Yeast control in different media can be reached by electroporation, as electroporation is a well-known technique for the permeabilization of cells in suspension and tissues [12]. The procedure is based on pulsed electric fields (PEF). PEF has

been used as a method for preservation and cold pasteurization of food [6]–[9], [13], [14], and as a cancer ablation treatment (*e.g.* electrochemotherapy) [15], [16]. Electroporation, accompanied by adequate detection, allows determining the appropriate electric pulse for cell control. PEF parameters can be optimized to reach the yeast irreversible electroporation threshold. Irreversible electroporation offers safe food with sensorial aspects more similar to the unprocessed, leading to a greater acceptance of the food. The use of PEF has been explored more intensely over the last few years, with the development of new and improved techniques [13], [17].

Macroscopic electrical properties measurements can be used to sense electroporation. The intact cell membrane is dielectric, and the opening of pores by electroporation causes a decrease in the membrane's electrical resistance. Moreover, leakage of intracellular ions may occur or complete cell membrane destruction. Those contribute to increasing the macroscopic conductivity. There are two main sensing approaches, measuring before and after the pulse (by using electrical impedance spectroscopy) or during an electroporation pulse (by current-voltage acquisition or electrodes current density). Macroscopic electrical measurements may take advantage of using the PEF-electrodes themselves, which facilitates implementation at sanitary controlled environments [17]–[19] without the need of extra equipment contacting the sample [20].

Analysis by electrical impedance spectroscopy may provide a wide range of information. The optimal cell sensing frequency range is between 100 Hz to 100 kHz [21]–[23]. Nevertheless, electrodes polarization up to 1 kHz is expected [23]. The impedance analysis method usually requires interruption in the electroporation protocol, and analysis may take seconds to complete, which may be a limitation of this procedure since electroporation occurs in nanoseconds [18]. Analysis during individual PEF pulses can be performed by measuring current and voltage. This method is also called 'instantaneous' or 'apparent' conductivity analysis, *i.e.,* the ratio between current and voltage at a given time point. The conductivity increase due electroporation was observed in high cell fraction suspensions of animal cells [12], [24], [25], bacteria [13] and yeast [26], [27], and tissues [15], [19], [28], [29]. High cell concentrations (typically over 5% volumetric fraction) are preferable since macroscopic effects on the conductivity are amplified. However, food industries typically use a low yeast load (< 10^8 cell/mL, *i.e.* lower than 2% volumetric fraction) [2], [11]. Yeast inactivation at industrial concentration is possible [30]. However, sensing the conductivity changes due to irreversible electroporation using industrial yeast concentration has not yet been discussed.

This work proposes sensing industrial wine yeast limit killed by electroporation via electrical properties measurements during the PEF protocol and using the PEF electrodes. We used a device to study electroporation detection techniques at industrial cell concentration. Currently, conductivity change can be used to sense electroporation in dense yeast suspension (> 10^8 cell/mL) [26], [27]. We propose using current-voltage sensing as a method of yeast control, as it is capable of sensing yeast cell death at low cell load (< 10^8 cell/mL) [2], [11]. Controlling cell death at the time of the pulse provides instantaneous feedback on cell death, and it is desired in industrial systems to perform closed-loop (or feedback loop) electroporation, *i.e.,* a real-time control system that adjusts voltage and number of pulses as a function of the change in the permeability of cells membranes. This type of control can enhance the optimization of the electroporation process and energy efficiency.

II. MATERIALS AND METHODS

A. Strains and cell suspension preparation

Saccharomyces cerevisiae ATCC® 36900™ were used in the *in vitro* experiments. Strains were obtained from a freeze-dried repository from the Laboratory of Bioprocesses (Microbiology, MIP) of the Federal University of Santa Catarina (UFSC). These cells were cultivated in 15 mL sterilized (autoclaving 120 °C, 15 minutes) YPD liquid media (2% peptone, 2% yeast extract, 2% glucose, pH 5.74) and incubated for 24 h at 30 ºC. This interval is necessary for yeasts reproduction. After incubation, the cell viability and density were measured using methods detailed in 'Cell viability assessment', and the electroporation experiment started. The cells viability at the beginning of the experiments was 97%. The cell suspension density was 2.5×10^7 cells/mL, representing a volumetric fraction or weight concentration (weight of yeast cells/total weight of suspension) of 0.43 % in water.

B. Electroporation setup

PEF protocol was generated by a custom made generator with embedded voltage-current data acquisition [31]. The protocols were 8 rectangular-shaped pulses of 100 μs and a repetition rate of 1 Hz (*i.e.,* 1-second pulses interval). This protocol is similar to the European Standard Operating Procedures of Electrochemotherapy [32]. We investigated the effects of amplitude changes as the electroporation mainly depends on it. The magnitude was estimated as the voltage applied divided by the distance between the electrodes. The voltage was measured at the electroporator's output which was directly connected to the electroporation chamber. It has been assessed the effect of amplitude applying protocols of 200 to 600 kV/m. Current-voltage measurements were collected during PEF protocol [25] and were used to calculate the absorbed energy, *i.e.,* $V*I*t/A$, where V and I are the voltage and current of the electrode, respectively, t the total protocol time (8×100 μs) and A the sample volume [3]. Averages were made based on 20 instant readings (200 kHz sampling rate system). This practice was used to mitigate transient effects, which occur at frequencies above 100 kHz [23]. A 100 kHz (4th order Butterworth) hardware anti-aliasing filter was used according to Nyquist theorem to avoid signal loss. The acquisition equipment was calibrated up to 600 V and 12 A and diagnosed by residuals using Rstudio 3.5.2 (RStudio, Inc., Boston, MA); the worst-case error is 1,66 %.

The electrical impedance study was performed before and after PEF using 4294A and 16047E adapter (Agilent Technologies, California, United States). The equipment was configured to obtain a real and imaginary part of the impedance (resistance and reactance) of 1 kHz, 10 kHz, and 100 kHz. Impedance measurements occurred 30 seconds before and after the PEF protocol.

The electrodes consist of two 6 × 7 mm AISI 304 stainless-steel parallel plates separated 1 mm (*d*) and mounted on a PVC

holder. Electrodes in the millimeter dimension facilitate obtaining high electric fields and are compatible with the sample tested. The electrodes' surface is larger than the samples surface contact; this avoids diffraction of the electric field. Therefore, all the cells were exposed to similar electric field magnitudes. Similar procedures are described in the literature [13], [33].

The electrodes were cleaned and dried with 70% ethyl alcohol, and a droplet of media (40 μL) was pipetted between the electrodes. We tested two groups: cell suspension (with the incubation YPD buffer to simulate wine) and the YPD buffer. The YPD conductivity was 0.415 S/m (measured with SX-650, San-Xin Instrumentation, Inc., China). The media remained in the electroporation chamber for a maximum of 45 seconds. The solution has enough intermolecular forces to not to overflow (no bucket required). The contents were removed using a micropipette after the PEF application (or not, in the case of the control) and follow to the microscopy studies (cell viability assessment and cell morphology studies). All samples were submitted to the same process (insertion and removal of the electrode system); this includes the control samples. All experiments were executed at 24.5 ºC room temperature.

C. Cell viability assessment

Methylene blue (0.2% $C_{16}H_{18}N_3SCl$) is a fast yeast viability tool and was used to describe the cell viability loss in all the experiments. Methylene blue penetrates all cells. If the cell is alive, methylene blue is reduced in colorless substance by an enzymatic process. The non-viable cells fail to reduce methylene blue and are stained in blue. Methylene blue was 1:1 diluted in the cell suspension samples by 30 seconds of manual shaking. A 5-minute waiting time was set for cell sedimentation and blue staining. No washing procedure or additional incubation period was required [34], [35]. The viable and non-viable cell counting was according to the hemocytometer method [11], and approximately 65 cells were counted per 0.25 x 0.25 mm² Neubauer chamber square area.

D. Cell morphology assessment by electron microscopy

The JSM-6390LV (JEOL Ltd., Tokyo, Japan) scanning electronic microscope (SEM) was used to characterize cell morphology and integrity. The equipment was configured with an accelerating voltage of 15 kV, magnification of 6000× and low vacuum mode.

The yeast suspensions were removed from electrodes and were centrifuged at 6200 rpm (approximately 2000×G) for 3 minutes. The yeast slurry was collected, washed three times with deionized water, deposited with adhesive carbon pads on stubs, dried in a vacuum desiccator for 1 h at 50 ºC (MA192 desiccator, Marconi Ltd., Piracicaba, Brazil) and gold plated (EM SCD500, Leica Microsystems GmbH, Wetzlar, Germany) [36]. The washing procedure is necessary to remove the YPD media that generate noises in the electron microscopy image.

E. Data analysis

Cell viability was performed with five replicates (N = 5), the impedance was performed seven times (N = 7), and in pulse current analysis was performed nine times (N = 9). The data was processed by Microsoft Excel (Office 365, Microsoft Corp., Redmond, Washington, United States). The statistical significance of differences for cell viability and current increase was calculated by Rstudio 3.5.2. Cell integrity assessment by electron microscopy was obtained in duality (N = 2).

Unpaired and parametric statistical tests were performed. Gaussian distribution was tested using Shapiro-Wilk normality test. All samples were found to be normally distributed. The one-way ANOVA test was used to compare groups.

F. Numerical and geometry modelling

The simulations were performed using the COMSOL Multiphysics® version 4.4 software package (COMSOL Inc., Burlington, MA) based on the finite-element method. The electric field distribution models were calculated using the steady current module. If the electric current density J in tissue is divergence-free, the solved equation is Poisson's equation:

$$-\nabla \cdot (\sigma \nabla V) = 0 \qquad (1)$$

where σ is the conductivity (S/m), and V is the electric potential (V).

Fig. 1 shows the spherical two-shell cell model used in our simulations. A grid independence study was performed to establish an optimized mesh. The COMSOL 'extremely fine' mesh was set on the cell membrane and 'fine' mesh in other geometries. The total mesh was 61,730 tetrahedral elements.
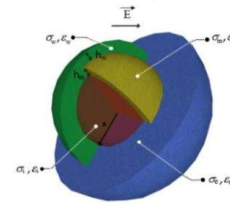
Fig. 1. Two-shell model of a yeast cell. The values of the radius R, thickness h, electric conductivity σ, and permittivity ε are available in Appendix A. The subscripts 'w', 'm', 'e' and 'i' refer to the wall membrane, cytoplasmic membrane, external and internal medium, respectively.

The ionic transport across the pores formed by electroporation increases cytoplasmic membrane conductivity. Assuming that the intact lipid matrix has negligible ionic mobility, all ionic transport should happen through the pores. The pores density, average membrane conductivity and pore conductivity equations were implemented and solved in numerical modelling (see Appendix A for details) [37]–[40]. The number of pores N(t), the electrical potential between faces of cytoplasmic membrane $V_m(t)$ (*i.e.,* transmembrane voltage) and cell wall differential voltage $V_w(t)$ were calculated for 200, 300, 400, 500 and 600 kV/m.

III. RESULTS

A. Impedance measurements

Impedance changes due to the PEF were compared between the cell suspension and YPD media. Chamber resistance and reactance (Ω) of cell suspension and YPD 'before PEF' and 'after PEF' 600 kV/m protocol are according to Table I. The 600 kV/m PEF was the highest protocol applied. The electrode-solution interface causes the increase of the reactance and resistance as the measurement frequency decreases in both media. Thus, measurements show a higher reactance at 1 kHz.

TABLE I
YPD AND CELL SUSPENSION CHAMBER IMPEDANCE (COLUMNS) BEFORE AND AFTER PEF AT 1, 10 AND 100 kHz (LINES). IMPEDANCE IS GIVEN AS
RESISTANCE AND REACTANCE (VALUES ARE EQUAL TO MEAN ± STANDARD DEVIATION).

	Frequency	Chamber resistance (Ω)		Chamber reactance (Ω)	
		YPD	Cell suspension	YPD	Cell suspension
Before PEF protocol	1 kHz	323.6 ±47.1	366.7 ±91.1	-200.9 ±50.9	-227.5 ±53.0
	10 kHz	195.3 ±17.5	188.9 ±41.3	-69.2 ±16.4	-92.6 ±27.6
	100 kHz	146.2 ±6.8	119.5 ±27.2	-23.4 ±6.1	-31.8 ±10.4
After PEF protocol	1 kHz	264.2 ±17.8	294.8 ±55.6	-106.8 ±11.8	-143.3 ±30.8
	10 kHz	189.3 ±11.6	178.4 ±33.5	-44.3 ±6.6	-66.2 ±14.9
	100 kHz	151.2 ±7.5	121.0 ±24.0	-17.7 ±2.3	-26.9 ±6.3

Significant changes (p ≤ 0,05) occur at 1 kHz in the YPD media resistance due to PEF, which may be explained by the PEF direct current altering the ion accumulation at electrodes (changing the impedance of the electrode-solution interface); this is called the electrode polarization and affects the sample's impedance approximately at 1 kHz. Electrode polarization and its interface makes the 1 kHz not an adequate frequency for sensing [23], [26], [41].

Information about cells membranes may be found at frequencies 10 and 100 kHz [21]–[23]. However, there is no statistical difference in resistance changes at 10 and 100 kHz for the YPD media and cell suspension (p > 0,05). The low cell concentration, typical of industrial alcoholic fermentation [2], [11], [42], may not permit detecting impedance differentiation between before and after electroporation treatment.

B. In pulse current rate

Fig. 2a shows the current during the PEF protocols. The absorbed energy is higher when there are cells in the media. Dozens to thousands of kJ/L are expected for microbial inactivation [3]. Due to the short burst (8 pulses of 100 μs), the theoretical temperature rise at the end of the 600 kV/m protocol is 3.5 °C [27]. The temperature increase should be lower in practice since thermal dissipation during the inter-pulse intervals (1 second). At 600 kV/m, we observed a conductivity plateau which may indicate the maximum ion exchange due to electroporation in our experiments. Other work reported similar conductivity saturation [15], [25], [27].

We analyzed the current changes in terms of in pulse current rate. We define the in pulse current rate as the average increase of current between the last (eight) and first pulse. Fig. 2b shows the in pulse current rate as a function of PEF amplitude. The YPD media were directly compared to the cell suspensions. At 200 kV/m there is a non-significant difference (ns). Over 300 kV/m we detected significant differences (when comparing equal kV/m magnitudes). When comparing in pulse current increase at similar delivered energy, 22-25 kJ/L has no significant difference, and 40-42 kJ/L has a significant difference. The phenomenon that changes current is related to the presence of cells and it is not associated with temperature. The polarization of the electrodes (seen in Table I) did not disrupt the differentiation between YPD and cell suspension.

C. Sensing electroporation effects

The compiled result of the current change and cellular viability due to the PEF protocol are shown in Fig. 3a. There is a correlation between cell viability reduction and current change. SEM images are shown in Fig. 3b. Using SEM, we observed that some cells were physically damaged, and others

were not. Zakhem *et al.* reported similar results [27]. Those are PEF triggered damage and not the actual PEF pores. The physical damage may be provoked by the combination of cell perturbations, *i.e.*, the PEF, the hypoosmotic medium passage and drying. The electroporation may weaker the cell surface and drain out the intracellular due to membrane destruction. We focused on showing the damaged cells, as shown in Fig. 3 (3c to 3f). At 200 and 300 kV/m, a smaller part of the cells presented the damage according to Fig. 3c and 3d. SEM is a qualitative tool to analyze if the physical damage occurred (as it cannot be seen using other studies). The viability curve (Fig. 3a) is a suitable way to inference in the cell population. The damage may be concentrated at yeast poles as those are the higher transmembrane voltage locations [39]; however, further studies are needed to study this hypothesis. SEM provided details of physical damage not seen using neither cell viability nor macroscopic electrical properties readings.

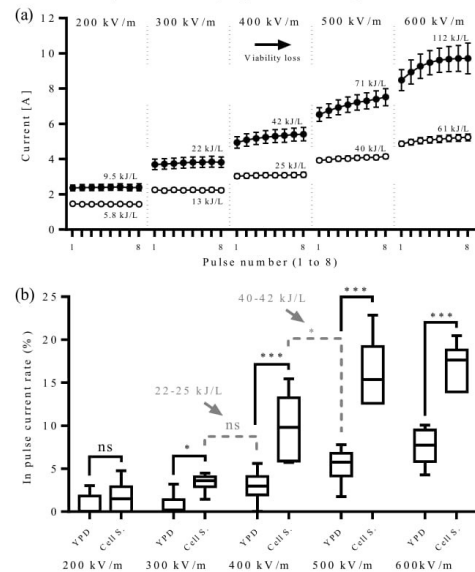Fig. 2. (a) Electrical currents at PEF protocol. The '●' means the cell suspensions data, and 'o' means the YPD data. (b) YPD and cell suspension ('Cell S.') conductivity change as a function of PEF protocol amplitude in kV/m. The significance levels are given upper the box plots. 'ns' means not significant (p>0.05), '*' means p<0.05 and '***' means p<0.001. Oscillations below zero at 200 and 300 kV/m are not shown.
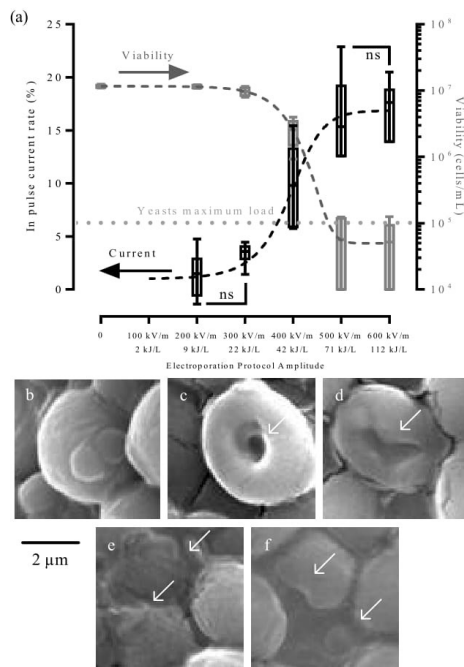
Fig. 3. (a) Cell viability and conductivity increase due to electroporation protocol amplitude. The errors bars are shorter than the height of the symbol in viability when 0, 200, 300 kV/m. Yeast maximum limit described as clear bottled white wine [2], unit adequation was realized with [43]. (b) SEM image of yeast cell without electroporation pulses. (c) 200 kV/m, (d) 300 kV/m, (e) 400 kV/m and (f) 500 kV/m. White arrows indicate surface damage.

At 500 kV/m, we detected yeast viability within limits accepted [2]. The yeast PEF-damage starts at 300 kV/m [44], and the irreversible electroporation threshold at dense cell suspension is reported to be 750 kV/m [27]. The measured threshold of 500 kV/m may be due to the lower cell density. Yeast clusters are formed at high cell density, which requires higher PEF [45]. The electroporation threshold may shift in the 300 to 800 kV/m range as it is also dependent on the external buffer [3], [13], yeast phase [45], temperature [9], and cell concentration [13], geometry and size distribution [46]. If the viability loss is greater than 90% (500 kV/m), it is possible to detect a greater current change than the 400 kV/m. Our results show that the current change method is not sensitive to detect a small viability loss (less than 10 %) or changes in the cell wall.

D. Modelling

Reversible electroporation usually occurs for transmembrane potentials (V_m) of 0.2 to 1 V [12], and irreversible electroporation may occur above 1 V [9]. Numerical simulations indicate that pores open in the cell membrane at all tested protocols, as shown in Fig. 4a (creation of pores as a function of time). Fig. 4b shows the behavior of the V_m. Accordingly, the 200 kV/m protocol may provoke reversible

electroporation, and the 300 kV/m protocol may provoke irreversible electroporation ($V_m > 1$ V). However, based on the viability test, 300 kV/m is not enough for irreversible electroporation, and protocols over 400 kV/m produced irreversible electroporation. 500 kV/m is in accordance with the yeast limit to clear white wine (seen in Fig. 3). The differential voltage in the cell wall shows a voltage peak, as Fig. 4c. The simulations show that the electroporation occurs in the order of microseconds, regardless of longer pulses of 100 μs.
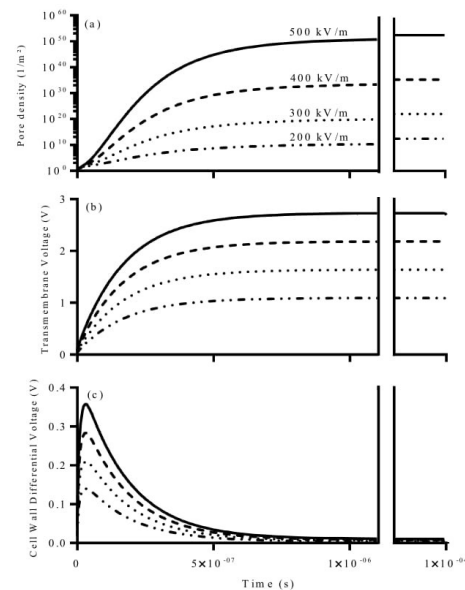
Fig. 4. Behavior of the (a) number of pores at cell membrane, (b) transmembrane voltage and (c) differential voltage in the cell wall as a function of the electroporation protocols of 200 to 500 kV/m and time. The graphs were cut from 0 (pulse start) to 1×10^{-6} seconds, since changes occur at these times.

IV. DISCUSSIONS

There are many reports showing microorganism inactivation capabilities of PEF at liquid food processing [3], [5], [7]–[9], [17], [47]–[49]. Detecting inactivation increases the safety of industrial use of this technique. Methods tested using cell suspension and YPD could be scaled to industry. Electrical measurement (i.e., impedance spectroscopy and current-voltage recording) may be used as a tool to detect and control inactivation. Give the need to detect the success of electroporation and reliability of current sensing during PEF protocol, we recommend in pulse current-voltage recording for low cell concentration. Moreover, hundreds of microseconds of pulsed current can be acquired and processed with simple equipment. Since some liquid foods (e.g., wine) is a sensitive medium (subject to oxidation and deterioration of organic substances) [2], future work may model other phenomena such as electrode failures and investigate other factors (e.g., conductivity, pH, sugar concentration and temperature).

Impedance analysis before and after the PEF protocol was not satisfactory for detecting electroporation in this work setup. This type of analysis only detected polarization of the electrodes at 1 kHz (see the 20% resistance decrease in the before and after results at Table 1) [23], [26], [50]. Besides this occurrence, changes in the 'instantaneous' conductivity in cell suspension (related to the electric current) were detected when using protocols over 300 kV/m (Fig. 2). There is evidence of a correlation between conductivity increase and cell viability loss using protocols over 400 kV/m (Fig. 3). Further analysis is needed to evaluate a similar correlation when using other cells and wine. The macroscopic current-voltage readings are not enough to detect cells physical changes showed by the SEM (SEM images at Fig. 3). Evidence of surface damage at the 200 kV/m may be correlated to V_m increase to approximately 1 V (observed in the numerical simulations in Fig. 4b), which may provoke irreversible electroporation [9].

Changes in the impedance spectrum (by impedance spectroscopy) due to electroporation are expected for high cell concentrations. Electroporation can extract ions and PEF could lead to membrane interface polarization (*i.e.*, ion accumulation in the membranes and cell walls) [12], [25], [26], [33]. In this work, there was no evidence of impedance changes before and after pulses due to electroporation. The lack of success when using impedance analysis may be explained by the low cell concentration used (2.5×10^7 cells/m, representing a volumetric fraction of 0.0043). The cell concentration used is typical of wine fermentation [42]. OIV suggests at least 5×10^6 cells/mL for fermenting wines [11].

Multiple effects are related to changes in electrical properties as a function of PEF (*e.g.*, electrochemical effects, joule heating and electroporation). This fact can difficult individual analysis of these phenomena. Heating by joule effect and electrode metal release may affect conductivity. Because of this, we adopted a direct comparison between YPD media and cell suspension (Fig. 2) [16], [51]. There is a significant difference in conductivity change when cells are in the medium if the protocol is higher than 300 kV/m (Fig. 2).

The techniques of measurement of current-voltage and impedance used in this work are similar to others reported in the literature [19], [25]. However, we used average current values from the last to the first pulse of the protocol. This type of practice favors sensing electroporation for real-time industry applications as it decreases computational and hardware costs. PEF is mostly studied with high voltage pulse generators without any feedback. Sensitization of irreversible electroporation and cell death can improve the detection of failures in the industry. In pulse current-voltage method is advantageous at implementation in an industry as it does not require interruption of the high voltage electroporation protocol. Impedance small-signal analysis may not be advantageous as it may require interruption of the high voltage application, which may be unsuitable for industrial process. The use of the electroporation electrodes themselves as sensors is advantageous since it is unnecessary to design electrodes with delicate mechanical parts, such as pH sensors or other extra equipment contacting the sample [20].

Current-voltage readings were suitable to detect the occurrence of irreversible electroporation using low cell density. With this, one can guarantee that the impedance measurement can measure yeasts death with a certain level of confidence. This makes this method beneficial since the overgrowth of yeast can cause it to become yeast spoilage where it can be responsible for economic losses [1]. We focused on indirect probing irreversible electroporation as it is desired in the industry. Further work may use methods to investigate reversible electroporation (*e.g.,* non-permeable dies) and compare it with conductivity. We believe the 300 kV/m PEF is a potential candidate for reversible electroporation, as it shows significant in pulse measurement difference (Fig. 2), it was insufficient for reducing viability (Fig. 3a), and the numerical simulation shows a $V_m > 1$ V (Fig. 4).

Electroporation may cause osmotic imbalance due to the leakage of ions and small molecules which provokes cell swelling and deformation [18]. Thus, the physical changes seen by SEM are expected. SEM detected changes in the membrane at 200 and 300 kV/m that were not perceived by the other methods. In addition to breakdown detail and destruction of cells at 400 and 500 kV/m, as shown in Fig. 3. However, cell-wall architecture may be involved with yeast inactivation. Fig. 4c shows the electric field in the cell wall above 1 MV/m for 400 kV/m. The cellulose dielectric breakdown strength is about 9 MV/m [52]. Our numerical findings support the evidence of Pillet *et al.* [53] that lost integrity of cell wall, and plasmatic membrane permeability were the causes of yeast inactivation.

New studies could apply high frequencies bursts, *i.e.*, 1 μs pulses waveform. It is observed that 97% of the signal energy is present in frequency up to 10 kHz. Frequencies above 10 kHz represent only 3% of the energy of this signal [16]. According to the results, electroporation occurs in microsecond time orders as shown in Fig. 4. Based on these facts, the reduction of the pulse time to sub microseconds should be adequate for electroporation; this is important in industrial applications, as it can represent energy savings. Moreover, high frequencies of bipolar pulses may mitigate electrodes polarization [50]. However, from the point of view of real-time analysis, this may be a problem as sub microseconds pulse acquisition may be contaminated with transient effects. Also, future work may use another viability assessment (e.g., CFU viability test) to provide better evidence on the correlation of increased current and inactivation. The methylene blue is used as a viability test in industries and literature; however, it measures enzymatic activity (at a specific point of time after treatment), indirectly associated with cell death [34].

In this work, the in pulse current rate has been analyzed as sensing to *S. cerevisiae* inactivation by irreversible electroporation for the wine industry. The increase of yeast concentration during the wine process may be a challenge for pasteurization by PEF. The in pulse current sensing may be a possible feedback to improve the PEF for efficient pasteurization. Future works could explore the control capacity of diverse microorganisms and yeasts strains with the methods proposed in this work.

V. CONCLUSIONS

This work demonstrates that inactivation of *S. cerevisiae* at low cell load, typically found on wines (< 10^8 cell/mL), can be detected by instantaneous current measurements during PEF. A 15% in pulse current increase is expected when reducing yeast

numbers to 10^5 cells/ml by 500 kV/m irreversible electroporation PEF. This result may enhance applications for liquid food pasteurization and preservation. The method described some industrial advantage as continuous monitoring, which optimizes the electroporation process.

APPENDIX

The nonlinear model of electroporation simplifies the Smoluchowski equation to describe the pore density $N(t)$, as [37]:

$$\frac{dN(t)}{dt} = \alpha e^{\left(\frac{V_m(t)}{V_{ep}}\right)^2}\left(1 - \frac{N(t)}{N_0}e^{-q\left(\frac{V_m(t)}{V_{ep}}\right)^2}\right) \qquad (2)$$

where $V_m(t)$ is the transmembrane voltage, V_{ep} is the electroporation voltage, N_o is the pore density at $V_m = 0$ V, and α and q are constants.

The regions where pores are formed present average conductivity of [38], [39]:

$$\sigma_m(t) = \sigma_{m_0} + N(t)\sigma_p\pi r_p^2 K \qquad (3)$$

where σ_{mo} is the membrane conductivity without electroporation, σ_p is the conductivity of pore, r_p is the pore radius, and K is:

$$K = \frac{e^{v_m}-1}{\frac{w_0e^{w_0-\eta v_m}}{w_0-\eta v_m}e^{v_m}-\frac{w_0e^{w_0+\eta v_m+\eta v_m}}{w_0+\eta v_m}} \qquad (4)$$

where w_o is the energy barrier inside the pore, η is the relative entrance length of the pore, and $v_m = \frac{qe}{kT}V_m$ is the non-dimensional transmembrane voltage.

The pore conductivity is [40]:

$$\sigma_p = \frac{\sigma_w - \sigma_i}{\ln\left(\frac{\sigma_w}{\sigma_i}\right)} \qquad (5)$$

The cell and electroporation model parameters are given in Table 2.

TABLE II
NONLINEAR ELECTROPORATION MODEL, ELECTRICAL AND GEOMETRIC PARAMETERS OF SIMULATION

Parameter	Symbol	Value	References
External conductivity	σ_e	$0.415\ S/m$	
External permittivity	ε_e	80	[54]
Membrane permittivity	ε_m	6	[55]
Wall membrane conductivity	σ_w	$0.05\ S/m$	[55], [56]
Wall membrane permittivity	ε_w	60	[57]
Cytoplasm conductivity	σ_i	$0.2\ S/m$	[54], [58]
Cytoplasm permittivity	ε_i	50	[54], [58]
Cell radius	R	$3.46\ \mu m$	
Thickness membrane	h_m	$8\ nm$	[54], [58]
Thickness wall	h_w	$220\ nm$	[54], [55]
Electroporation constant	q	2.46	[37], [38], [39]
Electroporation constant	α	$109\ m^2s^{-1}$	[37], [38], [39]
Pore density at V_m=0 V	N_0	$1.5 \times 10^9\ m^{-2}$	[37], [38], [39]
Electroporation voltage	V_{ep}	$258\ mV$	[37], [38], [39]
Pore energy barrier	w_0	2.65	[37], [38], [39]
Relative length of the pore	η	$0.15\ nm$	[37], [38], [39]
Pore radius	r_p	$0.8\ nm$	[37], [38], [39]
Boltzmann constant	k	$1.38 \times 10^{-23}\ m^2kgs^{-2}K^{-1}$	[37], [38], [39]
Temperature	T	$295\ K$	[37], [38], [39]

REFERENCES

[1] M. Eroglu S., Toprak S., Urgan O, MD, Ozge E. Onur, MD, Arzu Denizbasi, MD, Haldun Akoglu, MD, Cigdem Ozpolat, MD, Ebru Akoglu, *Yeasts in Food and Beverages*, vol. 33. 2012.

[2] V. Loureiro, "Spoilage yeasts in the wine industry," *Int. J. Food Microbiol.*, vol. 86, no. 1–2, pp. 23–50, Sep. 2003.

[3] E. Puértolas, N. López, S. Condón, J. Raso, and I. Álvarez, "Pulsed electric fields inactivation of wine spoilage yeast and bacteria," *Int. J. Food Microbiol.*, vol. 130, no. 1, pp. 49–55, Mar. 2009.

[4] G. H. Fleet, "Yeasts in foods and beverages: impact on product quality and safety," *Curr. Opin. Biotechnol.*, vol. 18, no. 2, pp. 170–175, Apr. 2007.

[5] H. Vega-Mercado, M. M. Gongora-Nieto, G. V Barbosa-Canovas, and B. G. Swanson, "Pulsed Electric Fields in Food Preservation," in *Handbook of Food Preservation*, Second., M. S. Rahman, Ed. Boca Raton, Florida: CRC Press, 2007, pp. 783–813.

[6] J. A. Couto, F. Neves, F. Campos, and T. Hogg, "Thermal inactivation of the wine spoilage yeasts Dekkera/Brettanomyces," *Int. J. Food Microbiol.*, vol. 104, no. 3, pp. 337–344, Oct. 2005.

[7] D. Branch, "Pulsed Electric Fields for Food Preservation : An Update on Technological Progress," in *Progress in Food Preservation*, no. January, Oxford, UK: Wiley-Blackwell, 2012, pp. 277–295.

[8] A. V. Charles-Rodríguez, G. V. Nevárez-Moorillón, Q. H. Zhang, and E. Ortega-Rivas, "Comparison of Thermal Processing and Pulsed Electric Fields Treatment in Pasteurization of Apple Juice," *Food Bioprod. Process.*, vol. 85, no. 2, pp. 93–97, 2007.

[9] A. Golberg, J. Fischer, and B. Rubinsky, "The Use of Irreversible Electroporation in Food Preservation," Springer Berlin Heidelberg, 2010, pp. 273–312.

[10] A. Lucera, C. Costa, A. Conte, and M. A. Del Nobile, "Food applications of natural antimicrobial compounds," *Front. Microbiol.*, vol. 3, p. 287, 2012.

[11] F. Castellucci, *OIV (2010) Organisation International de la Vigne et du Vin. Resolution OIV/OENO 206/2010. Microbiological Analysis of Wines and Musts —Revision of Resolution OENO 8/1995*. Tbilisi, Georgia, 2010.

[12] D. O. H. Suzuki *et al.*, "Theoretical and Experimental Analysis of Electroporated Membrane Conductance in Cell Suspension," *IEEE Trans. Biomed. Eng.*, vol. 58, no. 12, pp. 3310–3318, Dec. 2011.

[13] E. Emanuel, P. Roman, and R. Cahan, "Influence of the current density in moderate pulsed electric fields on P. putida F1 eradication," *Bioelectrochemistry*, vol. 126, pp. 172–179, Apr. 2019.

[14] M. E.A. and A. H. Amer Eiss, "Pulsed Electric Fields for Food Processing Technology," in *Structure and Function of Food Engineering*, no. April, InTech, 2012.

[15] R. E. Neal, P. A. Garcia, J. L. Robertson, and R. V. Davalos, "Experimental Characterization and Numerical Modeling of Tissue Electrical Conductivity during Pulsed Electric Fields for Irreversible Electroporation Treatment Planning," *IEEE Trans. Biomed. Eng.*, vol. 59, no. 4, pp. 1076–1085, Apr. 2012.

[16] Y. Zhao *et al.*, "Characterization of Conductivity Changes During High-Frequency Irreversible Electroporation for Treatment Planning," *IEEE Trans. Biomed. Eng.*, vol. 65, no. 8, pp. 1810–1819, Aug. 2018.

[17] F. J. Barba *et al.*, "Current applications and new opportunities for the use of pulsed electric fields in food science and industry," *Food

Res. Int., vol. 77, pp. 773–798, Nov. 2015.

[18] T. Batista Napotnik and D. Miklavčič, "In vitro electroporation detection methods – An overview," *Bioelectrochemistry*, vol. 120, pp. 166–182, Apr. 2018.

[19] Q. Castellví, B. Mercadal, and A. Ivorra, "Assessment of Electroporation by Electrical Impedance Methods," in *Handbook of Electroporation*, Cham: Springer International Publishing, 2017, pp. 671–690.

[20] P. Simonis, R. Garjonyte, and A. Stirke, "Mediated amperometry as a prospective method for the investigation of electroporation," *Sci. Rep.*, vol. 10, no. 1, p. 19094, Dec. 2020.

[21] S. Arndt, J. Seebach, K. Psathaki, H.-J. Galla, and J. Wegener, "Bioelectrical impedance assay to monitor changes in cell shape during apoptosis," *Biosens. Bioelectron.*, vol. 19, no. 6, pp. 583–594, Jan. 2004.

[22] D. Krinke, H.-G. Jahnke, O. Pänke, and A. A. Robitzki, "A microelectrode-based sensor for label-free in vitro detection of ischemic effects on cardiomyocytes," *Biosens. Bioelectron.*, vol. 24, no. 9, pp. 2798–2803, May 2009.

[23] Y. Xu, X. Xie, Y. Duan, L. Wang, Z. Cheng, and J. Cheng, "A review of impedance measurements of whole cells," *Biosens. Bioelectron.*, vol. 77, pp. 824–836, Mar. 2016.

[24] K. Kinosita and T. Y. Tsong, "Voltage-induced conductance in human erythrocyte membranes," *Biochim. Biophys. Acta - Biomembr.*, vol. 554, no. 2, pp. 479–497, Jul. 1979.

[25] M. Pavlin *et al.*, "Effect of Cell Electroporation on the Conductivity of a Cell Suspension," *Biophys. J.*, vol. 88, no. 6, pp. 4378–4390, Jun. 2005.

[26] A. Ramos and H. Farias D., "Numerical analysis of impedance spectra of yeast suspensions," *J. Microwaves, Optoelectron. Electromagn. Appl.*, vol. 12, no. 2, pp. 647–654, Dec. 2013.

[27] H. El Zakhem, J.-L. Lanoisellé, N. I. Lebovka, M. Nonus, and E. Vorobiev, "The early stages of Saccharomyces cerevisiae yeast suspensions damage in moderate pulsed electric fields," *Colloids Surfaces B Biointerfaces*, vol. 47, no. 2, pp. 189–197, Feb. 2006.

[28] C. Suárez, A. Soba, F. Maglietti, N. Olaiz, and G. Marshall, "The Role of Additional Pulses in Electropermeabilization Protocols," *PLoS One*, vol. 9, no. 12, p. e113413, Dec. 2014.

[29] J. Langus, M. Kranjc, B. Kos, T. Šuštar, and D. Miklavčič, "Dynamic finite-element model for efficient modelling of electric currents in electroporated tissue," *Sci. Rep.*, vol. 6, no. 1, p. 26409, Sep. 2016.

[30] Q. Zhang, A. Monsalve-González, B.-L. Qin, G. V. Barbosa-Cánovas, and B. G. Swanson, "Inactivation of saccharomyces cerevisiae in apple juice by square-wave and exponential-decay pulsed electric fields," *J. Food Process Eng.*, vol. 17, no. 4, pp. 469–478, Dec. 1994.

[31] G. B. Pintarelli, A. C. Antônio Jr, and D. O. H. Suzuki, "BR 10 2019 018097 8 - Equipamento para aplicação de pulsos de tensão elétrica de amplitude, período e forma de onda variáveis e análise de efetividade para técnicas de eletroporação na transfecção genética e tratamento de neoplasias," 2019.

[32] J. Gehl *et al.*, "Updated standard operating procedures for electrochemotherapy of cutaneous tumours and skin metastases," *Acta Oncol. (Madr).*, vol. 0, no. 0, pp. 1–9, Mar. 2018.

[33] J. Dermol and D. Miklavčič, "Mathematical Models Describing Chinese Hamster Ovary Cell Death Due to Electroporation In Vitro," *J. Membr. Biol.*, vol. 248, no. 5, pp. 865–881, Oct. 2015.

[34] M. Kwolek-Mirek and R. Zadrag-Tecza, "Comparison of methods used for assessing the viability and vitality of yeast cells," *FEMS Yeast Res.*, vol. 14, no. 7, p. n/a-n/a, Sep. 2014.

[35] K. Painting and B. Kirsop, "A quick method for estimating the percentage of viable cells in a yeast population, using methylene blue staining," *World J. Microbiol. Biotechnol.*, vol. 6, no. 3, pp. 346–347, Sep. 1990.

[36] S. M. Passmore and B. Haggett, "The Use of Scanning Electron Microscopy to Show Confluent Growth of a Saccharomyces and a Leuconostoc Species," *J. Appl. Bacteriol.*, vol. 36, no. 1, pp. 89–92, Mar. 1973.

[37] J. C. Neu and W. Krassowska, "Asymptotic model of electroporation," *Phys. Rev. E*, vol. 59, no. 3, pp. 3471–3482, Mar. 1999.

[38] K. C. Smith and J. C. Weaver, "Active Mechanisms Are Needed to Describe Cell Responses to Submicrosecond, Megavolt-per-Meter Pulses: Cell Models for Ultrashort Pulses," *Biophys. J.*, vol. 95, no. 4, pp. 1547–1563, Aug. 2008.

[39] G. Pucihar, D. Miklavcic, and T. Kotnik, "A Time-Dependent Numerical Model of Transmembrane Voltage Inducement and Electroporation of Irregularly Shaped Cells," *IEEE Trans. Biomed. Eng.*, vol. 56, no. 5, pp. 1491–1501, May 2009.

[40] L. Rems, M. Ušaj, M. Kandušer, M. Reberšek, D. Miklavčič, and G. Pucihar, "Cell electrofusion using nanosecond electric pulses," *Sci. Rep.*, vol. 3, pp. 1–10, 2013.

[41] S. Bhonsle, M. Lorenzo, A. Safaai-Jazi, and R. V. Davalos, "Characterization of Nonlinearity and Dispersion in Tissue Impedance during High Frequency Electroporation," *IEEE Trans. Biomed. Eng.*, pp. 1–1, 2017.

[42] J. Lleixà, V. Martín, M. del C. Portillo, F. Carrau, G. Beltran, and A. Mas, "Comparison of Fermentation and Wines Produced by Inoculation of Hanseniaspora vineae and Saccharomyces cerevisiae," *Front. Microbiol.*, vol. 7, p. 338, Mar. 2016.

[43] V. W. Mayer, C. J. Goin, and F. K. Zimmermann, "Aneuploidy and other genetic effects induced by hydroxyurea in Saccharomyces cerevisiae," *Mutat. Res. Mol. Mech. Mutagen.*, vol. 160, no. 1, pp. 19–26, Mar. 1986.

[44] D. Gášková, K. Sigler, B. Janderová, and J. Plášek, "Effect of high-voltage electric pulses on yeast cells: factors influencing the killing efficiency," *Bioelectrochemistry Bioenerg.*, vol. 39, no. 2, pp. 195–202, Mar. 1996.

[45] P. Molinari, A. M. R. Pilosof, and R. J. Jagus, "Effect of growth phase and inoculum size on the inactivation of Saccharomyces cerevisiae in fruit juices, by pulsed electric fields," *Food Res. Int.*, vol. 37, no. 8, pp. 793–798, 2004.

[46] N. I. Lebovka and E. Vorobiev, "On the origin of the deviation from the first-order kinetics in inactivation of microbial cells by pulsed electric fields," *Int. J. Food Microbiol.*, vol. 91, no. 1, pp. 83–89, 2004.

[47] B. L. Qin, G. V. Barbosa-Canovas, B. G. Swanson, P. D. Pedrow, and R. G. Olsen, "Inactivating microorganisms using a pulsed electric field continuous treatment system," *IEEE Trans. Ind. Appl.*, vol. 34, no. 1, pp. 43–50, 1998.

[48] S. Toepfl, V. Heinz, and D. Knorr, "High intensity pulsed electric fields applied for food preservation," *Chem. Eng. Process. Process Intensif.*, vol. 46, no. 6, pp. 537–546, Jun. 2007.

[49] S. Toepfl, V. Heinz, and D. Knorr, *Applications of Pulsed Electric Fields Technology for the Food Industry.* 2006.

[50] S. P. Bhonsle, C. B. Arena, D. C. Sweeney, and R. V Davalos, "Mitigation of impedance changes due to electroporation therapy using bursts of high-frequency bipolar pulses," *Biomed. Eng. Online*, vol. 14, no. Suppl 3, p. S3, 2015.

[51] G. Pataro, G. M. J. Barca, G. Donsì, and G. Ferrari, "On the modeling of electrochemical phenomena at the electrode-solution interface in a PEF treatment chamber: Methodological approach to describe the phenomenon of metal release," *J. Food Eng.*, vol. 165, pp. 34–44, Nov. 2015.

[52] I. Fernández *et al.*, "Thermal degradation assessment of Kraft paper in power transformers insulated with natural esters," *Appl. Therm. Eng.*, vol. 104, pp. 129–138, 2016.

[53] F. Pillet, C. Formosa-Dague, H. Baaziz, E. Dague, and M.-P. Rols, "Cell wall as a target for bacteria inactivation by pulsed electric fields," *Sci. Rep.*, vol. 6, p. 19778, 2016.

[54] C. Lyu, J. Wang, M. Powell-Palm, and B. Rubinsky, "Simultaneous electroporation and dielectrophoresis in non-electrolytic

1
2
3
4
5
6
7
8
9
10
11
12
13
14
15
16
17
18
19
20
21
22
23
24
25
26
27
28
29
30
31
32
33
34
35
36
37
38
39
40
41
42
43
44
45
46
47
48
49
50
51
52
53
54
55
56
57
58
59
60

113

micro/nano-electroporation," *Sci. Rep.*, vol. 8, no. 1, p. 2481, Dec. 2018.

[55] R. Hölzel and I. Lamprecht, "Dielectric properties of yeast cells as determined by electrorotation," *Biochim. Biophys. Acta - Biomembr.*, vol. 1104, no. 1, pp. 195–200, Feb. 1992.

[56] B. M. Geier, B. Wendt, W. M. Arnold, and U. Zimmermann, "The effect of mercuric salts on the electro-rotation of yeast cells and comparison with a theoretical model," *BBA - Biomembr.*, vol. 900, no. 1, pp. 45–55, 1987.

[57] R. Hölzel, "Electrorotation of single yeast cells at frequencies between 100 hz and 1.6 GHz," *Biophys. J.*, vol. 73, no. 2, pp. 1103–1109, 1997.

[58] Y. Huang, R. Holzel, R. Pethig, and X.-B. Wang, "Differences in the AC electrodynamics of viable and non-viable yeast cells determined through combined dielectrophoresis and electrorotation studies," *Phys. Med. Biol.*, vol. 37, no. 7, pp. 1499–1517, Jul. 1992.

G. B. Pintarelli (IEEE Member) received the B.S. degree (in 2016) and M.S. degree (in 2018) in electrical engineering from Federal University of Santa Catarina (UFSC, Brazil). Part of his B.S. (2014-2015) was done (with CNPq funding) in the Brunel University London (UK). He is a specialist in electronic product development (IFSC, Brazil). He is currently pursuing the Ph.D. degree in electrical engineering at UFSC.

Since 2016 he is a researcher at the Institute of Biomedical Engineering (IEB-UFSC). He has experience with hardware development, signal processing and modeling. His research interest includes the development of innovative electrical-based treatment and sensing techniques for medical and food industry.

C. T. S. Ramos is a researcher at the Institute of Biomedical Engineering of Federal University of Santa Catarina (IEB-UFSC). Her research interest includes the development of innovative electrical-based treatment and sensing techniques for cancer treatment.

J. R. da Silva received the B.S. degree (in 2018) in electronic engineering from Federal University of Santa Catarina (UFSC, Brazil). She is currently pursuing the M.S. degree in electrical and electronic engineering at UFSC.

Since 2015 she is a researcher at the Institute of Biomedical Engineering (IEB-UFSC). She has experience with signal processing, biomedical modeling, and software development. Her research interest includes the development of electrochemotherapy.

M. J. Rossi received the B.S. degree in chemical engineering from the Federal University of Santa Maria (UFSM, Brazil), in 1994, and the M.S. degree (in 2001) and Ph.D. degree (in 2006) in chemical engineering from the Federal University of Santa Catarina (UFSC, Brazil).

Since 2006 he has been an adjunct professor in the Department of Microbiology, Immunology and Parasitology at the Federal University of Santa Catarina. He has experience in the field of biotechnological processes using microorganisms to produce biomass and metabolites for various applications (agricultural, forest, food, biological control and health) and bioreactors design. His research interests include the development of biotechnological processes.

D. O. H. Suzuki received the B.S. degree (in 1996), M.S. degree (in 2003) and Ph.D. degree (in 2009) in electrical engineering from Federal University of Santa Catarina (UFSC, Brazil).

Since 2011 she has been an adjunct professor in the Department of Electrical Engineering at the Federal University of Santa Catarina. She has experience with the application of electrochemotherapy (new cancer treatment), veterinary medical equipment, sensors, applied electronics, biomedical experiments, mathematical modeling of biological phenomena, genetic transfer and bio electromagnetism. Her research interests include biomedical instrumentation, modeling biological processes, numerical investigation of membrane electroporation, and electrophysiological phenomena.

APPENDIX C – Dielectric Dispersion Modulated Sensing of Yeast Suspension Electroporation

Creative Common CC BY license. Reprinted, with permission, from PINTARELLI, G. B. *et al.* Dielectric Dispersion Modulated Sensing of Yeast Suspension Electroporation. **Sensors**, v. 22, n. 5, p. 1811, 2022. Available at: https://doi.org/10.3390/s22051811. This appendix contains the published version of the article. Any part of the article may be reused.

sensors

MDPI

Article

Dielectric Dispersion Modulated Sensing of Yeast Suspension Electroporation

Guilherme B. Pintarelli [1,*] , **Jessica R. da Silva** [1], **Wuqiang Yang** [2] **and Daniela O. H. Suzuki** [1]

[1] Department of Electrical and Electronics Engineering, Institute of Biomedical Engineering, Federal University of Santa Catarina (UFSC), Florianopolis 88040-370, Brazil; jessica.rodrigues@posgrad.ufsc.br (J.R.d.S.); daniela@ppgeel.ufsc.br (D.O.H.S.)

[2] Department of Electrical and Electronic Engineering, The University of Manchester, Manchester M13 9PL, UK; wuqiang.yang@manchester.ac.uk

* Correspondence: guilherme.pintarelli@ufsc.br

Abstract: A specific pulsed electric field protocol can be used to induce electroporation. This is used in the food industry for yeast pasteurization, in laboratories for generic transfer and the medical field for cancer treatment. The sensing of electroporation can be done with simple 'instantaneous' voltage-current analysis. However, there are some intrinsic low-frequency phenomena superposing the electroporation current, such as electrode polarization. The biological media are non-homogeneous, giving them specific characterization in the broad frequency spectrum. For example, the cell barrier, i.e., cell membrane, causes so called β-dispersion in the frequency range of tens to thousands of kHz. Electroporation is a dynamic phenomenon characterized by altering the cell membrane permeability. In this work, we show that the impedance measurement at certain frequencies could be used to detect the occurrence of electroporation, i.e., dielectric dispersion modulated sensing. This approach may be used for the design and implementation of electroporation systems. Yeast suspension electroporation is simulated to show changes in the frequency spectrum. Moreover, the alteration depends on characteristics of the system. Three types of external buffers and their characteristics are evaluated.

Keywords: pulsed electric field; bio-impedance; biological system modeling; bio-technology; bio-membranes

check for **updates**

1. Introduction

Pulsed Electric Field (PEF) is a non-thermal electricity-based process to control cells. PEF is used in bio-technology [1], veterinary [2] and medical research [3], and food industry [4,5]. These applications require specific levels of electroporation control. Techniques and sensing electroporation improve safety and optimization applications of PEFs. Recent progress on electroporation methods propose studies of PEF using nanoparticles [6], gels [7,8], microdevices [9], and electrospun PCL [10].

The PEF approach makes use of a combination of pulse amplitudes, pulse durations and pulse repetitions. Usually, high amplitude, short duration, and rectangular PEF (hundreds of kV/m and tens to hundreds of μs) is used for the permeabilization of the cell membrane, also known as electroporation or electro-permeabilization [11,12]. Electroporation can arise as reversible or irreversible, mainly depending on the PEF amplitude. If PEF is configured as low amplitude and long duration (tens of kV/m and tens ms), it is possible to primarily cause electrolysis, which may induce chemical ablation [13,14].

The electroporation theory is based on formation of nano-pores in the cell membrane due to excessive accumulation of transmembrane ionic charges. Pore hypothesis evidence is given by measurements showing the increase in ionic permeability due to PEF. Pore creation and expansion is described to change the membrane electrical properties (e.g., electrical conductivity) [15]. The pore number can be described by the Smoluchowski equation [16]. The membrane changes affect the macroscopic scale electrical properties,

which can be modeled using a macroscopic current. This concept is mostly used to describe PEF tissue response, which enables the pre-treatment of PEF-based cancer therapies [17,18].

PEF is usually delivered in the signature of 100 μs rectangular pulses burst, which is described by diverse sub-4.4 kHz frequency components. Current models use instantaneous current-voltage measurements to describe the PEF electrical current [18,19], which is a sum of conduction current, dispersive effects, electrode-biological-media polarization, and electroporation. From the engineering point of view, differentiating the electroporation current from other PEF-current is complex. We call the electroporation current the superimposed non-physiological displacement current in the cell membrane due to pore opening. It is known that the biological systems are electrolytes and charges are subject to changes in polarization, i.e., orientation and displacement of charges. The polarization delay is given in the time domain, and it is called relaxation, which can be transposed to the frequency domain, so-called dispersion. Biological systems are characterized by the three most expressive relaxation factors: ions diffusion outside the cells, cell's membrane interface charging, and molecule orientation, which contribute to Schwan's dispersions, α, β, and γ, respectively [20]. The α-dispersion and electrode-biological-media-dispersion are located at sub-10 kHz, which is where the PEF burst energy spectrum is. Those phenomenon dynamics have not been completely understood, interfering in the direct current measurement.

Besides the complexity of characterizing biological samples using sub-10 kHz measurements, the electroporation itself is not entirely understood. Thus, PEF systems usually do not have electroporation feedback because there is no adequate PEF probing method. We have recently shown that it is possible to eliminate yeast using irreversible electroporation and the macroscopic current changes due to cell breakage [4]. Yeasts are a problem in the industry, as their contamination can cause financial loss. If contaminated yeast is injected into a human body, it can cause health problems. However, there are no efficient methods to sense electroporation for probing the actual electroporation current, which can be ultimately used to directly probe the membrane conductivity or electroporation pore density. In this work, we evaluated the effects of electroporation on the dielectric spectrum of cell suspensions. This evaluation can provide insights into the development of electroporation/PEF high frequency (>10 kHz) sensors. New sensors can be designed to operate in a frequency range adequate for detecting membrane changes while avoiding sub-10 kHz PEF direct current polarization disturbances. This technique provides more accurate readings of electroporation mechanisms to control and optimize industrial processes.

To demonstrate the feasibility of supervising electroporation, we propose a numerical study on the sensing of the suspension dielectric dispersion. Yeast cell suspension is known to have well-defined β-dielectric dispersion in the frequency range of 0.1–1 MHz due to the cell membrane. The electroporation model is used to calculate changes in the membrane conductivity (σ_m) during electroporation. System invariance is assumed on a small scale, and the suspension dielectric spectrum is calculated. A computer model is used to demonstrate that the system dielectric dispersion changes due to the cells' membrane and their interaction with the extracellular media and electroporation. This technique may be applied at a microsensor embedded at an industrial electroporation line or an electroporation lab on a chip device.

2. Materials and Methods

Analytical approaches to solving electric fields at the cellular level are based on spatially dependent, partial differential equations [21,22]. It is challenging to assume modeling conditions, such as irregular cell shape, nearby cells, and non-linear cell membrane change due to electroporation [23]. This research uses a finite element method (FEM) to deal with those conditions at a computational cost.

In the following, the effects of electroporation and extracellular buffers on the equivalent (bulk) electrical properties are evaluated theoretically. A two-shell model is used to represent the yeast cell (see Figure 1a) under 50 μs (10 to 60 μs) and 1 μs (2 to 3 μs),

400 kV/m PEF (see Figure 1d). The PEF induce higher transmembrane voltages at cell poles, which provokes electroporation. The electroporation model describes the pore density $N(t)$ and average membrane conductivity due to PEF (see Figure 1b,c). The 'electroporated' yeast cell is in the center of an infinitesimal cylindrical volume (see Figure 1e). The cylinder is used to evaluate conduction current density J during PEF. The infinitesimal volume describes the yeast suspension (see Figure 1f). The data are calculated and analyzed in terms of the cell's membrane conductivity, the transmembrane voltage, and equivalent relative permittivity ε_{eq} of the infinitesimal cylinder during the PEF protocol. Membrane conductivity and transmembrane voltage are given as function of θ angle (see Figure 1e). The low-frequency current increases due to the cell's membrane interface change, altering the sample's electrical characteristic, i.e., β-dispersion.
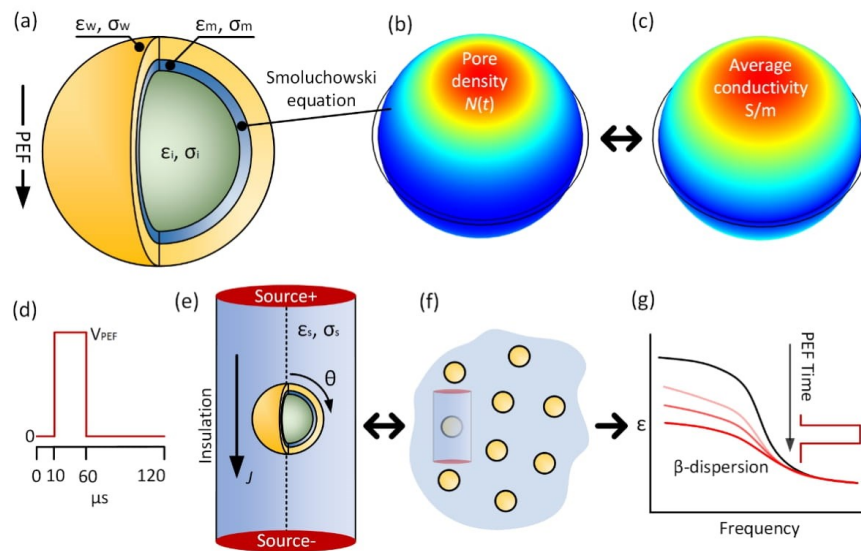
Figure 1. (**a**) Two-shell whole yeast cell model under PEF. PEF induces higher transmembrane voltages, which increases (**b**) pore density $N(t)$ and (**c**) the average membrane conductivity. The color map values are as follows: red means higher and blue means lower. (**d**) The 50 µs stimulus signal profile, where V_{PEF} is calculated to obtain 400 kV/m maximum PEF. (**e**) An infinitesimal cylindrical model with one 'electroporated' cell. The θ angle is used to address membrane conductivity and transmembrane voltage results. (**f**) The infinitesimal cylinder describes a cell suspension with 1% yeast concentration ratio. (**g**) The decrease in the membrane conductivity affects the β-dispersion of the yeast suspension.

2.1. Numerical Modeling

The time-harmonic conduction and displacement currents are solved according to Maxwell-Ampère's law, as given by Equation (1). In this equation, it is assumed that all variations in time occur as steady-state sinusoidal signals. Because of a non-linear condition due to electroporation, the observation is considered to be time-dependent, and linearity is assumed over a small-scale step. Thus, the time step is a stationary problem in the frequency domain using complex values. The fields are represented by amplitude and phase (i.e., phasors), while the frequency is specified as a predefined sweep sinusoidal

signal input. A frequency range from 100 to 1 MHz is employed, as they are the optimal frequencies for cell membrane sensing [24]:

$$J = \sigma E + j\omega\varepsilon E \qquad (1)$$

where J is the conduction current density and E is the electric field (V/m), computed as $E = -\nabla V$ (where V is the electric potential) [25].

The whole cell geometry model is a two-shell yeast model located at a cylindrical spatial media. The model is 2D axisymmetric, and a revolution in the cylinder axis is used to obtain volumetric results (see the dotted line in Figure 1e). The volumetric model containing one cell is shown in Figure 1e. The whole cell simulation parameters and their description are given in Table 1. Cells of the yeast *Saccharomyces cerevisiae* are used because detailed electrical properties literature and their ellipsoidal shape are often approximated as a two-shell sphere [26–28]. In this research, a 1% yeast concentration ratio (i.e., the ratio between cell's volume divided by the total solution) is used, which is approximately 2×10^8 cells/mL. This is a typical yeast concentration from the experimental point of view [29]. The cell concentration is controlled by adjusting the cylinder volume, i.e., changing the total buffer volume to match the desired concentration.

Table 1. Geometric simulation parameters.

Symbol	Value
Infinitesimal volume cylinder heigh	30 μm
Infinitesimal volume cylinder radius	16.8 μm
Cell wall thickness	220 ηm [1]
Cell membrane thickness	8 ηm [1]
Cell radius	4 μm [1]

[1] Data from [30].

COMSOL Multiphysics® version 4.4 software is used for FEM modeling and 2D electric currents application ('ec', from the COMSOL's AC/DC Module). The electroporation model is solved in the time domain (as described previously [4,31]), giving results of pore density $N(t)$ and average membrane electrical conductivity (see Appendix A Equations (A1) and (A2)). The simulation steps are defined as linear and were 0.5 μs when using 50 μs PEF and 0.01 μs when using 1 μs PEF. The simulation is run until 120 μs (for 50 μs PEF) and 20 μs (for 1 μs PEF) to calculate post-PEF transient effect. The small signal frequency domain is used to calculate equivalent complex permittivity. The boundary conditions were insulation on the curved cylinder surface, and the top and bottom bases were used as sinusoidal and PEF voltage sources. There is a differential bias of 1×10^{-4} V between the top and bottom boundaries used for small signal analysis. We suppose that our simulation volume behaves as an infinitesimal volume in a whole yeast suspension as the gradient of the voltage in the insulation is less than 2.5% of the source voltage, and the gradient of the current in the top and bottom sources is less than 2.5%. Those parameters are critical and must be as small as possible. If the gradient in the boundary layers is negligible, then there is no field diffraction in the boundary so that we can assume an infinitesimal volume design model.

A custom mesh is designed for this study. The mesh is edge mapped for bilateral symmetry and mapped as 10 per 1000 quadratic elements for each cell's membrane and wall. Other elements are made using COMSOL's free triangular semiconductor 'fine' pre-set. The maximum element size is set as 3.3×10^{-7} m. The mesh consists of 171,416 tetrahedral elements. The transmembrane voltage due to PEF can be analytically calculated using the Laplace equation [32]. We validated the numerical calculations by comparing them to the analytical solution proposed by Gimsa and Wachner [33]. The maximum relative error between the analytical solution and the computer simulation was 5.18% (using the

parameters shown in Table 1). Therefore, we considered our model to be sufficiently accurate for our study.

2.2. Yeast Cell Passive Properties

The electrical parameters of the tested materials are listed in Table 2. Low conductivity media (also called 'electroporation buffer') are preferred for mitigating electrolysis during PEF [34], and some buffer composition is reported to improve electroporation efficiency [35]. For the in vitro experiment, the conductivity and osmolality of the buffer can be modulated by changing salts (e.g., KCl and NaCl) and sugars (e.g., sucrose). However, caution must be taken for modeling, as the buffer conductivity influences the cell's wall and membrane conductivity and intracellular conductivity [26–28]. We computed results using three conductivities situations: 1×10^{-3} S/m (low σ), 50×10^{-3} S/m (medium σ) and 0.1 S/m (high σ) buffer. It is found that the conductivity of laboratory deionized water is typically 1×10^{-3} S/m and final yeast's suspension solutions in a range from 50×10^{-3} to 0.2 S/m [26]. The membrane channels state is 'closed' (i.e., the lower conductivity end at approximately 0.25×10^{-6} S/m) at 1 to 10×10^{-3} S/m buffers and 'increasingly opening' for buffers over 20×10^{-3} S/m. For a typical 50×10^{-3} S/m buffer [35], the membrane conductivity is approximately 0.1×10^{-3} S/m [27]. The cell wall is a known negative charged sieve-like structure. Thus, it is the first selective barrier [36]. Some reports say that for a highly conductive medium, the conductivity of the cell's walls is approximately 10 to 20% of medium conductivity, which may be explained by the wall's porosity and its charges [26]. The cytoplasm is known to be a highly conductive medium, as it holds the necessary salt and protein for a cell's life.

Table 2. Non-linear electroporation model, electrical and geometric parameters of the simulation.

Parameter	σ_{Low} Buffer	σ_{Med} Buffer	σ_{High} Buffer
External solution conductivity (σ_s)	1×10^{-3} [S/m]	50×10^{-3} [S/m]	0.1 [S/m]
External solution permittivity (ε_s)	78	78 [1]	77
Cytoplasm's conductivity (σ_i)	0.2 [S/m]	0.55 [S/m]	0.6 [S/m]
Cytoplasm's relative permittivity (ε_i)	50	50 [1]	58
Initial membrane's conductivity (σ_{m0})	0.25×10^{-6} [S/m]	0.1×10^{-3} [S/m]	0.1×10^{-3} [S/m] [2]
Membrane's relative permittivity (ε_m)	6	7.6	5.2
Cell wall's conductivity (σ_w)	14×10^{-3} [S/m]	5×10^{-3} [S/m]	20×10^{-3} [S/m]
Cell wall's relative permittivity (ε_w)	60	60 [1]	60

[1] Data were not informed in [27]. We used data from [30]. [2] Data were considered as 0 S/m in [26]. We considered 0.1×10^{-3} S/m, which is the minimum physiological conductivity for yeast membranes.

3. Results

The membrane conductivity, transmembrane voltage, and solution's relative permittivity when using 50 µs PEF is shown in Figure 2. During 10 to 60 µs, the PEF is enabled. All buffers are adequate to induce electroporation transmembrane voltages. The σ_{Low} buffer has the slowest time dynamics (see the post-60 µs dynamism of membrane conductivity and transmembrane voltage). This occurs due to the poor buffer-cell interface conductive coupling, which leads to slower capacitive charging and discharging processes. The membrane state change is practically instantaneous when using σ_{Med} and σ_{High} buffers. Additionally, the extent of membrane area affected by electroporation is higher when σ_{High} buffer is used (approximately $-\pi/2$ to $\pi/2$).
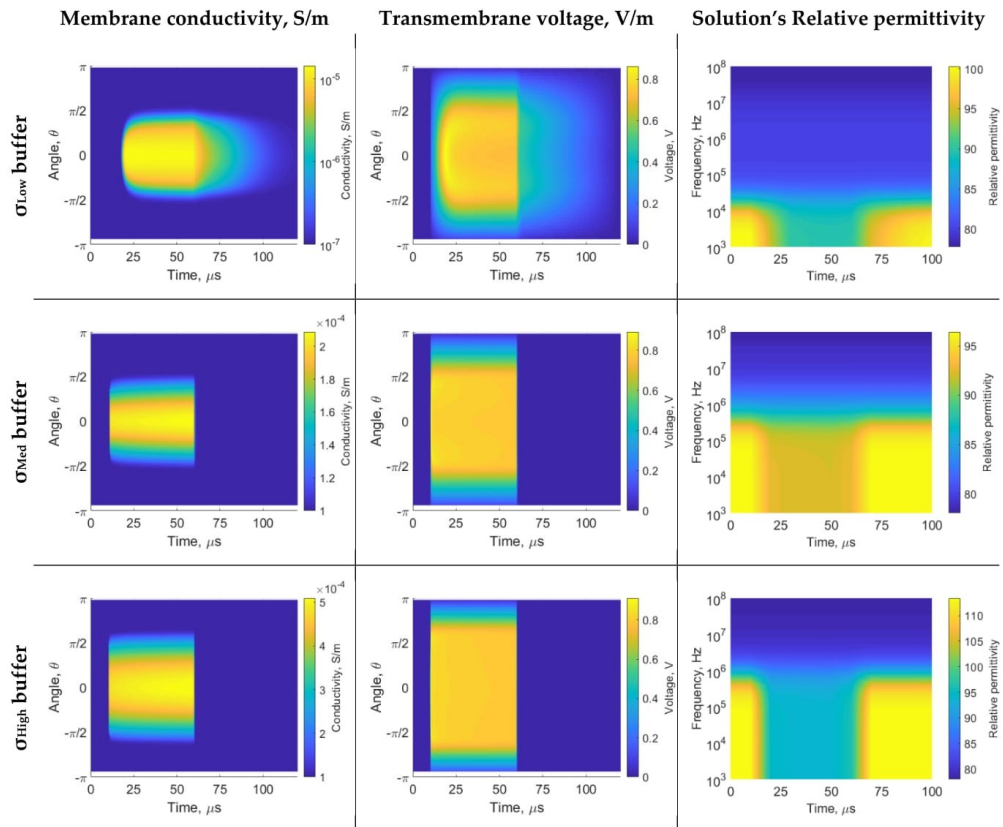
Figure 2. Results of 50 μs PEF: Membrane conductivity, transmembrane voltage and solution equivalent relative permittivity. The horizontal axis is the time in μs. The PEF starts at 10 μs and ends at 60 μs. The vertical axis of the membrane conductivity and transmembrane voltage figures represent the angle location in the membrane. The vertical axis of the solution relative permittivity figures is the sensing frequency (1 kHz to 100 MHz range).

Figure 3 shows the cell suspension dielectric properties before and during electroporation, using data from 8 μs and 50 μs time step, respectively (from 50 μs PEF). The membrane interface changes due to electroporation and affects the β-dispersion magnitude. The dispersion center depends on the system's characteristics; the dispersion center is approximately 10 kHz for σ_{Low} buffer and 500 kHz for σ_{Med} and σ_{High} buffer (see the blue arrows at Figure 3 solution's relative permittivity). Frequencies higher than 1 MHz are not suitable for sensing the membrane dispersion, as the displacement current can flow through the cell, which is called 'electrically invisible'. The β-dispersion is mainly explained by the cell barrier (membrane and wall). The cell wall is described to be electrically distinct from the membrane. Thus, a sub-β-dispersion is provoked by the cell wall and interfere with the 'main' β-dispersion. The wall interference starts at 0 Hz when using σ_{Med} and σ_{High} buffer, as the wall is less conductive than external media. The wall primarily impacts the σ_{Med} buffer β-dispersion as electrical characteristics of wall and membrane are more similar than σ_{High} buffer. The wall sub-β-dispersion has its peak indicated by the gold arrows in Figure 3 (gold arrows show the peak trans-wall voltage).
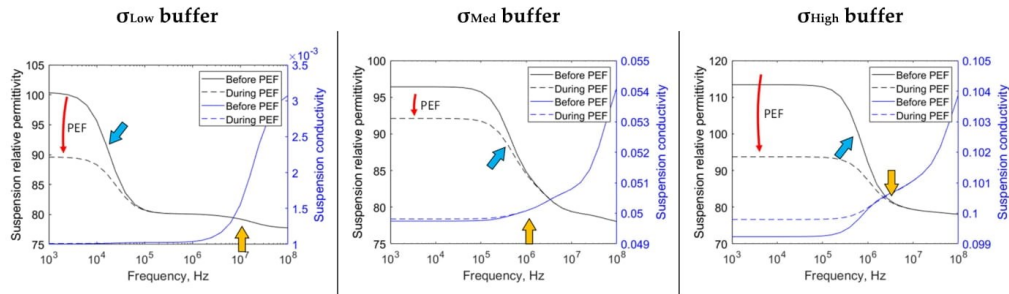
Figure 3. Cell suspension dielectric properties before and during PEF. The electroporation decreases the equivalent solution permittivity. The red arrow indicates the time direction. The blue arrow indicates the membrane main-β-dispersion. The gold arrow indicates the yeast wall peak sub-β-dispersion.

The 1 μs PEF results are shown in Figure 4. During 2 to 3 μs, the PEF is enabled. The σ_{Low} buffer slow dynamic cannot charge the membrane sufficiently for electroporation (the membrane charges up to 200 mV). Thus, the membrane conductivity change is negligible, and the spectrum does not change significantly (i.e., unsuccessful electroporation). The σ_{Med} buffer can charge the membrane sufficiently for electroporation. However, the 1 μs does not saturate conductivity, as seen in 50 μs PEF (Figure 2). Thus, σ_{Med} buffer β-dispersion decays only at the end of the 1 us pulse.

Figure 4. *Cont.*

Figure 4. Results of 1 μs PEF: membrane conductivity, transmembrane voltage and solution equivalent relative permittivity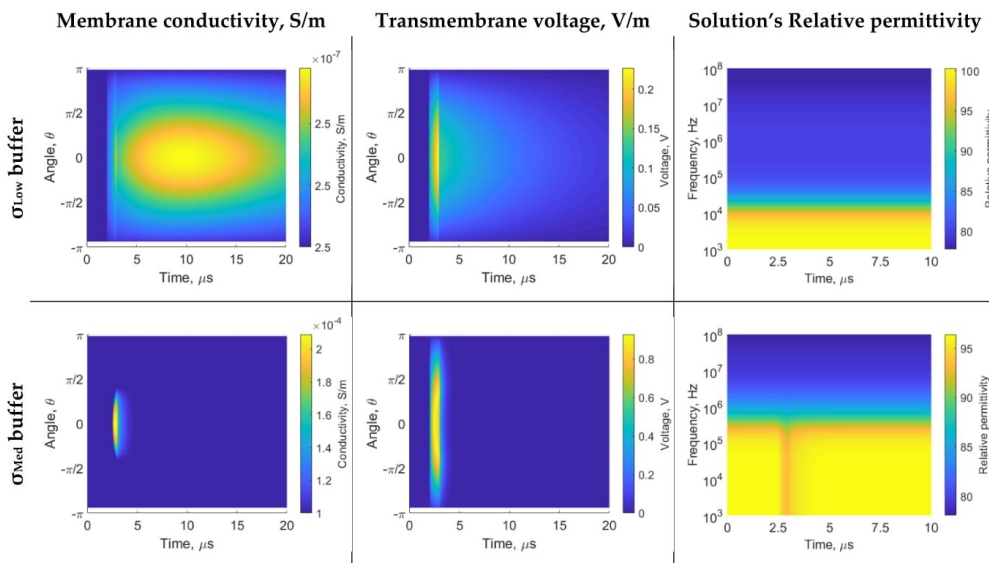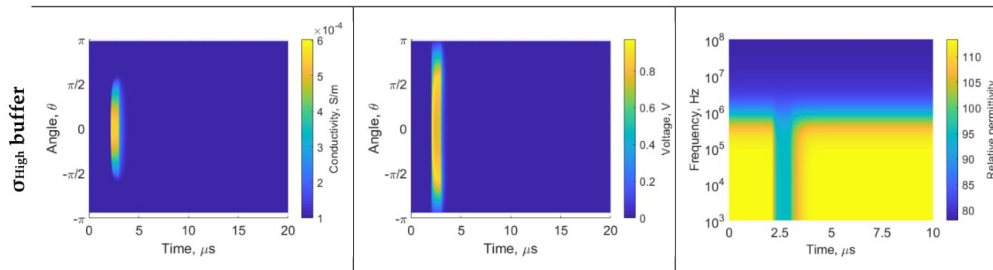. The axis description is used within Figure 3. The PEF starts at 2 μs, and ends at 3 μs. When using σ_{Low}, the membrane conductivity changes are lower than 0.1%.

4. Discussion

This study is focused on the impact of cells' relative parameters on the frequency spectrum of impedance, particularly how individual electrical properties affect the dielectric β-dispersion center. The β-dispersion is mostly described by the cell membrane interface. The dielectric dispersion dynamics can be used as a design parameter for micro/nano dielectric dispersion modulated sensors. Those sensors may be used for industrial irreversible electroporation or lab on a chip electroporation device [9]. FEM simulation has been used to find the equivalent ε, which depends on the inhomogeneous media. We have shown that an impedance sensor operating up to 1 MHz can perceive the alteration caused by electroporation in cells if the buffer conductivity is higher than 50 mS/m. An infinitesimal volume has been used to simulate a cell suspension, which is a reasonable approach for low density suspension. The electroporation analysis of cells attached or very closed to the microelectrodes [9] can use similar dielectric dispersion dynamics modulated sensors. However, specific cell geometry and properties, cell density, and electrode/chamber design may be simulated to determine appropriate sensor operating frequency and minimum buffer conductivity. The electroporation model is used to assess the membrane conductivity during PEF. The change in membrane conductivity affects the overall, i.e., 'equivalent', properties.

The maximum membrane conductivity for σ_{Low}, σ_{Med}, and σ_{High} buffers are 0.01 mS/m, 0.2 mS/m, and 0.5 mS/m, respectively, as shown in Figure 2. Even though we did not replicate the recent electroporated membrane conductivity of 3 mS/m to 30 mS/m [37–39], our results are consistent with some early experimental and theoretical works (0.01 mS/m to 1 mS/m) [32,40–42]. Ramos et al. [43] shows a membrane conductivity of 1 μS/m to 0.01 mS/m (conversion $\sigma_m = h \cdot G_m$ [44]) for yeast cells with 0.28 volumetric fraction. These reduction of electroporated membrane conductivity may be caused by volumetric fraction [45]. The present studies are similar to very low cell density, without reduced transmembrane potential caused by cells proximity. Despite the limitations, our findings are consistent with the previous reports of membrane conductivity.

The σ_{Low} buffer, i.e., deionized water, is a 'reasonable' insulator from a biological media perspective. We have observed that some cell types may not be compatible with this medium's osmolarity. The electrical characteristics of this buffer are similar to the cell wall. Therefore, the effects of the buffer-wall interface are reduced, i.e., diffraction of the electric field and wall voltage drop. Because most of the dispersion is created only by the cell membrane, it tends to have the dispersion center at low frequency due to the thin membrane (the dispersion center, in this case, is near 10 kHz). The σ_{High} medium is more typical for liquid foods [4,38,46]. The σ_{Med} and σ_{High} buffers are more similar regarding dispersion center location. Those have the dispersion center near 500 kHz. From the membrane sensing point of view, it is interesting to see that the cell's interface dispersion is higher than 10 kHz, as frequencies sub-10 kHz are probably contaminated with the chambers'

electrolytic double layer effect, i.e., electrode polarization and α-dispersion [26]. Therefore, this sensing approach can mitigate the unwanted impact by using measurements higher than 100 kHz. However, we cannot exceed 1 MHz, as the membrane and wall become 'electrically invisible'. In other words, the voltage drop due to the cell's interface is primarily linear. We did not notice changes in the spectrum at the time of electroporation (see the relative permittivity in Figure 2). Other researchers reported similar values [23,39,47].

The electroporation is modeled as the change in membrane conductivity due to the transmembrane voltage. When the transmembrane voltage reaches a certain value (~0.2–1 V) [48], membrane permeability increases as a consequence of the formation of hydrophilic pores in the lipid bilayer, leading to an increase in membrane conductivity (see Appendix A Equation (A2)). The σ_{Low} buffer has slower membrane (dis)charging dynamics (see the transmembrane voltage dynamics in Figure 2). Therefore, there is a direct effect on the conductivity of the membrane and the overall relative permittivity. For applications of molecule transfer, using a low conductivity buffer may be interesting to provide a slower dynamic transfer window, which is easier to operate from a control system perspective. Some authors have shown that a low conductivity buffer affects electroporation or enhances cell uptake [49–51]. Furthermore, the low conductivity buffer is attractive, as it results in lower electrical currents, and consequently, mitigates thermal or electrochemical effects. For purely irreversible electroporation PEF or arc plasm applications, this is the most suitable buffer to destroy the cell's membrane. We observe that caution is needed if using fast PEF protocols. The 1 μs was not adequate to provoke electroporation when using σ_{Low} buffer. Additionally, the 1 μs PEF combined with σ_{Med} buffer is not fast enough to saturate the transmembrane voltage; thus, it may be the approximate lower threshold conductivity buffer to be used with 1 μs PEF. The dielectric dispersion sensing mechanism is capable of detecting the electroporation state: there are no alterations at σ_{Low} buffer (unsuccessful electroporation), late alterations at σ_{Med} buffer (caution state), and alterations at σ_{High} buffer (successful electroporation, see Figure 4).

The two-shell models are widely used in scientific research. However, they rely on various assumptions, e.g., spheric cells, nothing embedded in the wall or membrane, and homogeneous intracellular media [30]. Those may be a limiting factor in the analysis above 10 MHz [26,28]. However, this work, as well as others in the literature, have demonstrated that to sense the cell's primally barrier (i.e., cell membrane), we should not exceed approximately 1 MHz [23,24,39]. The sub-β-dispersion (see Figure 2 gold arrow) is caused by the cell wall. The yeast experimental and simulations results described by Asami attributes sub-dispersions due to cell wall and vacuole [26]. It is known that the entire spectrum is interdependent (as dispersive effects overlap) [52], and PEF is reported to induce permeabilization in the entire cell barrier [53]. Therefore, we believe that at present, it is appropriate to evaluate the electroporation as a sum of effects (mixed results of membrane and wall). Even if the information generates a discrete event, it would be suitable in some scenarios, such as cold pasteurization by PEF. The membrane electroporation state change is almost instantaneous with a medium or high conductivity buffer. Thus, if a single pulse is used in these cases, the reversible electroporation may be modeled as a discrete event.

5. Conclusions

Yeasts may contaminate liquid food, causing financial or health problems. The PEF systems can eliminate microorganisms. However, those systems lack a directly electroporation feedback. This type of sensing is complex, as other phenomena result from direct current in an ionic media, i.e., electrode polarization. Disturbances in the spectrum due to electrode polarization are usually up to 10 kHz. We have demonstrated that it is feasible to supervise electroporation using impedance. The biological media are characterized by the β-dispersion, which is provoked mainly by the cell membrane. If the cell membrane changes due to electroporation, the biological media dispersion changes. A numerical study of a yeast suspension process can calculate the dielectric dispersion due to the cell

barrier, external medial (buffer), and electroporation. Yeast cell suspension β-dispersion reduces due to the increase in the membrane conductivity. This approach may be used to develop a microsensor for use on an industrial electroporation line or an electroporation lab on a chip device.

Appendix A

A non-linear model of electroporation can be used to simplify the Smoluchowski equation to describe the pore density $N(t)$, as [54]:

$$\frac{dN(t)}{dt} = \alpha e^{\left(\frac{V_m(t)}{V_{ep}}\right)^2}\left(1 - \frac{N(t)}{N_0}e^{-q\left(\frac{V_m(t)}{V_{ep}}\right)^2}\right) \tag{A1}$$

where $V_m(t)$ is the transmembrane voltage, V_{ep} is the electroporation voltage, N_0 is the pore density at $V_m = 0$ V, and α and q are constants. Equation (A1) was implemented in COMSOL using the Weak Form Boundary PDE physics application mode on all membrane surfaces.

The regions where pores are formed present average conductivity of [42,45,55]:

$$\sigma_m(t) = \sigma_{m_0} + N(t)\sigma_p \pi r_p^2 K \tag{A2}$$

where σ_{m0} is the membrane conductivity without electroporation, σ_p is the conductivity of pore, r_p is the pore radius, and K is:

$$K = \frac{e^{v_m} - 1}{\frac{w_0 e^{w_0 - \eta v_m}}{w_0 - \eta v_m}e^{v_m} - \frac{w_0 e^{w_0 + \eta v_m} + \eta v_m}{w_0 + \eta v_m}} \tag{A3}$$

where w_0 is the energy barrier inside the pore, η is the relative entrance length of the pore, and $v_m = \frac{q_e}{kT}V_m$ is the non-dimensional transmembrane voltage.

The pore conductivity is [56]:

$$\sigma_p = \frac{\sigma_w - \sigma_i}{\ln\left(\frac{\sigma_w}{\sigma_i}\right)} \tag{A4}$$

The cell and electroporation model parameters are given in Table A1.

Table A1. Non-linear electroporation model, electrical and geometric parameters of simulation.

Parameter	Symbol	Value	References
External conductivity	σ_e	See Table 2	-
External permittivity	ε_e	See Table 2	-
Membrane permittivity	ε_m	See Table 2	-
Wall membrane conductivity	σ_w	See Table 2	-
Wall membrane permittivity	ε_w	See Table 2	-
Cytoplasm conductivity	σ_i	See Table 2	-
Cytoplasm permittivity	ε_i	See Table 2	-
Cell radius	R	5 μm	[30]
Thickness membrane	h_m	8 nm	[30,57]
Thickness wall	h_w	220 nm	[27,30]
Electroporation constant	q	2.46	[54,55]
Electroporation constant	α	109 m^2s^{-1}	[42,54,55]
Pore density at $V_m = 0$ V	N_0	1.5×10^9 m^{-2}	[42,54,55]
Electroporation voltage	V_{ep}	258 mV	[42,54,55]
Pore energy barrier	W_0	2.65	[42,54,55]
Relative length of the pore	η	0.15 nm	[42,54,55]
Pore radius	r_p	0.8 nm	[42,54,55]
Boltzmann constant	k	1.38×10^{-23} $\text{m}^2\text{kgs}^{-2}\text{K}^{-1}$	[42,54,55]
Temperature	T	295 K	[42,54,55]

References

1. Ozyigit, I.I. Gene transfer to plants by electroporation: Methods and applications. *Mol. Biol. Rep.* **2020**, *47*, 3195–3210. [CrossRef]
2. Rangel, M.M.M.; Luz, J.C.S.; Oliveira, K.D.; Ojeda, J.; Freytag, J.O.; Suzuki, D.O. Electrochemotherapy in the treatment of neoplasms in dogs and cats. *Austral J. Vet. Sci.* **2019**, *51*, 45–51. [CrossRef]
3. Geboers, B.; Scheffer, H.J.; Graybill, P.M.; Ruarus, A.H.; Nieuwenhuizen, S.; Puijk, R.S.; van den Tol, P.M.; Davalos, R.V.; Rubinsky, B.; de Gruijl, T.D.; et al. High-Voltage Electrical Pulses in Oncology: Irreversible Electroporation, Electrochemotherapy, Gene Electrotransfer, Electrofusion, and Electroimmunotherapy. *Radiology* **2020**, *295*, 254–272. [CrossRef] [PubMed]
4. Pintarelli, G.B.; Ramos, C.T.S.; Da Silva, J.R.; Rossi, M.J.; Suzuki, D.O.H. Sensing of Yeast Inactivation by Electroporation. *IEEE Sens. J.* **2021**, *21*, 12027–12035. [CrossRef]
5. Reineke, K.; Schottroff, F.; Meneses, N.; Knorr, D. Sterilization of liquid foods by pulsed electric fields-an innovative ultra-high temperature process. *Front. Microbiol.* **2015**, *6*, 400. [CrossRef]
6. Ghorbel, A.; Mir, L.M.; García-Sánchez, T. Conductive nanoparticles improve cell electropermeabilization. *Nanotechnology* **2019**, *30*, 495101. [CrossRef]
7. Pintarelli, G.B.; Berkenbrock, J.A.; Rassele, A.; Rangel, M.M.M.; Suzuki, D.O.H. Computer simulation of commercial conductive gels and their application to increase the safety of electrochemotherapy treatment. *Med. Eng. Phys.* **2019**, *74*, 99–105. [CrossRef]
8. Lopes, L.B.; Pintarelli, G.B.; dos Santos, C.S.F.; Suzuki, D.O.H. Computer optimization of conductive gels for electrochemotherapy. *Med. Eng. Phys.* **2021**, *98*, 133–139. [CrossRef]
9. Zhang, Y.; Yan, Z.; Xia, X.; Lin, Y. A novel electroporation system for living cell staining and membrane dynamics interrogation. *Micromachines* **2020**, *11*, 767. [CrossRef]
10. Bazzolo, B.; Sieni, E.; Zamuner, A.; Roso, M.; Russo, T.; Gloria, A.; Dettin, M.; Conconi, M.T. Breast cancer cell cultures on electrospun poly(ε-caprolactone) as a potential tool for preclinical studies on anticancer treatments. *Bioengineering* **2021**, *8*, 1. [CrossRef]
11. Kotnik, T.; Kramar, P.; Pucihar, G.; Miklavcic, D.; Tarek, M. Cell membrane electroporation- Part 1: The phenomenon. *IEEE Electr. Insul. Mag.* **2012**, *28*, 14–23. [CrossRef]
12. Haberl, S.; Miklavcic, D.; Sersa, G.; Frey, W.; Rubinsky, B. Cell membrane electroporation-Part 2: The applications. *IEEE Electr. Insul. Mag.* **2013**, *29*, 29–37. [CrossRef]
13. Weaver, J.C.; Smith, K.C.; Esser, A.T.; Son, R.S.; Gowrishankar, T.R. A brief overview of electroporation pulse strength–duration space: A region where additional intracellular effects are expected. *Bioelectrochemistry* **2012**, *87*, 236–243. [CrossRef] [PubMed]

14. Rubinsky, L.; Guenther, E.; Mikus, P.; Stehling, M.; Rubinsky, B. Electrolytic Effects During Tissue Ablation by Electroporation. *Technol. Cancer Res. Treat.* **2016**, *15*, NP95–NP103. [CrossRef]

15. Zhuang, J.; Kolb, J.F. Time domain dielectric spectroscopy of nanosecond pulsed electric field induced changes in dielectric properties of pig whole blood. *Bioelectrochemistry* **2015**, *103*, 28–33. [CrossRef]

16. Mescia, L.; Chiapperino, M.A.; Bia, P.; Gielis, J.; Caratelli, D. Modeling of Electroporation Induced by Pulsed Electric Fields in Irregularly Shaped Cells. *IEEE Trans. Biomed. Eng.* **2018**, *65*, 414–423. [CrossRef]

17. Kotnik, T.; Rems, L.; Tarek, M.; Miklavčič, D. Membrane Electroporation and Electropermeabilization: Mechanisms and Models. *Annu. Rev. Biophys.* **2019**, *48*, 63–91. [CrossRef]

18. Zhao, Y.; Bhonsle, S.; Dong, S.; Lv, Y.; Liu, H.; Safaai-Jazi, A.; Davalos, R.V.; Yao, C. Characterization of Conductivity Changes During High-Frequency Irreversible Electroporation for Treatment Planning. *IEEE Trans. Biomed. Eng.* **2018**, *65*, 1810–1819. [CrossRef]

19. Pavlin, M.; Kandušer, M.; Reberšek, M.; Pucihar, G.; Hart, F.X.; Magjarevićcacute, R.; Miklavčič, D. Effect of Cell Electroporation on the Conductivity of a Cell Suspension. *Biophys. J.* **2005**, *88*, 4378–4390. [CrossRef]

20. Schwan, H.P. Electrical Properties of Tissue and Cell Suspensions. In *Advances in Biological and Medical Physics*; Elsevier: Amsterdam, The Netherlands, 1957; pp. 147–209.

21. Pauly, H.; Schwan, H.P. Über die Impedanz einer Suspension von kugelförmigen Teilchen mit einer Schale. *Zeitschrift für Naturforsch. B* **1959**, *14*, 125–131. [CrossRef]

22. Weaver, J.; Astumian, R. The response of living cells to very weak electric fields: The thermal noise limit. *Science* **1990**, *247*, 459–462. [CrossRef] [PubMed]

23. Gowrishankar, T.R.; Weaver, J.C. An approach to electrical modeling of single and multiple cells. *Proc. Natl. Acad. Sci. USA* **2003**, *100*, 3203–3208. [CrossRef] [PubMed]

24. Xu, Y.; Xie, X.; Duan, Y.; Wang, L.; Cheng, Z.; Cheng, J. A review of impedance measurements of whole cells. *Biosens. Bioelectron.* **2016**, *77*, 824–836. [CrossRef] [PubMed]

25. Bastos, J.P.A.; Sadowski, N. *Magnetic Materials and 3D Finite Element Modeling*; CRC Press: Boca Raton, FL, USA, 2017; Volume 40, ISBN 9781315215624.

26. Asami, K.; Yonezawa, T. Dielectric behavior of wild-type yeast and vacuole-deficient mutant over a frequency range of 10 kHz to 10 GHz. *Biophys. J.* **1996**, *71*, 2192–2200. [CrossRef]

27. Hölzel, R.; Lamprecht, I. Dielectric properties of yeast cells as determined by electrorotation. *Biochim. Biophys. Acta-Biomembr.* **1992**, *1104*, 195–200. [CrossRef]

28. Raicu, V.; Raicu, G.; Turcu, G. Dielectric properties of yeast cells as simulated by the two-shell model. *Biochim. Biophys. Acta-Bioenerg.* **1996**, *1274*, 143–148. [CrossRef]

29. El Zakhem, H.; Lanoisellé, J.-L.; Lebovka, N.I.; Nonus, M.; Vorobiev, E. The early stages of Saccharomyces cerevisiae yeast suspensions damage in moderate pulsed electric fields. *Colloids Surf. B Biointerfaces* **2006**, *47*, 189–197. [CrossRef]

30. Lyu, C.; Wang, J.; Powell-Palm, M.; Rubinsky, B. Simultaneous electroporation and dielectrophoresis in non-electrolytic micro/nano-electroporation. *Sci. Rep.* **2018**, *8*, 2481. [CrossRef]

31. Costa, J.A.; de Oliveira, P.X.; Pereira, L.S.; Rodrigues, J.; Suzuki, D.O.H. Sensitivity Analysis of a Nuclear Electroporation Model—A Theoretical Study. *IEEE Trans. Dielectr. Electr. Insul.* **2021**, *28*, 1850–1858. [CrossRef]

32. Suzuki, D.O.H.; Ramos, A.; Ribeiro, M.C.M.; Cazarolli, L.H.; Silva, F.R.M.B.; Leite, L.D.; Marques, J.L.B. Theoretical and Experimental Analysis of Electroporated Membrane Conductance in Cell Suspension. *IEEE Trans. Biomed. Eng.* **2011**, *58*, 3310–3318. [CrossRef]

33. Gimsa, J.; Wachner, D. Analytical Description of the Transmembrane Voltage Induced on Arbitrarily Oriented Ellipsoidal and Cylindrical Cells. *Biophys. J.* **2001**, *81*, 1888–1896. [CrossRef]

34. Saulis, G.; Lapė, R.; Pranevičiūtė, R.; Mickevičius, D. Changes of the solution pH due to exposure by high-voltage electric pulses. *Bioelectrochemistry* **2005**, *67*, 101–108. [CrossRef] [PubMed]

35. Sherba, J.J.; Hogquist, S.; Lin, H.; Shan, J.W.; Shreiber, D.I.; Zahn, J.D. The effects of electroporation buffer composition on cell viability and electro-transfection efficiency. *Sci. Rep.* **2020**, *10*, 3053. [CrossRef] [PubMed]

36. Aouida, M.; Tounekti, O.; Belhadj, O.; Mir, L.M. Comparative roles of the cell wall and cell membrane in limiting uptake of xenobiotic molecules by Saccharomyces cerevisiae. *Antimicrob. Agents Chemother.* **2003**, *47*, 2012–2014. [CrossRef]

37. Guo, F.; Qian, K.; Zhang, L.; Deng, H.; Li, X.; Zhou, J.; Wang, J. Anisotropic conductivity for single-cell electroporation simulation with tangentially dispersive membrane. *Electrochim. Acta* **2021**, *385*, 138426. [CrossRef]

38. Yan, Z.; Hao, C.; Yin, L.; Liu, K.; Qiu, J. Simulation of the influence of temperature on the dynamic process of electroporation based on finite element analysis. *IEEE Trans. Plasma Sci.* **2021**, *49*, 2839–2850. [CrossRef]

39. Chiapperino, M.A.; Bia, P.; Lamacchia, C.M.; Mescia, L. Electroporation modelling of irregular nucleated cells including pore radius dynamics. *Electronics* **2019**, *8*, 1477. [CrossRef]

40. Schmeer, M.; Seipp, T.; Pliquett, U.; Kakorin, S.; Neumann, E. Mechanism for the conductivity changes caused by membrane electroporation of CHO cell-pellets. *Phys. Chem. Chem. Phys.* **2004**, *6*, 5564–5574. [CrossRef]

41. Kakorin, S.; Neumann, E. Ionic conductivity of electroporated lipid bilayer membranes. *Bioelectrochemistry* **2002**, *56*, 163–166. [CrossRef]

42. Pucihar, G.; Miklavčič, D.; Kotnik, T. A time-dependent numerical model of transmembrane voltage inducement and electroporation of irregularly shaped cells. *IEEE Trans. Biomed. Eng.* **2009**, *56*, 1491–1501. [CrossRef]

43. Ramos, A.; Schneider, A.L.S.; Suzuki, D.O.H.; Marques, J.L.B. Sinusoidal signal analysis of electroporation in biological cells. *IEEE Trans. Biomed. Eng.* **2012**, *59*, 2965–2973. [CrossRef] [PubMed]

44. Arnold, W.M.; Schmutzler, R.K.; Schmutzler, A.G.; van der Ven, H.; Al-Hasani, S.; Krebs, D.; Zimmermann, U. Electro-rotation of mouse oocytes: Single-cell measurements of zona-intact and zona-free cells and of the isolated zona pellucida. *Biochim. Biophys. Acta (BBA)-Biomembr.* **1987**, *905*, 454–464. [CrossRef]

45. Ramos, A.; Suzuki, D.O.H.; Marques, J.L.B. Numerical study of the electrical conductivity and polarization in a suspension of spherical cells. *Bioelectrochemistry* **2006**, *68*, 213–217. [CrossRef]

46. Al-Hilphy, A.R.S. Electrical Field (AC) for Non Thermal Milk Pasteurization. *J. Nutr. Food Sci.* **2012**, *2*, 177–181. [CrossRef]

47. Li, S.; Chen, X.; Han, F. Simulation of Cell Dielectric Properties Based on COMSOL. *Proc. Int. Conf. Artif. Life Robot.* **2018**, *23*, 603–606. [CrossRef]

48. Teissié, J.; Rols, M.P. An experimental evaluation of the critical potential difference inducing cell membrane electropermeabilization. *Biophys. J.* **1993**, *65*, 409–413. [CrossRef]

49. Silve, A.; Leray, I.; Poignard, C.; Mir, L.M. Impact of external medium conductivity on cell membrane electropermeabilization by microsecond and nanosecond electric pulses. *Sci. Rep.* **2016**, *6*, 19957. [CrossRef] [PubMed]

50. Muraji, M.; Taniguchi, H.; Tatebe, W.; Berg, H. Examination of the relationship between parameters to determine electropermeability of Saccharomyces cerevisiae. *Bioelectrochem. Bioenerg.* **1999**, *48*, 485–488. [CrossRef]

51. Djuzenova, C.S.; Zimmermann, U.; Frank, H.; Sukhorukov, V.L.; Richter, E.; Fuhr, G. Effect of medium conductivity and composition on the uptake of propidium iodide into electropermeabilized myeloma cells. *Biochim. Biophys. Acta-Biomembr.* **1996**, *1284*, 143–152. [CrossRef]

52. Di Biasio, A.; Ambrosone, L.; Cametti, C. The Dielectric Behavior of Nonspherical Biological Cell Suspensions: An Analytic Approach. *Biophys. J.* **2010**, *99*, 163–174. [CrossRef]

53. Stirke, A.; Celiesiute-Germaniene, R.; Zimkus, A.; Zurauskiene, N.; Simonis, P.; Dervinis, A.; Ramanavicius, A.; Balevicius, S. The link between yeast cell wall porosity and plasma membrane permeability after PEF treatment. *Sci. Rep.* **2019**, *9*, 14731. [CrossRef]

54. Neu, J.C.; Krassowska, W. Asymptotic model of electroporation. *Phys. Rev. E* **1999**, *59*, 3471–3482. [CrossRef]

55. Smith, K.C.; Weaver, J.C. Active Mechanisms Are Needed to Describe Cell Responses to Submicrosecond, Megavolt-per-Meter Pulses: Cell Models for Ultrashort Pulses. *Biophys. J.* **2008**, *95*, 1547–1563. [CrossRef] [PubMed]

56. Rems, L.; Ušaj, M.; Kandušer, M.; Reberšek, M.; Miklavčič, D.; Pucihar, G. Cell electrofusion using nanosecond electric pulses. *Sci. Rep.* **2013**, *3*, 3382. [CrossRef] [PubMed]

57. Huang, Y.; Holzel, R.; Pethig, R.; Wang, X.-B. Differences in the AC electrodynamics of viable and non-viable yeast cells determined through combined dielectrophoresis and electrorotation studies. *Phys. Med. Biol.* **1992**, *37*, 1499–1517. [CrossRef]

APPENDIX D – Liquid Food Conductivity

The conductivities of four beers were measured with conductometer Hanna HI 8733. Measurements were at 5-10 ºC using the temperature correction (as 25º measurements). The measurements are at Table 4. It is noted that the conductometer manufacturer does not provide the measurement frequency, which is typically 1 kHz.

Table 4 – Conductivities of beer.

Type	Conductivity σ, S/m (mean ± SD)
Handmade Dark Lager	0.156 ± .011
Handmade Pale Lager	0.139 ± .002
Kairos Kapital Cream Ale	0.161 ± .005
Eisenbahn Pilsen	0.102 ± .005

Source: Author.

APPENDIX E – Potato Tissue Impedance Monitoring During Time and Sample
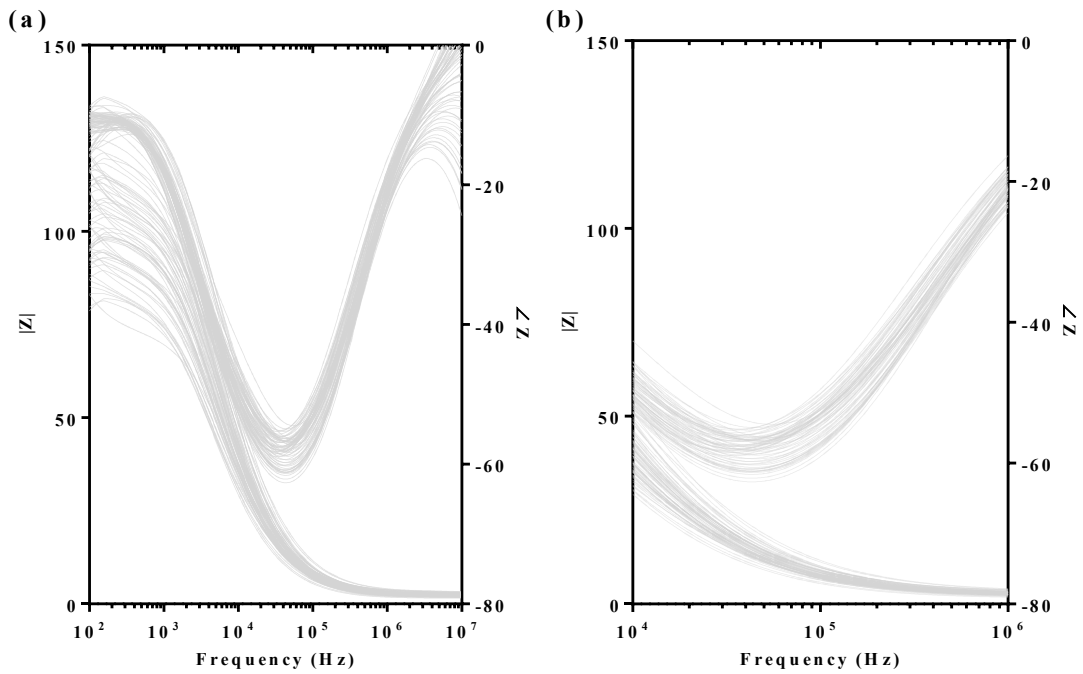
The sample has an accommodation time, which implies changes in its spectrum up to approximately 100 kHz. The measurements using 2 minutes intervals (i.e. delay) are as Figure 49. The variations of the samples themselves, as well as deviations in the positioning between electrodes and cutting are shown in Figure 50.

Figure 49 – (a) Sample frequency spectrum under time to the measurement. (b) Zoom in the 100 kHz. The time steps are in minutes (*i.e.* t2 = 2 minutes waiting time to the measurement).
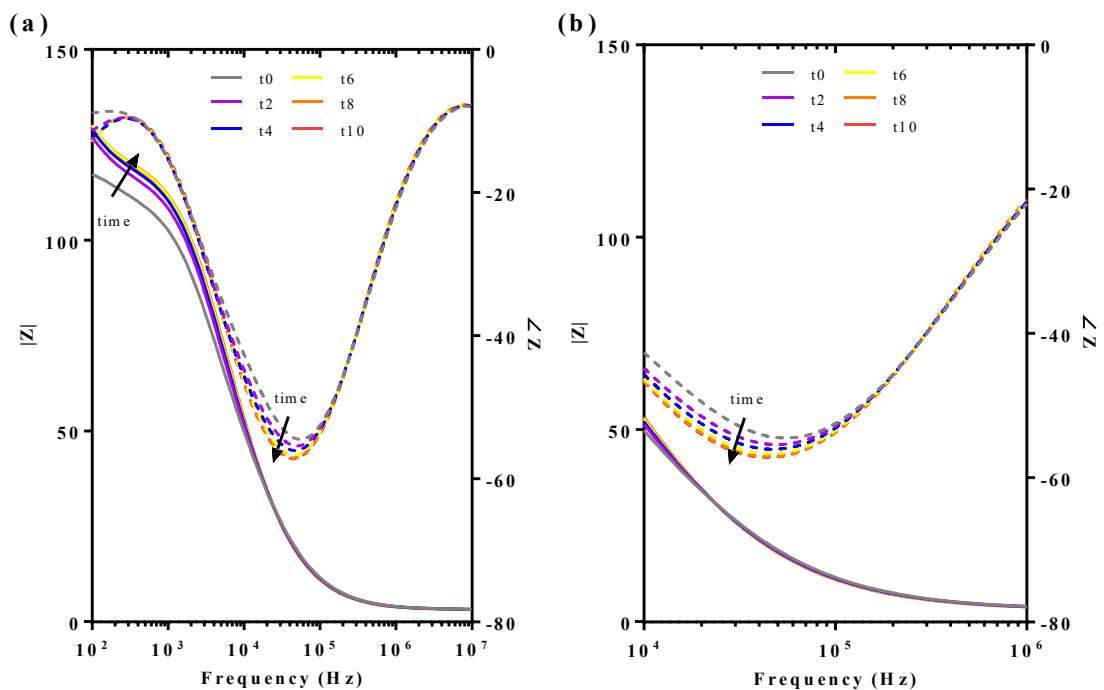
Source: Author.

Figure 50 – (a) All samples spectrum used in this work. (b) Zoom in the 100 kHz. Those are the data from before PEF. The |Z| and ∠Z graphs are composed by 69 lines each.

Source: Author.